EXPLORING SELECTED MODERN MASS SPECTROMETRY TECHNIQUES IN APPLIED SCIENCES

MARYAM YOUSEFI-TAEMEH

A DISSERTATION SUBMITTED TO
THE FACULTY OF GRADUATE STUDIES
IN PARTIAL FULLFILLMENT OF THE
REQUIREMENTS
FOR THE DEGREE OF
DOCTOR OF PHILOSOPHY

GRADUATE PROGRAM IN CHEMISTRY
YORK UNIVERSITY
TORONTO, ONTARIO

July 2023

Abstract

Mass Spectrometry (MS) is a powerful analytical technique that has revolutionized our ability to analyze complex mixtures and has diverse applications in various scientific disciplines. It is widely used in chemistry and biology to determine the molecular composition, structure, and quantification of samples. In this dissertation, we aimed to explore novel applications of mass spectrometry techniques, including electrospray ionization (ESI) and tandem mass spectrometry (MS/MS), as well as mass spectrometry imaging (MSI) techniques such as matrix-assisted laser desorption/ionization (MALDI) and desorption electrospray ionization (DESI). The objective was to strengthen our knowledge and skills in various MS methodologies and gain practical experience in using these techniques, for developing methods to chemically profile, separate, detect, map, and quantify a wide range of targeted and untargeted analytes from complex matrices.

Given the versatility of MS-based techniques, we focused on specific applications within this field. First and foremost, forensic and pharmaceutical cannabis-related applications require accurate and sensitive analytical methods. Hence, we developed and validated a DESI-MS method for detecting cannabinoids in cannabis-infused chocolate, utilizing TLC-DESI-MS and QuEChERS extraction for THC quantification.

Additionally, we investigated metabolic differences associated with soybean alleles (QTLs E and M) conferring resistance to leaf-chewing insects. Non-targeted mass spectrometry reveals distinct metabolite sets influenced by the QTLs, highlighting daidzein as a significant marker. This suggests a novel mechanism impeding the insects' ability to evolve tolerance.

Moreover, we explored the sublimation technique for the application of a matrix coating in MALDI-MSI. Specifically, we investigated the optimal conditions for sublimation of the 5-chloro-2-mercaptobenzothiazole (CMBT) matrix on mouse kidney samples. We successfully obtained high-quality MALDI-MSI images of phospholipids (PC, PG) and phosphatidylinositol (PI) in mouse kidney sections, providing valuable spatially resolved information.

Lastly, we discussed the importance of phosphatidylinositols (PI) and phosphoinositides and their involvement in various diseases, emphasizing the need to optimize the MALDI-matrix type and thickness for enhanced sensitivity in detecting these molecules. The label-free data obtained through this optimized approach holds the potential for investigating the relative *m/z* factors associated with PI-related pathogenesis.

Overall, this dissertation demonstrated the versatility and potential of mass spectrometry techniques. The findings lay the groundwork for future research in the field of MS analysis, particularly in the detection, quantification, and understanding of phosphatidylinositols and phosphoinositides in biological systems and disease pathologies.

Acknowledgements

I would like to express my sincere gratitude to Professor Demian Ifa, my supervisor, for providing me with the incredible opportunity to join his research group. I am truly thankful for his mentorship, which not only introduced me to the fascinating world of mass spectrometry but also allowed me to explore diverse projects and research throughout my graduate studies. My time in his lab has been incredibly valuable and transforming me into a more confident and experienced individual.

I would also like to extend my appreciation to Professors Derek Wilson and Trevor VandenBoer, who served as my supervisory committees. Their invaluable suggestions and feedback during the annual Research Evaluation have played an important role in improving the quality of my research and enhancing its overall impact. Additionally, I would like to offer my special thanks to Professors Arash Zarrine-Afsar and Satinder Brar for graciously accepting the invitation to be part of my examination committee. I am grateful for their willingness to contribute their expertise to this important milestone in my academic journey.

I extend my heartfelt gratitude to Dr. Udo Verkerk for generously devoting his time and expertise to review my dissertation comprehensively and engaging in a thorough discussion pertaining to potential queries arising from its content. His valuable input and support are deeply appreciated, and I am truly grateful for this invaluable experience.

To all past and current members of Professor Ifa's lab: Consuelo, Shamina, Aafreen, Adriana, Mayara, Alessandro. I want to express my deepest gratitude for the opportunity to work alongside each and every one of you. Talita, Leonardo, and Laurentiu, I am beyond grateful for the chance of working closely with you over the past year. The memories we have created together, the laughter we shared, and the countless brainstorming sessions about different research topics, will forever hold a special place in my heart. I will never forget the challenging days when our experiments didn't go as planned, and how we rallied together to lift each other's spirits. And let's not forget the exhilarating moments when our experiments succeeded, and we celebrated as a team. I genuinely wish we could have had more time to continue working side by side. The memories of

the gummi bear extraction and the multimeter measurement experiments will stay with me for a lifetime. Thank you all for your friendship, support, and the remarkable experiences we shared. Each of you has made a lasting impact on my journey in the lab, and I am grateful for the knowledge and experience we have built together.

On a personal note, I want to take a moment to express my deepest gratitude and honor the memory of my dear father, Reza Yousefi-Taemeh, the extraordinary man who inspired me to pursue a lifelong passion for science. From my earliest memories, you nurtured a love of learning within me. I can still remember our conversations about the wonders of the universe, with you patiently answering my questions and sharing your knowledge. You believed that we could become anything we wanted if we pursued our passions and gave our utmost effort. I carried your spirit with me, knowing that you believed in me wholeheartedly. Your influence remains a source of strength and motivation. I am forever grateful to have had you as my father and mentor. Your support and encouragement continue to guide me on my path, towards the fulfillment of my dreams. I am committed to honoring your memory by making meaningful contributions to the field, with the hope that I can make you proud.

To my incredible mother, Shadi Derakhshan Nejad, words cannot fully express my gratitude for your dedication and boundless love. Your love and support have made a big difference in my life. You've always been there for me, guiding me through the ups and downs. Your sacrifices and care have played a big part in my success and happiness. As I move forward, I carry with me the valuable lessons you've taught me – to face challenges with courage, to embrace kindness in all interactions, and to cherish the beauty of life's journey. Thank you, Mama, for being the guiding force in my life. Your love has been the anchor that has kept me grounded, and your presence has filled my world with warmth and love. I am forever indebted to you for shaping me into the person I am today.

To my amazing sister, Melika Yousefi-Taemeh, thank you for always bringing laughter into my life and supporting me with your love throughout this journey. Our bond is not just that of siblings, but also of lifelong friends, and I am grateful for the enduring friendship we share.

And to my incredible partner, Iman Hashemi, the biggest thank you for being by my side throughout this journey. Your presence and support have been invaluable. You have always prioritized my studies above all else, making every step of the way more enjoyable with your constant care and support.

I am grateful for each and every one of you, as it is because of your support that I have been able to turn this dream into a reality.

Table of Contents

List of Tables

List of Figures

List of Abbreviations

Δ^8-THC	(-)-Δ^8-trans tetrahydrocannabinol
Δ^9-THC	(-)-Δ^9-trans-tetrahydrocannabinol
2D	Two dimension
3D	Three dimension
9AA	9-aminoacridine
µJ	Microjoule
µm	Micrometer
^oC	Degrees Celsius
ACN	Acetonitrile
AIDS	Acquired immunodeficiency syndrome
AMS	Ambient mass spectrometry
ANOVA	Analysis of Variance
API	Atmospheric pressure ionization
Bt	*Bacillus thuringiensis*
CBC	Cannabichromene
CBD	Cannabidiol
CBE	Cannabielsoin
CBG	Cannabigerol
CBL	Cannabicyclol
CBN	Cannabinol
CBND	Cannabinodiol
CBT	Cannabitriol
CEM	Chain ejection model
CID	Collision induced dissociation
CMBT	5-chloro-2-mercaptobenzothiazole
CRM	Charged residual model
CV	Coefficient of variation
Da	Dalton
DAN	1,5-Diaminonapthalene
DESI	Desorption electrospray ionization
DESI-MS	Desorption electrospray ionization mass spectrometry
DESI-MSI	Desorption electrospray ionization mass spectrometry imaging
DHA	2,5-Dihydroxyacetophenone
DHB	2,5-dihydroxybenzoic acid
dSPE	Dispersive solid-phase extraction
ESI	Electrospray ionization mass spectrometry
ESI-MS	Electrospray ionization mass spectrometry
EtOH	Ethanol
FDA US	Food and drug administration of the United States of America
g	Grams
G. max	Glycine max
G. soja	Glycine soja
GC-MS	Gas chromatography-mass spectrometry
H&E	Hematoxylin and Eosin
HCD	Higher Energy Collisional Dissociation

HPLC	High-Performance Liquid Chromatography
Hr(s)	Hour/hours
Hz	Hertz
IEM	Ion evaporation model
IS	Internal standard
ITO	Indium tin oxide
kV	Kilovolt
LADI	Laser ablation direct analysis in real time imaging
LC	Liquid Chromatography
LG	Linkage Group
LOD	Limit of detection
LOQ	Limit of quantitation
LTQ	Linear trap quadrupole known as linear ion trap
m/z	Mass-to-charge ratio
MALDI	Matrix assisted laser desorption ionization
MALDI-MS	Matrix assisted laser desorption ionization mass spectrometry
MALDI-MSI	Matrix assisted laser desorption ionization mass spectrometry imaging
Mb	Megabase
MeOH	Methanol
min	Minute
mm	Millimeter
ms	Milliseconds
MS	Mass spectrometry
MS^n	Multiple stages of tandem mass spectrometry
MSI	Mass spectrometry imaging
MS/MS	Mass spectrometry/Mass spectrometry
MW	Molecular weight
nano ESI-MS	Nano electrospray ionization mass spectrometry
Nd:YAG	Neodymium-doped Yttrium Aluminum Garnet
NH_4OH	Ammonium Hydroxide
nm	Nanometer
PC	Phosphatidylcholine
PCA	Principal component analysis
PG	Phosphatidylglycerol
PI	Phosphatidylinositol
PIP	Phosphatidylinositol phosphate
PIP_2	Phosphatidylinositol bisphosphate
PIP_3	Phosphatidylinositol trisphosphate
PLS-PA	Partial least squares path modeling
ppm	Parts per million
psi	Pounds per square inch
Q1	First mass analyzer
q2	Reaction cell
Q3	Second mass analyzer
QC	Quality control
QTL	Quantitative trait loci
QuEChERS	Quick, easy, cheap, effective, rugged, and safe
RE	Relative error
RF	Radiofrequency

Rf	Retention factor
rpm	Revolutions per minute
RSD	Relative standard deviation
S/N	Signal-to-noise ratio
SD	Standard deviation
SIM	Selected ion monitoring
SPE	Solid-phase extraction
THC-D_3	Isotopically labeled form of THC
THCA	Tetrahydrocannabinolic acid
THCV	Tetrahydrocannabivarin
TLC	Thin layer chromatography

Chapter One: General Introduction

1.1. History and the Fundamental Principles of Mass Spectrometry

The continuous development of mass spectrometers began with the discoveries of W. Wien and J.J. Thomson in the late 19th century. [1] Thomson's analysis of the deflection of cathode rays in an electric field in 1897 allowed him to determine the mass-to-charge ratio of the electron, leading to the discovery of this subatomic particle. [1] [2] Furthermore, Wien's discovery of the proton in 1898 was made possible through his analysis of positive anode rays, which enabled him to determine the mass of the hydrogen atom. [1] [3] The inception of mass spectrometry can be tracked back to 1907 when J.J. Thomson proposed his hypothesis that channel rays consist of charged particles, with the lighter particles being more deflected than the heavier ones. This principle formed the basis of mass spectrometry. [1]

Mass Spectrometry (MS) is a powerful analytical technique that has become an integral part of many fields of scientific disciplines, such as chemistry and biology. [4] It is used to determine the molecular composition and structure of a sample, as well as to quantify its components. To achieve this, the molecules of interest are introduced into the ionization source of the mass spectrometer, where they are ionized to produce positive or negative gas-phase ions. [5] [6] These ions then travel through the mass analyzer, get sorted based on their mass-to-charge ratio (*m/z*), and reach the detector. [6] [7] The detectable ions are recorded and the computer displays the signals as a mass spectrum, which indicates the relative abundance of the signals based on their *m/z* ratio. [6] [7]

MS has revolutionized our ability to analyze complex mixtures and has diverse applications, ranging from drug discovery to environmental analysis and forensic science. The coupling of MS with other techniques can be advantageous and often leads to more reliable results. [5] [7] The method is additionally applied in proteomics and metabolomics research to understand the functions of proteins and metabolites in biological systems. As a result, there is a deeper understanding of the molecular mechanisms underlying various diseases, and the development of new drugs and therapies has been possible. [8]

All mass spectrometers require a sample input system, an ionization source, a mass analyzer, and a detector. [7]

1.2. Electrospray Ionization Mass Spectrometry

"*A few years ago, the idea of making proteins or polymers "fly" by electrospray ionization (ESI) seemed as improbable as a flying elephant, but today it is a standard part of modern mass spectrometers*" – Professor John Fenn–2003 [9]

Attempts to establish mass spectrometry techniques to study large biomolecules, have faced significant challenges due to the difficulty of converting these molecules into ions that can be analyzed in gas phase. [10] Due to the extensive decomposition that occurs, the vaporization of these molecules is not possible. Therefore, traditional ionization methods that rely on gas-phase interactions with the molecule cannot be used. [10]

In 1989, Fenn introduced electrospray ionization as a soft ionization technique that allowed intact chemical species to be ionized by multiple charging, successfully addressing previous problems in this field. [11] Electrospray Ionization (ESI) is a category of ionization methods which utilized strong electric fields to desorb ions. [10] The technique is considered a soft ionization method due to the fact that it results in very little residual energy being retained by the analyte, and generally no fragmentation occurs upon ionization. [11] Furthermore, the multiple charging during ESI causes the resulting ions to have lower *m/z* values, which allows them to fall within the mass ranges compatible with common mass analyzers. [11] [12] Prior to the development of ESI-MS, existing ionization methods were not sufficient to accurately measure biologically important macromolecules such as proteins. [11]

In more details, ESI employs electrical energy to facilitate the transfer of ions from solution into gas-phase prior to mass spectrometric analysis. [6] A mist of charged droplets carrying the same polarity as the capillary voltage in then produced. [6] With the aid of a pressure gradient and potential gradient, the charged droplets move towards the analyzer region of the mass spectrometer. [6] The charged droplets undergo continuous reduction in size by solvent evaporation, resulting in an increase in surface charge density and decrease in droplet radius until it reaches a point called Rayleigh limit where the Coulomb force of repulsion among the shrinking charged droplets overcomes the surface tension, causing them to break up into smaller droplets that also evaporate. [6] [11] [10] This sequence of events repeats with cycles of evaporation and disintegration of charged droplets, until they eventually break up into droplets with radii of a few

nanometers which consequently produce gaseous analyte ions that are detectable by MS (Figure 1.1). [10] [12]

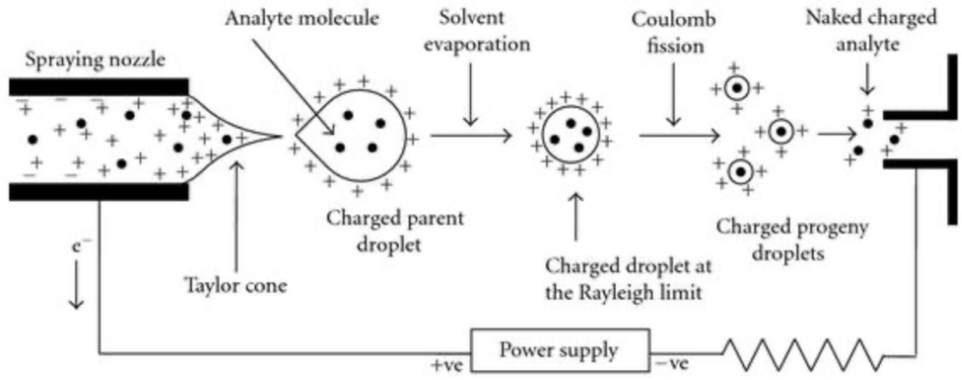

Figure 1.1. Adapted from Banerjee et al. [11] Schematic representation of electrospray ionization process.

There are three different mechanisms of formation of charged gaseous species by ESI: (a) low molecular weight species in solution are believed to be transferred into gas-phase following ion evaporation model (IEM); (b) larger globular species such as native proteins are transferred into gas-phase via charged residual model (CRM); and (c) partially hydrophobic, disordered polymer chains are transferred to gas-phase via chain ejection model (CEM) (Figure 1.2). [12]

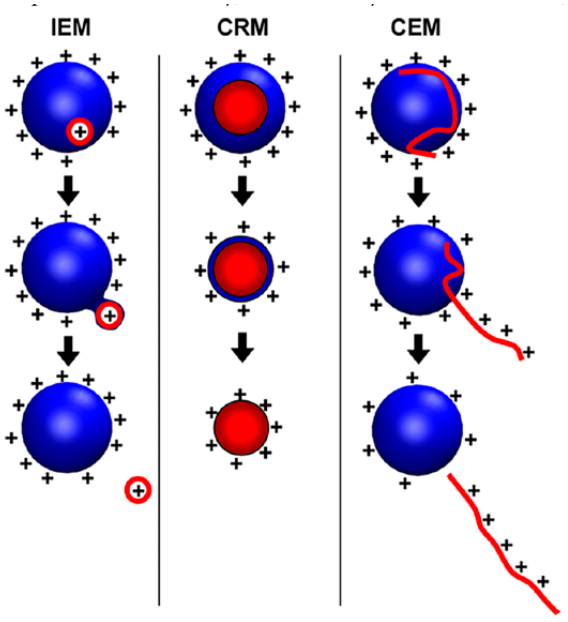

Figure 1.2. Adapted from Konermann et al. [12] Summary of ESI mechanisms. (a) IEM: Small ion ejection from a charged nanodroplet. (b) CRM: Release of a globular protein into the gas phase. (c) CEM: Ejection of an unfolded protein.

Therefore, electrospray ionization mass spectrometry (ESI-MS) has become a significantly important and useful technique in the production of gas-phase ions from large macromolecules and also to investigate the structural characterization, identification, and quantitative measurement of metabolites present in a complex biological sample. [6] [11] [10] It is a sensitive, reliable, and robust technique that enables the analysis of non-volatile and thermally labile biomolecules at very small sample volumes. [6]

1.3. Tandem mass spectrometry (MS/MS):

Tandem mass spectrometry (MS/MS) is a technique where gaseous ions are analyzed in two or more stages of mass analysis, which may be separated spatially or temporally. [11] During a tandem mass spectrometry experiment, a precursor ion is selected by a mass analyzer (Q1) and directed to a reaction cell (q2) to undergo a gas-phase chemical reaction or fragmentation. As a result of this reaction, different product ions with varying masses are formed which are then passed on to the second mass analyzer (Q3) to generate a product ion spectrum. [6] [11]

Due to the soft ionization characteristic of ESI, analytes get transferred in gas-phase without breaking any covalent bonds and thus provides the information about the molecular weight of the compound. [11] Relying on the MW alone is insufficient to establish the structure of an unknown analyte. Therefore, fragmentation of the gaseous analyte is necessary for elucidating its structure. [11] A typical method of activating a precursor ion within a collision cell (q2) involves raising its internal energy to cause cleavage of the chemical bonds. [11] Various techniques can be employed for the activation of precursor ions. Collision-induced dissociation (CID) is among the most common methods in which the gaseous precursor ion is made to collide with a gaseous target (inert and neutral such as nitrogen, helium, or argon) in the collision cell, which leads to the fragmentation of the precursor ions into product ions. [6] [11] The product ions can also be trapped and subjected to another cycle of CID reaction, which can be repeated multiple times for further fragmentation. This process is referred to as MS^n in which n is the number of CID reactions. [6]

1.4. Mass Spectrometry Imaging (MSI)

In recent years, mass spectrometry imaging (MSI) has been proven to be a promising and powerful tool for mapping and spatial analysis of the distribution of a wide range of molecules on

biological samples surfaces. [13] [14] This technique allows for the detection and spatial analysis of multiple chemical compounds based on their *m/z*. Through the analysis of metabolite expressions and biomarker measurements from disease versus healthy tissue comparisons, MSI can help identify the cause of certain diseases. [13] The distribution patterns of one or more molecular species and their correlation with the morphological aspects of a biological sample section are crucial for comprehensive analysis, leading to disease diagnosis. [14]

Mass spectrometry imaging instruments are classified based on how ions are generated from the sample. Matrix-assisted laser desorption ionization (MALDI) and desorption electrospray ionization (DESI) are widely used mass spectrometry imaging techniques for generating ion maps of diverse samples. The MALDI-MSI is a laser-based technique where ions are produced from specific locations (pixels) on the sample surface using laser irradiation. [15] [14] On the other hand, DESI-MSI is an ambient mass spectrometry imaging technique which employs charged solvent droplets to extract and ionize analytes present on the surface of a given sample. [16]

MALDI experiments are conducted in a vacuum, while DESI is performed at atmospheric pressure, making each a unique method, and leading to their fundamental differences. [17]

1.4.1. Desorption Electrospray Ionization Mass Spectrometry Imaging (DESI-MSI)

Desorption Electrospray Ionization (DESI) was introduced by Professor Cooks and his team in 2004 as the first ambient ionization technique. [17] This technique is a variation of the ESI that involves spraying the surface of a sample with an ESI spray and leading the extracted ions from the surface into a mass spectrometer. [18] This ambient technique can analyze the sample directly and under open-air conditions, with little or no prior preparation, and in its native state. [16] Using this technique, the analyst can perform a direct, rapid, real-time, and high-throughput analysis for a wide range of chemical classes such as small molecules, organic compounds, carbohydrates, industrial polymers, and complex biological materials. [16] [17]

To put in simply, DESI proceeds via a “droplet pick-up” mechanism that involves the process of directing electrosprayed charged droplets and ions of solvent onto the surface of the sample that needs to be analyzed. The spray solvent comes into contact with the sample surface,

creating a thin liquid film. This liquid film aids in extracting the analyte from the surface. The successive collisions between primary electrospray droplets and the thin solvent film generates secondary droplets at the opposite end of the impacted film. The extracted analyte is carried by these secondary droplets, which are then pulled into the mass spectrometer's reduced pressure region through a longer capillary inlet (Figure 1.3). [18] [19] Selective ionization of specific compounds, including those present in biological matrices, can be achieved by modifying the composition of the solution that is sprayed. [18]

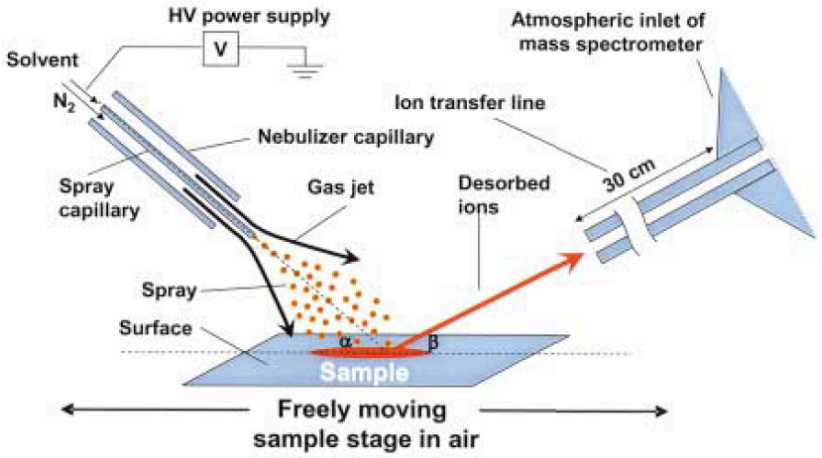

Figure 1.3. Adapted from Takáts et al. [18] Schematic of typical DESI experiment. The sample solution was deposited from solution and dried onto a PTFE surface, and methanol-water (1:1 containing 1% acetic acid or 0.1% aqueous acetic acid solution) was sprayed at a flow rate of 3 to 15 µl/min under the influence of a high (4 kV) voltage. The nominal linear velocity of the nebulizing gas was set to 350 m/s.

This ionization technique utilizes a sprayer probe that is connected to an adjustable XYZ positional mount, which enables the spray nozzle to be directed towards sample surface. [19] During the DESI-MS analysis, it is possible to continuously move or change the orientation of the sample in space. [18]

To produce small, charged solvent microdroplets, a coaxial high flow nebulizing gas is provided from a pressurized source (ranging from 100-200 psi). [19] Similar to the process in ESI, the generation of primary electrically charged droplets that are released from the spray nozzle requires a high voltage connection. [19]

There are five key geometrical factors to take into account while adjusting a DESI source: (1) the incident angle (α), (2) the collection angle (β), (3) the sample spot-to MS inlet distance (x), (4) the tip-to-surface height (d_1), and (5) the MS orifice-to-surface height (d_2). [19] For most routine analysis, these variables remain relatively constant and as follows: α set to 45−60° relative to the surface, x set to 2−3 mm, d_1 is usually 1−3 mm, and d_2 set to ∼1 mm. [19] The collection angle (β) is determined by several factors, including the composition of the solvent, the velocity of the spray jet and the properties of the surface (such as its hardness, hydrophobicity, and porosity). [19] The solvent flow rate can vary depending on factors such as its composition and the substance being analyzed, but it typically falls between 1.5-10 μL min^{-1} (Figure 1.4). [19]

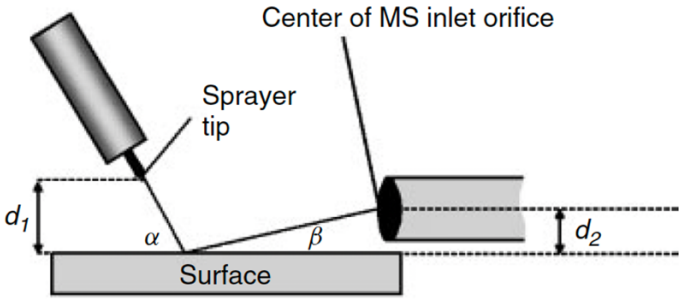

Term	Definition
α	Incident angle
β	Collection angle
d_1	Tip-to-surface distance
d_2	MS inlet-to-surface distance

Figure 1.4. Adapted from Takáts et al. [17] Definitions of terms used in conjunction with DESI.

The mass spectra obtained as a result of this process are comparable to regular ESI mass spectra, as they predominantly display singly or multiply charged molecular ions of the analyte. [18]

1.4.2. Matrix Assisted Laser Desorption Electrospray Ionization Mass Spectrometry Imaging (MALDI-MSI)

Matrix-assisted laser desorption/ionization (MALDI) mass spectrometry imaging (MSI), is a laser-based system in which ions are formed from discrete x and y locations (pixels) across a sample surface using laser irradiation. [15] [14] With its unique feature to analyze complex mixtures from small drugs to large proteins, this technique encompasses broad applicability to

various fields such as proteomic studies, small molecules imaging, drug metabolism, disease pathology, synthetic polymers, and many more. [15] [20]

Efforts to produce ions of organic molecules using lasers can be traced back to early 1970s. [21] Researchers have utilized a diverse range of lasers with significantly differing wavelengths and pulse durations, and have combined them with every available type of mass spectrometer. [21] Given the substantial variation in basic parameters, it is expected that distinct outcomes have been achieved, leading to the development of various combinations of lasers and spectrometers for specific applications. [21] After years of systematic observations, two general principles have developed for the usage of laser in this application: firstly, it is necessary for the molecules to absorb the laser wavelength through resonance for efficient and controllable energy transfer to the sample. Secondly, it is necessary for the energy to be transferred within a very brief period of time to prevent breakdown of thermally labile molecules. [21]

This method involves incorporating the analyte into an excess amount of a matrix compound. [22] For analytes in solution, a common method of sample preparation includes co-spotting a small volume of sample with a matrix solution on to a metal plate and analyze it when dried. [22] While drying, matrix-analyte co-crystals are generated. [23] To analyze a tissue sample, a section is affixed to a sample plate, and a thin layer of matrix is deposited on the tissue. [22] Following that, the crystals are then subjected to short laser pulses, which result in the ionization and desorption of the analyte molecule. [23] The Neodymium-doped Yttrium Aluminum Garnet (Nd:YAG) type laser is among the most typically used ones due to its short pulse width range, and the ability of its laser beam to be focused to small spot sizes. [21]

To conduct MALDI-MSI, thin and frozen tissue section mounted on a stainless-steel target plate or an indium tin oxide (ITO) slide, is coated with the matrix of choice via various matrix application methods. Then the matrix coated sample section is introduced to the vacuum for further mass spectrometric analysis. The image analysis is carried out through a scanning process where a focused laser beam systematically irradiates different spots on the sample surface, and moves across the surface in parallel lines, separated by a defined distance. As a result, an averaged mass spectrum is generated from compounds available within the irradiated area (Figure 1.5). [22] [24]

The MS imaging softwares are used to generate ion images by mapping the intensities of specific *m/z* across the sample's spatial dimensions. [22] [24] This involves assigning color-coded intensity values to each pixel in the image based on the ion's abundance at that location. By using MSI, the analyte of interest can be selected and its distribution over the scanned area can be displayed. This represents both the location as well as the intensity of the corresponding MS signal simultaneously as molecular images. [22]

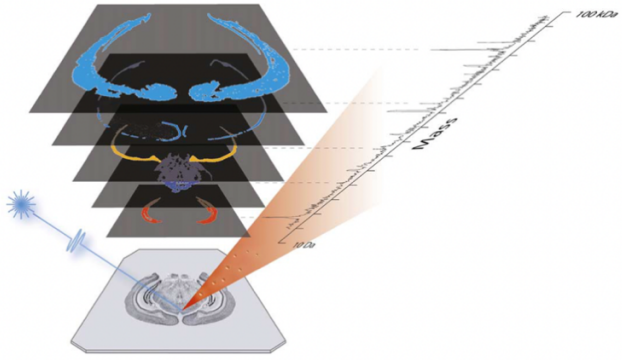

Figure 1.5. Adapted from Rohner et al. [22] MALDI mass spectrometric imaging. A laser is rastered over a tissue sample while acquiring a complete mass spectrum from each position, resulting in molecular images for multiple analytes.

1.4.2.1. Matrices and Matrix application methods

MALDI uses a small organic compound called matrix to facilitates the desorption and ionization of analytes from the sample surface. [20] The matrix absorbs energy at the wavelength of the irradiating laser, and transfers it to the analyte, causing it to become ionized and detectable. [23] Choosing the appropriate matrix is a critical factor for the success of a MALDI-MSI experiment. The kind and thickness of the matrix compound have a direct effect on the signal intensities. They are chosen based on their ability to provide sufficient ionization efficiency for a specific analyte, and their structures, pH, proton affinity and other properties can influence the observed analyte sensitivity. [20] Therefore, careful consideration is needed in selecting the matrix to achieve optimal results in MALDI-MSI.

Since the introduction of MALDI-MSI instrumentation, numerous candidates have been studied for their ability to function as a matrix. [25] In addition to matrix selection, proper matrix application is of importance in analyzing different compounds using MALDI-MSI. [25] [26] Improvements toward higher resolution and greater image details have been an ongoing demand for MSI technology. [27] Factors such as matrix uniformity, matrix crystal size, and unwanted delocalization of analytes during matrix deposition using matrix solutions (especially for lipids due to their relatively low molecular weight and high solubility in organic solvents used to dissolve matrices) can affect the image resolution in MALDI-MSI. [27]

The two methods that are widely used for achieving good matrix deposition are matrix spraying and matrix sublimation, although there have been a number of other methods, such as micro-spotter, hand-held aerosol sprayers, and air brushers reported for MALDI-MSI analysis as well. [26] [27] [28] [29] Except the sublimation technique, all these techniques require matrix dissolution in a water/organic solvent mixture. [27] In addition, when using spraying techniques, the size of the droplet has an effect on the maximum achievable spatial resolution and improvements will be needed in order to produce maximum matrix coverage of the sample yet without delocalizing the analyte. [15] On the other hand, over-spraying the matrix solution can increase the analyte migration from the extraction location. Although automated sprayers can minimize operator variability, it is necessary to repeat overlapping passes when applying the matrix to areas larger than the aerosol diameter, which may introduce variations in ion intensity. [15] The uneven matrix crystal deposition compromises the detection sensitivity of the experiment. [30] So, applying the matrix compound uniformly to the sample surface is a critical step in determining the spatial resolution, the number, and the intensity of ions detected. [15]

Inspired by the sublimation (solid to vapour-phase transition) technique that has been used by chemists for centuries, a solvent free matrix deposition method for MALDI-MSI was introduced by Hankin et. al. [27] It was discovered that under specific conditions of high temperature and low pressure, MALDI matrices could undergo sublimation without decomposition. [27] This inexpensive technique avoids the use of solvents and resolve analyte delocalization during matrix application. [27] It applies a uniform matrix coating over a large sample plate, forms fine microcrystals, and increases the matrix's purity and, consequently, the analyte signal. [27]

Matrix sublimation/deposition for MALDI MSI analysis:

The vacuum sublimation apparatus is consisted of two main pieces: an upper flat-bottom, water-cooled condenser and lower sublimator chamber that acts as the matrix holder. The process for matrix sublimation using the sublimation apparatus can be described as follows:
Firstly, an ITO coated glass slide or stainless steel MALDI plate insert loaded with sample section or dried sample droplet is prepared. The slide or the plate is then affixed to the underside of the flat-bottom condenser of the sublimation apparatus, commonly using copper tape for sufficient and consistent thermal contact. Matrix (300 mg) is added to the bottom of the sublimator chamber, and the two pieces are assembled using an O-ring seal. The system is then connected to a cold trap and a vacuum pump. After pressure reaches the intended value (0.05 Torr for our system), the condenser is filled with cold water (below 15 ºC). After 5 additional minutes, heat is provided to the base of the sublimator chamber by a heating mantle, heated sand bath, or heated oil bath. Time is recorded from the onset of heat application. The matrix is heated, gradually sublimated, and deposited on the sample attached to the cold condenser. After giving the system the intended amount of time for the matrix sublimation and deposition process, the heat application is paused, and while the vacuum is maintained, the condenser and the sublimator chamber are gradually brought to room temperature. Once the system is ventilated, it is opened, and the sample plate is carefully removed from the underside of the condenser. The sample is ready for further MALDI-MSI analysis.

The thickness of the matrix layer on the surface of the sample plays a crucial role in determining the quality of the MALDI-MSI images obtained. If the matrix layer is too thin, it results in production of small amount of ion signals upon laser irradiation, whereas if the matrix layer is too thick, it only generates ions from the matrix. [27] The obtained amount of deposited matrix on the sample surface is determined empirically by adjusting parameters of temperature of the heating system, time of sublimation, pressure of the system, initial amount of matrix at the bottom of the chamber. [27]

Despite significant efforts to enhance the understanding of the mechanisms involved in the desorption/ionization of MALDI processes, the exact comprehension of these mechanisms is still under

study. Several theories and pathways have been studied and examined with regards to both ionization and desorption. [31] [32] [33] [34] [35] [36]

The general process can be summarized in the following steps: initially, the analyte-matrix mixture, consisting of both neutral and pre-charged analytes produced during sample preparation, is subjected to laser ablation. During this process, the matrix molecules absorb most of the energy and release it as heat to the surroundings, causing thermal expansion. This leads to desorption of the matrix and analyte from the surface, resulting in a hot plume of gaseous molecules that contain a combination of charged and neutral matrix molecules. The reactive matrix species and the analyte molecules engage in protonation or deprotonation events, which result in the ionization of the analyte molecules. Simultaneously, some pre-charged analytes that are desorbed manage to maintain their charge even after separating from their counterions. Ultimately, depending on the extraction voltage, either cations or anions are sent to the mass analyzer in a mass spectrometer.

Some authors claimed that the phospholipid standards analyzed using this MALDI-MSI showed that applying matrix by sublimation produced more intense and consistent signals with less sodium adducts compared to the electrospray matrix application technique. [27] This potential could be significantly important in studying lipids in tissue due to their relatively low molecular weight and high solubility in common organic solvents like methanol, ethanol, or acetonitrile used for matrix dissolution in spraying applications. [27]

Figure 1.6. Photograph of sublimation apparatus used to apply matrix to sample surfaces for MALDI-MSI experiments. The sample on the ITO glass slide or MALDI plate insert is attached to the underside of the condenser be thermal conducting tape.

1.5. Mass Spectrometers

The following sections will cover a general overview of mass spectrometers used in my research, including the Thermo Finnigan™ LTQ™ and the QExactive™ Quadrupole-Orbitrap hybrid mass spectrometers.

1.5.1. Thermo Finnigan™ LTQ™ Mass Spectrometer

The Finnigan LTQ comprises of an atmospheric pressure ionization (API) source, ion optics, a mass analyzer, and an ion detection system to measure the mass-to-charge ratios of ions.

The instrument operates by guiding ions produced in the source through the ion optics to the mass analyzer, where they are trapped in stable orbits by a time-varying electric field. The lenses and ion optics are used to regulate the transmission of ions. The ions enter the tube lens via the ion transfer capillary, where they undergo additional desolvation, and are focused towards the skimmer opening. The skimmer acts as a vacuum barrier between the high (ion source) and low (Q00 ion guide) pressure regions of the instrument. The ions then move towards the Q00 ion guide, and their injection into the mass analyzer is controlled by the gate lens. The mass analyzer which is made up of a front lens, linear ion trap, and a back lens, is where the ions are analyzed. The basic design of the linear ion trap is shown in figure 1.8. The linear ion trap consists of a precisely engineered square arrangement of hyperbolic rods that are aligned with great accuracy. Within this structure, two of the rods located in the center section are referred as the exit rods, which contain a slit through which the ions are ejected during the scan out. The mass analyzer measures the mass-to-charge ratios of the ions, and selected ions are ejected and detected by the ion detection system, which produces a signal that is amplified by the detection system electronics. [37]

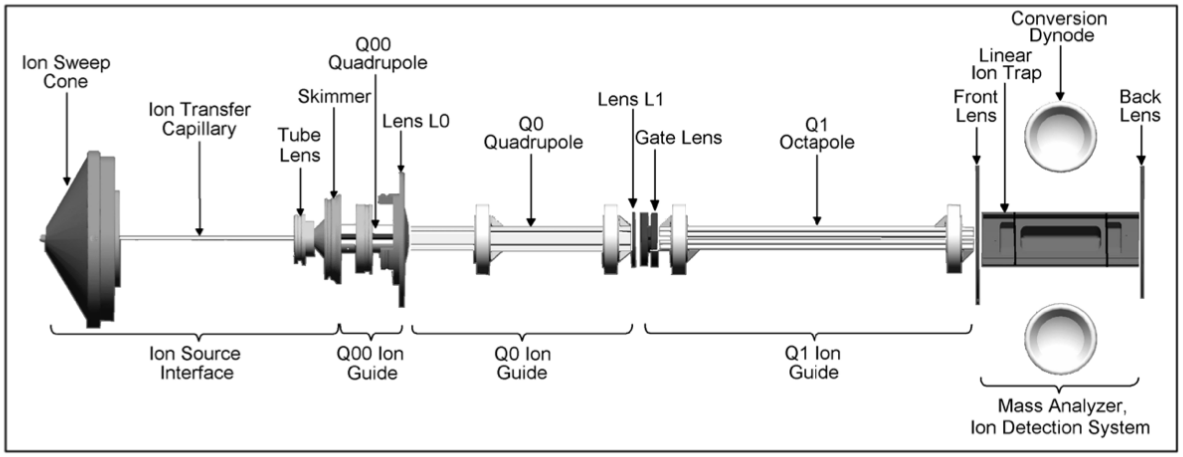

Figure 1.7. Adapted from Thermo Electron Corporation LTQ hardware manual. [37] Construction details of the Thermo Finnigan™ LTQ™ mass spectrometer.

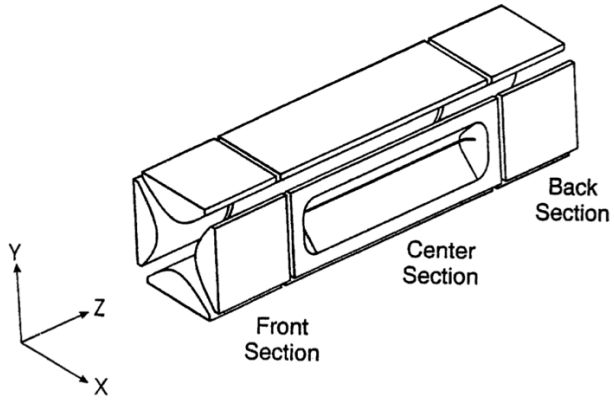

Figure 1.8. Adapted from Thermo Electron Corporation LTQ hardware manual. [37] Linear ion trap quadrupole rod assembly.

1.5.2. Thermo Scientific™ QExactive™ Hybrid Mass Spectrometer

The Exactive series of mass spectrometers are Orbitrap instruments that use an atmospheric pressure ionization (API) source for liquid chromatography (LC) or nano electrospray ionization (nano-ESI) mass spectrometry applications. The instrument is also capable of being linked to a matrix assisted laser desorption/ionization (MALDI) source for mass spectrometry imaging applications. The QExactive mass spectrometers consist of five main components: ion source, quadrupole mass filter, intermediate storage device (C-Trap), collision cell for performing Higher Energy Collisional Dissociation (HCD) experiments, and an Orbitrap analyzer.

The schematic of a Thermo Scientific QExactive is shown in figure 1.9.

The instrument can receive samples from a variety of ion sources. The injection flatapole focuses and transfers ions from the source to the quadrupole which serves as an ion transmission device that has the capacity to separate ions based on their mass-to-charge ratio. The ions are then transferred to the C-Trap where they are accumulated, and their energy is reduced using nitrogen gas. Next, a lens system called "Z-lens" transfers the ions into the Orbitrap analyzer where mass spectra are acquired. [38]

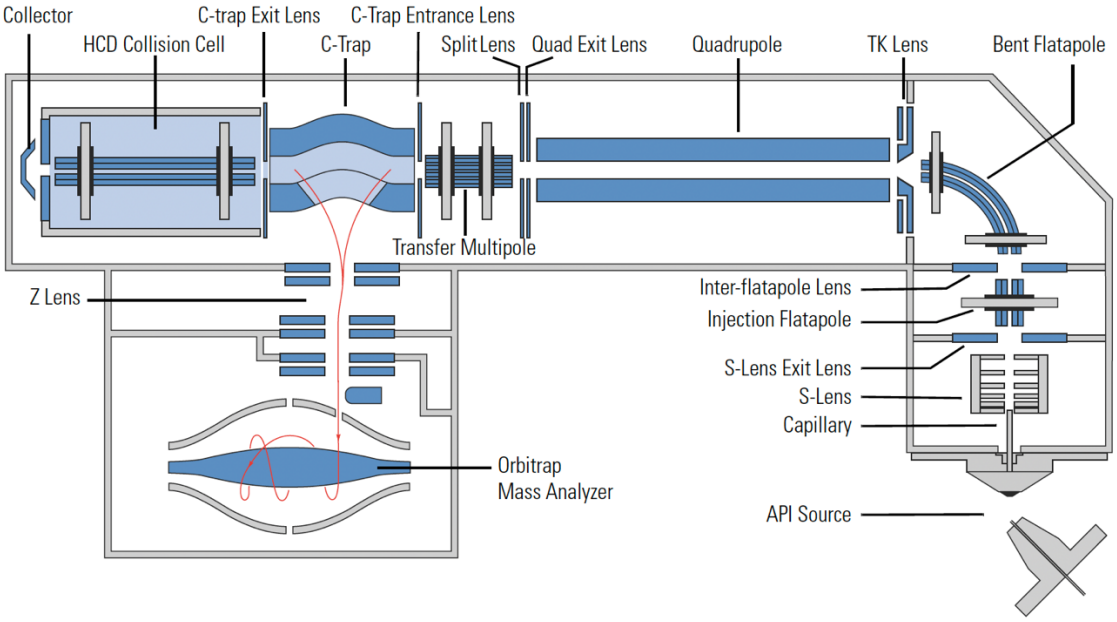

Figure 1.9. Adapted from Thermo Fisher Scientific Exactive series operating manual. [38] Construction details of the Thermo Scientific™ QExactive™ mass spectrometer.

1.6. MALDI mass spectrometry imaging of Phosphatidylinositols (PIs)

Among different metabolites, lipids deserve particular and extensive study as they are involved in and play important roles in many biological aspects, such as structural components, energy storage, biochemical processing in living systems, membrane permeability, functional lipid biosynthesis, and other regulatory and signaling roles on molecular recognition processes beyond genes and proteins. [39] Studies on abundance variation and spatial localization of lipids can expand our understanding of lipid-related disease pathogenesis.

One of the main categories of lipids is phospholipids. The minority of phospholipids in all eukaryotic cellular membranes are phosphatidylinositols (PI), an acidic phospholipid attached to a myo-inositol head group. [40] After binding to the phospholipid, the cyclic inositol is left with five free hydroxyl moieties around it, from which three are readily available for phosphorylation. [40] As a result, a combination of seven phosphorylated derivatives known as phosphoinositides can be formed that are known to play fundamental roles in different structural and instructional processes, including protein interaction and regulation, membrane transport, cytoskeletal function, plasma membrane signalling and more. [40] [41] This category includes phosphatidylinositol phosphate (PIP), phosphatidylinositol bisphosphate (PIP_2), and phosphatidylinositol trisphosphate (PIP_3).

Abnormalities in phosphatidylinositols and phosphoinositides, as well as their relative kinase activities and levels, have been associated with various diseases, such as human nervous system diseases [41], cancer [42] [43] [44], inflammation and thrombosis related diseases [42], immune system diseases [42], acute renal inefficiency in infancy [45], and pregnancy-related diseases [43], to name a few.

Previous studies have reported the identification and visualization of PI molecular species in different tissues. The results suggest that MALDI and DESI-MSI techniques are promising tools for assessing the distribution and abundance of different PI molecular species in different tissues. Enomoto et al. investigated the distribution of PI species in pork chops using MALDI-MSI.

In contrast to studies involving lipid extractions that are time and solvent consuming and may result in the loss or depletion of some lipid classes, MALDI-MSI facilitates the simultaneous detection and data analysis of multiple lipid classes within their biological environment. This makes it a useful tool for unbiased preclinical and clinical lipidomic studies.

Phospholipids tend to ionize in one of the two forms: either as phosphate anions (which is the case for PIs) or nitrogen-centered cations during the MALDI process. [46] The intensity of PI compounds generated in MS experiments relates to the quantity of molecules present in a tissue sample. [46] Phosphatidylinositols are not as numerous as other phospholipids. The most abundant

PI in many tissues is PI(18:0/20:4), with a signal observed at *m/z* 885.5 in negative ion mode. [46] Polyphosphoinositol lipids or phosphoinositides (PIP, PIP_2, PIP_3) are products of PI kinases and have crucial intracellular roles. [46] However, their abundant is so low that detecting them with MSI requires extensive method optimizations and developments.

1.7. Research Objectives

In this dissertation, the main objective was to explore novel applications of mass spectrometry techniques including ESI and tandem mass spectrometry, as well as MSI techniques such as MALDI and DESI. The aim was to gain a better understanding and experience of these various techniques for developing methods to chemically profile, separate, detect, map, and quantify a wide range of targeted and untargeted analytes from complex matrices.

Below, I have outlined the contributions to each corresponding publication, including the publication titles, co-authors names, and the specific roles I played in the research process.

Chapter 2:

Analysis of Tetrahydrocannabinol Derivative from Cannabis-Infused Chocolate by QuEChERS-Thin Layer Chromatography-Desorption Electrospray Ionization Mass Spectrometry.

(Maryam Yousefi-Taemeh, Demian R. Ifa)

I contributed to this work by designing the experiments and conducting all sample preparation, extraction, TLC experiment, mass spectrometry analysis, and data interpretation. Prof. Demian Ifa provided mentorship during the data analysis and manuscript publication process.

Chapter 3:

Metabolomics Differences of *Glycine max* QTLs Resistant to Soybean Looper.

(Maryam Yousefi-Taemeh, Jie Lin, Demian R. Ifa, Wayne Parrott, Nik Kovinich)

I contributed to this project by designing and performing all mass spectrometry experiments, including MS/MS experiments and putative data identification through library searching. However, I was not involved in the soybean sampling, extraction, or statistical analysis through principal component analysis (PCA) and data interpretations. Prof. Demian Ifa provided guidance

and feedback on the manuscript. Wayne Parrott provided the soybean samples. Sample preparations such as extractions, were performed by Prof. Nik Kovinich and Jie Lin, who also assissted with data interpretation through statistical analysis. Prof. Nik Kovinich also provided feedback on the manuscript, especially in areas related to the biological aspects of the soybean samples and soybean loopers.

Chapter 4:

Sublimation application of 5-chloro-2-mercaptobenzothiazole (CMBT) matrix for MALDI mass spectrometry imaging (MSI) of mouse kidney.

(Maryam Yousefi-Taemeh, Ergi Duli, Laurentiu G. Dabija, Mathieu Lemaire, Demian R. Ifa)

I conducted all mass spectrometry imaging experiments, interpret the results, and wrote the manuscript for this project. Ergi Duli and Prof. Mathieu Lemaire provided the mouse kidney tissues. Laurentiu Dabija assisted with experimentation and methodological approaches. Prof. Demian Ifa provided guidance and feedback throughout the project as well as manuscript publication process.

Chapter 5:

Assessment of MALDI matrices for phosphoinositide detection and visualization in mouse kidney models through Matrix Assisted Laser Desorption Ionization (MALDI) imaging techniques.

(Maryam Yousefi-Taemeh, Laurentiu G. Dabija, Ergi Duli, Mathieu Lemaire, Demian R. Ifa)

I made contributions to this research project by designing the experimental framework and optimizing the appropriate thickness for each matrix compound. Together with Laurentiu, we conducted mass spectrometry imaging analysis and interpreted the acquire data. Ergi Duli and Prof. Mathieu Lemaire provided valuable support by supplying the mouse kidney tissues and guiding us in the phosphoinositide-related aspects of the study. Throughout the project, Prof. Demian Ifa provided guidance, feedback, and assistance during the manuscript publication process.

Chapter Two: Analysis of Tetrahydrocannabinol Derivative from Cannabis-Infused Chocolate by QuEChERS-Thin Layer Chromatography-Desorption Electrospray Ionization Mass Spectrometry

Chapter 2 is a version of the published manuscript:

Yousefi-Taemeh, M., Ifa, D.R. Analysis of tetrahydrocannabinol derivative from cannabis-infused chocolate by QuEChERS-thin layer chromatography-desorption electrospray ionization mass spectrometry. *J Mass Spectrom*. **2019**; 54 (10): 834-842.

2.1. Abstract

Recently in Canada and some states of the United States, marijuana (cannabis) has become fully legalized and regulated, for both medical and recreational purposes. This fact is going to make cannabis products such as edibles even more popular than ever before. Therefore, it is assumed that there will be a high demand for analytical methods, which are accurate and sensitive enough to be used in different forensic and pharmaceutical cannabis–related applications. Cannabis derivatives have an extreme range and number of constituents with possible interactions with one another. Thus, this characteristic leads to their vast and highly complex chemistry, which requires robust analytical tools to be able to quantify and qualify them precisely and accurately. We developed and validated an analytical method using desorption electrospray ionization (DESI)–mass spectrometry (MS) to accurately detect, characterize, and quantify cannabinoids and also offer an easy, cost-effective, and reliable technique, which can be performed in a short time for infused edibles in complex matrices such as chocolate. We evaluated a quantitative analysis of tetrahydrocannabinol (THC) in cannabis-infused chocolate with thin-layer chromatography (TLC)–DESI-MS and QuEChERS extraction method. Both techniques of TLC and QuEChERS are cost-effective and can be run in short time.

2.2. Introduction

2.2.1. Cannabis and cannabinoids

Marijuana (or cannabis) has remained the most extensively cultivated and widespread illegal recreational drug worldwide, with 9.5% of adults and 23.7% of youth reporting use in the United States within 2015. [47] [48] The increasing number of users is related to the decreased perception of harm from cannabis and its legalization by many states. [47] [49] Among different forms of available cannabis products, edibles have become more interesting among users. Although there have not been enough studies performed yet to scientifically evaluate and confirm the accuracy of these factors, it is reported that the growing interest for edibles can be due to factors such as the convenient and discreet rout of cannabis consumption [47]; for instance, patients with chronic conditions on medicinal cannabis prefer to choose an extended type of the drug with the

longer duration of analgesic effect in the workplace since smoking cannabis in public is not comfortable or still prohibited in some states. Another factor is the calmer and more relaxing "high" result of edible usage compared with smoking cannabis and also the lower health risk (mainly the ones that are associated with lung inflammation and bronchitis) of edibles compared with smoking cannabis. [47] Either for recreational or medicinal purposes, the core idea of using cannabis is to "feel better" that may range from feeling "high" (e.g., recreational use) to relieving an unpleasant mental or physical condition (e.g., anxiety, pain, or nausea). [47]

Because of the presence of abundant natural components, cannabis are known as chemically complex species. [48] For instance, over the last decades, the number of natural constituents isolated from *Cannabis Sativa* (*C sativa*) has continued to increase, with more than 120 cannabinoids reported in 2017. [48] In general, cannabinoids are the C_{21} terpenophenolic skeleton chemicals isolated from *C sativa*, which can be categorized into 11 types: (-)-Δ^9-trans-tetrahydrocannabinol (Δ^9-THC), (-)-Δ^8-trans tetrahydrocannabinol (Δ^8-THC), cannabigerol (CBG), cannabichromene (CBC), cannabidiol (CBD), cannabinodiol (CBND), cannabielsoin (CBE), cannabicyclol (CBL), cannabinol (CBN), cannabitriol (CBT), and miscellaneous-type cannabinoids. [48]

Among psychological and physiological effects of cannabis, euphoria, analgesia, sedation, memory and cognitive impairment, appetite stimulation, and antiemesis can be mentioned, which are mostly caused by Δ^9-THC. [47] [48] On the other hand, the therapeutic applications of cannabis have contributed to the treatment of glaucoma, migraine headaches, spasticity, anxiety, as an analgesic, control of nausea, and vomiting associated with chemotherapy, and for appetite stimulation of AIDS patients suffering from the wasting syndrome. [47] [48] Δ^9-THC and CBD are two major phytocannabinoids that have been extensively contributed to these therapeutic applications. A vast number of techniques have been performed for quantitative and qualitative analysis of various cannabis-related experiments with the main focus on THC, CBD, CBG, CBN, CBC, and tetrahydrocannabivarin (THCV) because of their possible medicinal and therapeutic properties. [48]

Cannabis and cannabinoid detection is an interesting and growing area of research nowadays. Many testing laboratories in different fields are searching for reliable, cost-effective, efficient, and easy analytical tools and methods to be able to analyze different cannabis related materials both qualitatively and quantitatively. [50] Edible labelling (baked goods, infused edibles, and beverages) has brought in some new challenges for the market, because of cannabinoids differences from each other and also from the original plant. [50] [51] Inaccurate labelling of a product may cause the risk of consuming higher dose of cannabinoids and therefore having unpleasant side effects for consumers. On the other hand, people taking edibles in substitution for medical purposes may suffer from their symptoms (pain) because of receiving lower than mentioned cannabinoid dose. [50] Having reliable techniques capable of comparing the claimed amount of cannabinoids versus the actual one in the sample, in a short time, has a significant importance.

Therefore, our aim was to examine the qualitative and quantitative ability of desorption electrospray ionization (DESI)–mass spectrometry (MS) for cannabis analysis and offer an easy, cost-effective, and reliable technique, which can be performed in a short time for infused edibles in complex matrices such as chocolate. Here, we evaluate a quantitative analysis of tetrahydrocannabinol (THC) in cannabisinfused chocolate with thin-layer chromatography (TLC)–DESI–mass spectrometry and QuEChERS extraction method. Both techniques are cost-effective and can be run in short time.

2.2.2. DESI mass spectrometry

Mass spectrometry is one of the essential and prevalent analytical tools in the chemical and biological sciences. [52] Among many types of ionization methods commercially available today, electrospray ionization (ESI) has become the most popular technique for biological studies. [7] DESI is the first ambient ionization technique introduced in 2004 by Professor Cooks and his team. [17] The extracted ions from the surface are directed to the inlet of the mass spectrometer through air at atmospheric pressure and then mass analyzed. [17] DESI has the ability to record mass spectra on samples in their native environment, without sample preparation or preseparation for qualitative analysis, by creating ions outside the instrument. [17] [16]

2.2.3. QuEChERS method

Sample preparation (extraction and separation of cannabinoid of interest) was required for quantitative experiment. Since the infused chocolate, gummy, candy, and butter matrices are very complicated, most significant challenges are matrix related, which increase variability. [51] For instance, because of their variety in preparation and composition of the compound they are going to mix with, each one of different types of edibles may require different sample preparation strategies to isolate the cannabinoids for an effective analytical examination. In edibles analysis, all the normal food's components, such as fatty acids, sugars, sugar alcohols, proteins, and fibers, must be taken into consideration. For example, sugars and glycerin in gummy bears, the ethanol present in cannabis-infused fermented beverages, and the ingredients in baked goods such as fats, proteins, and fibers can impact the extraction and analysis of targeted cannabinoids. [53] Moreover, the hydrophobicity of cannabinoids can result variable binding to individual compounds of edible products. [53]

Surprisingly, there is little published literature on the isolation and extraction of cannabis or cannabis products before analysis. [54] Hence, we decided to choose a chocolate matrix removal technique rather than cannabinoids extraction, and consequently, QuEChERS method fits well with our protocol.

Quick, easy, cheap, effective, rugged, and safe technique, known as QuEChERS method, has been developed by Anastassiades and Lehotay in 2003 for pesticides analysis. [54] This approach has been assessed in matrix removal and extraction of different analytes from different complex substances. The method is consisted of salting out step and, if necessary, dispersive solid-phase extraction (dSPE) in some cases. [54] Applications of QuEChERS coupled to different mass spectrometry techniques have been reported for some quantitative and high throughput analysis. [55] [56]

Some of the advantages of this method over traditional liquid-liquid extraction techniques are the low required amount of undesirable, costly, and toxic solvents and consequently less volume of organic solvent waste, as well as the ease of batch processing. [50] In addition,

QuEChERS is more reproducible, cost-effective, easy to learn for technicians and to adapt as a routine analysis technique for any laboratory, and fast in comparison with solid-phase extraction (SPE). [50]

2.2.4. TLC separation method

For quantitation, the extracted solution from QuEChERS method is not clean, and there is the possibility of the presence of other analytes, which can cause ion suppression in the mass spectra. To address this problem in this experiment, a separation technique is required. The acidic form of THC is Δ^9-tetrahydrocannabinolic acid (THCA) and is psychologically inactive. [57] This compound is thermally labile and may be converted to THC via decarboxylation. [57] Therefore, analytical methods that include thermal sample manipulations such gas chromatography are not efficient and suitable separation techniques for cannabis analysis. [57] Coupling TLC with ambient mass spectrometry offers a very simple, cost-effective, and robust separation methodology with a detector that exhibits the ability to qualitatively and quantitatively identify and detect target analytes with great selectivity.

Thus, here, we evaluated the use of DESI-MS to assess and quantitate analytes separated on TLC plates. The goal of this project is to use DESI-MS technique to provide identification, separation, and quantification of cannabis from edible cannabis-infused products. A simple, robust, and automated TLC-DESI-MS system is evaluated with QuEChERS extraction technique for the analysis of THC in the cannabis-infused chocolate. It is believed to be a valuable technique for discrimination and detection of cannabinoids in complex matrices such as chocolates, candies, and gummies.

2.3. Methods

2.3.1. Materials

“Shatter Bars” cannabis-infused milk chocolate by Euphoria Extractions has been chosen as a sample to be analyzed using DESI-MS. The standard THC and internal standard THC-D_3 were

obtained from Cerilliant Sigma-Aldrich Corporation. The concentrations of the stock solution of standard and internal standard were 1 mg/mL and 100 μg/mL in methanol, respectively. The cannabis-infused milk chocolate was purchased from a legal cannabis dispensary in Toronto, Canada. The QuEChERS extract pouches (AOAC method) containing 6.00 g of magnesium sulfate and 1.50 g of sodium acetate were purchased from Agilent Technologies. Silica gel TLC glass plates used had 250.00-μm thickness and were purchased from Silicycle. All solvents used in this experiment were acquired from Sigma-Aldrich.

According to the nutrition fact sheet on the chocolate bar, the chocolate bar is 85.00 g, which includes 135.00 mg of THC. So, there is 1.59 mg/g of THC present in each gram of chocolate. The chocolate contains other different cannabinoids in various amounts, such as 2.04 mg of CBN, 47.00 mg of THCA, 1.13 mg of THCV, 2.60 mg of CBG, 0.29 mg of CBD, and 2.16 mg of CBC.

2.3.2. QuEChERS extraction

The experiment started with the matrix removal step performing the QuEChERS technique. To demonstrate the accuracy and precision of the methodology, the analysis was performed in triplicate. A small piece of chocolate was placed in a zipper plastic bag and kept in the refrigerator (4 $^{\circ}$C) for 10 minutes. Using a pestle, the frozen chocolate was crushed. Approximately 1.00 gram of the crushed chocolate was weighed for each run with an analytical balance. Then each part of chocolate was added to a 50-mL centrifuge tube containing 15 mL of water and sonicated for 20 minutes. The purpose of this step was to remove water soluble components of the matrix. Next, 15 mL of acetonitrile was added and mixed thoroughly, following the addition of one pouch of salt. Then the tube was shaken, and the mixtures were centrifuged at 3000 x g for 5 minutes. The resultant was a centrifuge tube with four layers, which from top to bottom were acetonitrile layer with cannabinoids, insoluble chocolate matrix components, water soluble components, and excess extraction salt. Using a transfer pipette, the top layer acetonitrile was carefully transferred into a clean vial, ready for use. For cannabinoid content analysis, dSPE was not necessary because of the high cannabinoid concentration in the organic solvent extract. [50]

In order to find the optimal extraction solvent with the highest THC signal intensity (recovery), the same process was performed with different organic systems such as chloroform, acetonitrile with 1% acetic acid, acetonitrile with 1% formic acid, and hexane.

2.3.3. DESI solvent spray optimization

The extracted solutions were then spotted on silica gel TLC plates with no development, to test the presence of THC. The spotted plates were analyzed using different ranges of solvents in positive and negative ion polarities, in search for the spray solvent with the best ionization efficiency. The spray solvent systems used are acetonitrile:methanol (8:2), acetonitrile, methanol, methanol:water (9:1), acetonitrile: chloroform (1:1), acetonitrile with (0.1%, 0.5%, and 1%) NH_4OH, acetonitrile with 1% formic acid, acetonitrile with 1% acetic acid, and acetonitrile:methanol (8:2) with 1% NH_4OH.

2.3.4. Quantitative analysis

After assessing the solvent with the highest ionization efficiency, the quantitative analysis was performed to achieve a calibration curve in each run. To do so, serial dilution mixtures of THC standards and THC-D_3 solutions were made in methanol in a range of 20- to 80-µg/mL concentration for THC standard and a constant concentration of 50 µg/mL for THC-D_3.

Of each solution, 1.5 µL was spotted on a silica gel-TLC plate 0.5 mm from the bottom. The TLC plate was then air dried. A development chamber was saturated with different mobile phases such as hexane, chloroform, hexane:dichloromethane (1:1), hexane:ethylacetate (9:1), hexane:ethylacetate (6:3), and hexane:dichloromethane: acetone (5:4:1), for some minutes. The spotted plate was then kept inside the chamber and developed with the mobile phase followed by air drying.

The green color of the solution containing cannabinoids makes the starting points on the TLC plates very visible. The sprayer angle and moving stage were adjusted carefully so that the TLC plates can be scanned in a straight line. The TLC plates were scanned along the x-axis starting

a little before the point where the solution was spotted till the point where the TLC plate was developed. As a test, three different line scans were acquired for the first trial, and it was concluded that the first line scan for all concentrations had the highest intensity of the analytes. Therefore, only one line scan was carefully acquired for each run during the experiment.

This type of scanning helps to determine all the analytes present in one line, which are not observable without staining. The DESI source was connected to a moving stage for a consistent speed over the analysis.

2.3.5. Instrument parameters for scanning

All data were collected using a Thermo Fisher Scientific LTQ linear ion trap mass spectrometer (San Jose, CA, USA), which is controlled by Xcalibur 2.0 software (Thermo Fisher Scientific) and is connected to a lab-build automated DESI ion source. [17] [58] The parameters for DESI direct identification: Nitrogen at 100 psi was used as the nebulizing gas for all the experiments. The incident angle was 52^{o}; the distance from spray tip to inlet capillary and spray tip-to-surface distance were kept at 5 and 2.5 mm respectively, for all experiments.
For the TLC dilution series analysis, the instrument was set to collect negative ion, SIM mode spectra for a maximum ion trap injection time of 100 milliseconds using three microscans per spectrum. The range was *m/z* 313 with a window of *m/z* 10 to include the *m/z* 316 for THC-D_3 internal standard. The main experimental parameters used were as follows: solvent flow rate, 10 μL min^{-1}; spray voltage, ±5 kV; capillary temperature, 220 ^{o}C. All optimization experiments conducted were done in both negative and positive ion polarities in full scan mode at a mass range from *m/z* 100 to *m/z* 1000.

2.4. Result and Discussion

2.4.1. Qualitative analysis

In this work, first, the qualitative ability of DESI-MS for detecting cannabinoids, especially THC which is the most psychoactive cannabinoid, was evaluated by experimenting a small piece

of cannabis-infused chocolate sample, in its native environment with no sample preparation. The clear presence of THC was then confirmed by DESI-MS, and this success had led the progress to quantitative analysis.

2.4.2. Quantitative analysis

A cost-effective and reliable quantitative analysis of THC in cannabis-infused chocolate with TLC-DESI-MS and QuEChERS extraction method was performed, and the quantitative ability of DESI-MS was evaluated.

2.4.3. Solvent optimization

For the purpose of this project, we required to run various experiments to provide the optimal factors for the best result. Among these factors, solvent in each step has a very important role in both extraction and ionization efficiency. The signal intensity of an analyte in MS is not only related to its concentration but to its ionization efficiency and environmental extractability as well. [59] Solvent optimization is an important procedure in DESI. [60] An increase in selectivity in the DESI-MS measurements can be achieved for different analytes by the solvent choice and composition. The signal intensities for the polar analytes enhance by using an aqueous solvent whereas the nonpolar analytes present optimal signals with a high organic content solvent spray. [61] This phenomenon can be explained by “like dissolve like” principle where the analyte shows higher solubility in the similar polarity spray solvent and, therefore, more efficient desorption of the analyte from the surface. [61] Moreover, sometimes, adding a small amount (0.1%-1%) of acid or base additives may enhance the formation of protonated and deprotonated molecules, respectively. Among these additives, formic acid and ammonium hydroxide are very common. [61] It has also become clear that the analyte should be soluble in the localized liquid thin film (or simply in the spray solvent) to facilitate its transfer from the surface. [60] The differences in signal levels among different solvents appeared to be caused by two competing processes: dissolution and subsequent desorption of the analyte from the surface or dissolution and elution of analyte material away from the DESI plume before desorption could take place. [62] This elution versus desorption phenomenon makes solvent optimization a necessity for DESI-MS experiments. Δ^9-

THC has a tricyclic 21 carbon structure without nitrogen and with two chiral centers in trans-configuration. [63] Δ^9-THC is volatile viscous oil with high lipid solubility, low aqueous solubility, and a pKa of 10.6. [63] For this experiment, first, the extraction procedure was performed with different extraction solvents, and as a result, hexane has been chosen as the best solvent with the highest detected experimental THC in the spectra (Figure 2.1A).

Several solvent mixtures were prepared to assess their ionization efficiency with the THC compound in the extracted solution, in both polarities. Acetonitrile:methanol (8:2) with 1% NH_4OH shows the most efficient desorption or ionization by resulting in the highest signal intensity for the THC at *m/z* 313 in negative ion mode, $[M–H]^-$, compared with other solvents. The ammonium hydroxide has a crucial role in favoring the deprotonation of the THC compound by making the solvent more basic. Moreover, after performing MS/MS at *m/z* 313, the spectrum shows fragment pattern that is consistent with the literature by Ifa et al, confirming the presence of THC in our solution (Figure 2.1B). [64]

Next, for the serial dilution spots, multiple TLC developer mixtures were tested for the most efficient separation of different components. Hexane:ethylacetate (9:1) shows the best result with showing highest peak area for THC compound.

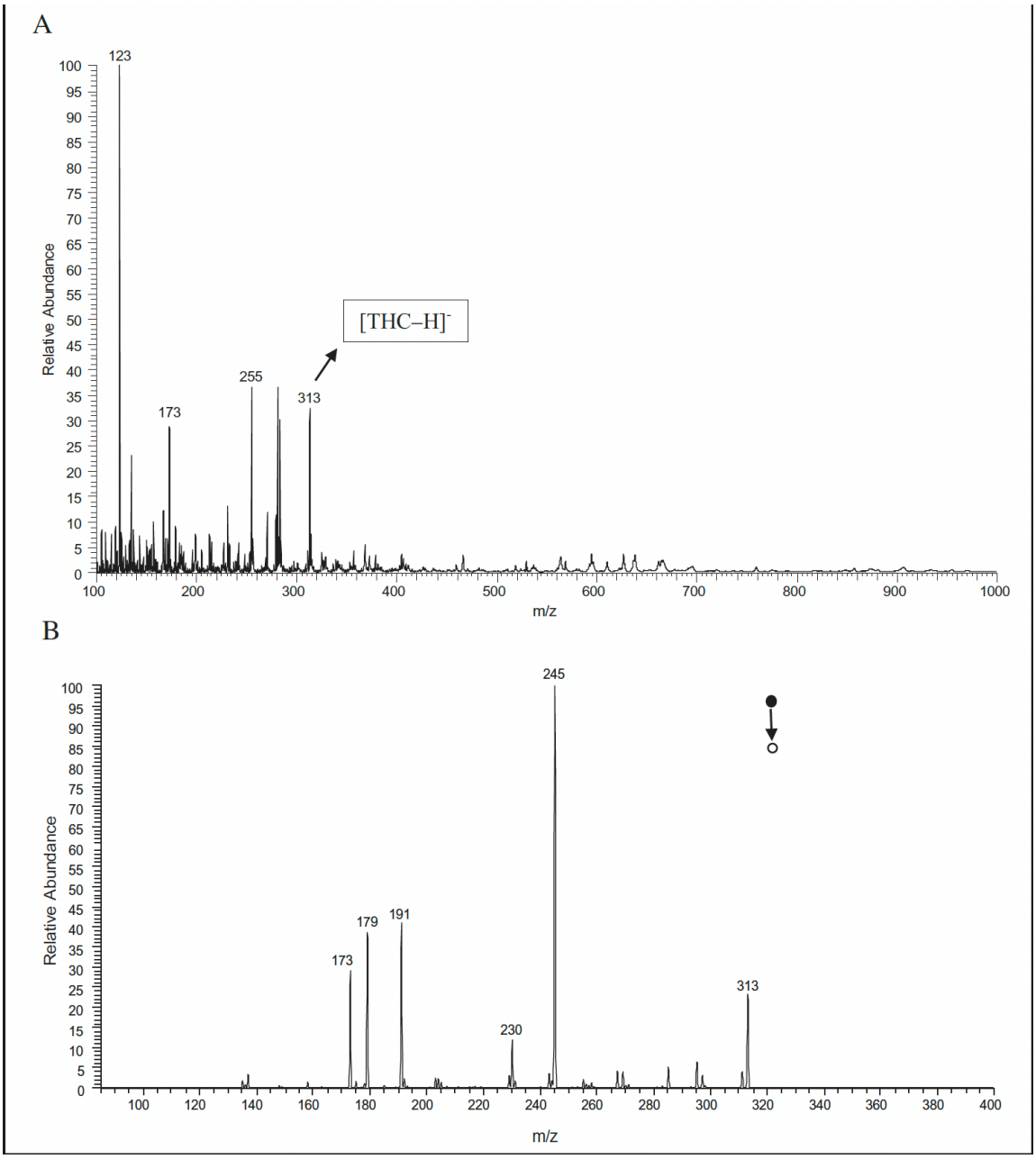

Figure 2.1. (A) Negative ion DESI mass spectrum of THC extract in hexane with acetonitrile:methanol (8:2) +1% NH_4OH spray solvent. (B) The tandem mass spectrum of THC which matches the literature by Ifa et al. [64]

2.4.4. Serial dilution experiments

For the quantitation purpose, appropriate standards and internal standards were required. Isotopically labeled THC-D_3 standard was added to the dilution series in known quantities. When a synthetic, stable isotope-labeled analyte is used as an internal standard, the concentration can be measured by the ratios of the signals from the labelled internal standard and the unlabeled standard.

The reason for this is the fact that these compounds have the same physico-chemical properties and differ only by mass, and by using them, we can correct for inefficiencies in the extraction process of analytes from complex matrices. Six dilution mixtures were prepared in the range of 20 to 80 µg/mL of THC standard, and a constant concentration of 50 µg/mL of THC-D_3 isotopically labelled internal standard (IS) was added to the series (Table 2.1). The reason for choosing this range was due to the theoretical calculation and estimation of THC concentration from the extraction, which is 52.94 µg/mL after dilution in 15 mL of ACN. The range was chosen in a way for the theoretical concentration and the IS to be in the middle of the curve.

The dilution mixtures of cannabinoid standards and IS were separated on a normal phase silica gel TLC plate and detected via DESI-MS in negative ion SIM scan mode.

The data shown in Figure 2.2 represent the calibration line-scanning mode of TLC-DESI-MS analysis for THC and THC-D_3, in negative ion SIM mode. Figure 2.2A and B show the DESI-MS extracted ion chromatograms of THC-D_3 and THC after using smoothing function of 15 points with Xcalibur software, respectively. Figure 2.2C is the total SIM mode scan range. As it is expected, Figure 2.2B represents more than one peak for the chosen range of *m/z* 313. This is due to the presence of other isomer cannabinoids for *m/z* 313, such as CBD and CBC in the extract, and their well separation on the TLC plate.

Table 2.1. Calibration curve for THC concentration determination

	Volume of Each Component for Making Serial Dilutions for the Total Volume of 100 µL			Area of S/Area of IS					
Standard THC Concentration, µg/mL	THC standard, µL	THC-D_3 IS, µL	Methanol Solvent, µL	Run 1	Run 2	Run 3	Average	Standard Deviation	Relative Standard Deviation
20	2	50	48	0.45	0.36	0.20	0.34	0.13	38%
30	3	50	47	0.53	0.51	0.54	0.53	0.02	4%
40	4	50	46	0.73	0.81	0.69	0.74	0.06	8%
50	5	50	45	0.89	0.83	0.81	0.84	0.04	5%
60	6	50	44	1.12	1.08	1.03	1.08	0.04	4%
80	8	50	42	1.26	1.31	1.50	1.36	0.13	10%
Extract	50-µL Extract (no standard)	50	0	1.04	1.09	1.04	1.06	0.03	3%

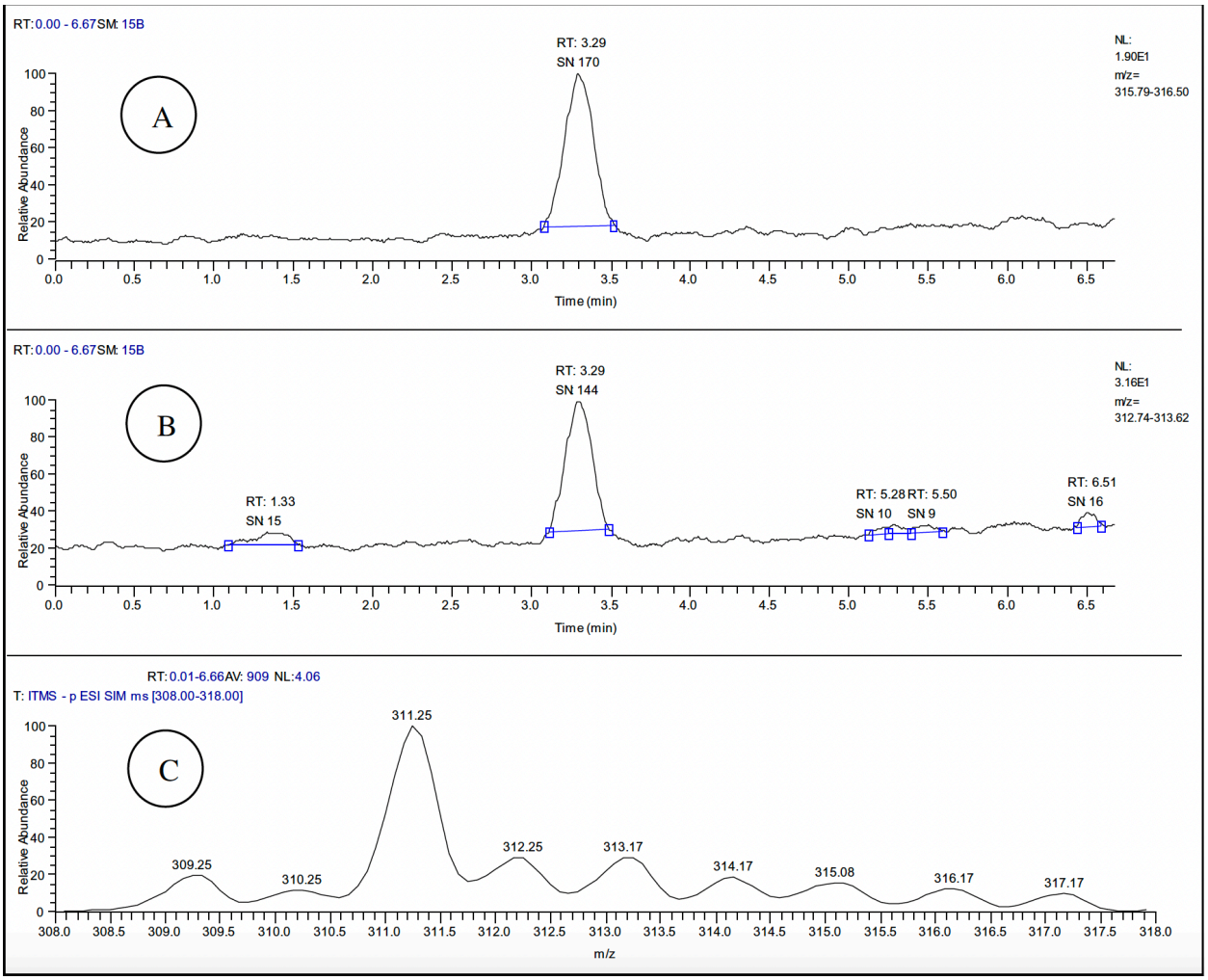

Figure 2.2. Line-scanning mode of TLC-DESI-MS analysis for the mixture of extracted THC and THC-D_3, in negative ion SIM mode using acetonitrile:methanol (8:2) +1% NH_4OH spray solvent, for quantitative analysis. (A) Ion chromatogram of THC-D_3 internal standard and (B) extracted THC from the chocolate, after using smoothing function of 15 points. (C) Total SIM mode scan range for the mixture of THC and THC-D_3.

2.4.5. Limit of detection and limit of quantification

The limits of detection and quantification for THC were in the range of 20 and 30 µg/mL, when experimenting 1.5 µL of extracted sample. The spots with 20 and 30 µg/mL diluted mixtures represent S/N of 2 to 4 and 8 to 15, respectively. For this reason, the 20-µg/mL concentration spots were removed from the average calibration curve in Figure 2.3.

Table 2.2. Summary of theoretical and calculated data for THC from the extract

	Run 1	Run 2	Run 3	Average curve
Measured chocolate, g	1.0058	1.0074	1.0078	1.0070
Theoretical concentration, µg/mL	53.2	53.3	53.3	53.3
Chocolate extract concentration, µg/mL	61.2	63.4	58.4	60.6 ± 1.1
Calibration curve R^2	0.97	0.97	0.98	0.99

2.4.6. Calibration curve resulting from TLC-DESI- MS

Figure 2.3 demonstrates the calibration curve resulting from the triplicate TLC-DESI-MS analysis of dilution series. For the quantitation purpose, the calibration curve of concentration range versus ratio of area of standard and IS was plotted. The concentration of extracted THC can be calculated from the equation of line of each graph. Table 2.2 represents calculated concentration of THC for runs 1, 2, and 3 obtained from individual and average runs.

The obtained data show a higher-than-expected values for concentration of THC in the extract solutions. It has been shown that cannabis samples of various types lose potency over time. [65] this fact is more pronounce in the conversion of THCA to THC by exposing to air, heat, and light. According to this, interday analysis of cannabis compounds might show measurably different results from each other. [65] The chocolate sample used for this experiment contains 47.00 mg of THCA, which is expected to be around 0.5 mg per 1 g of chocolate. According to this, in each extraction sample, we had a ratio of approximately 3:1 THC:THCA, which makes the higher concentration of THC in our result more explainable.

Interday and intraday precision and accuracy of quality control samples were calculated with the requirement that the mean of each concentration must be within 15% of the nominal value

and must have a precision not exceeding 15% CV. [57] Our mean value for the three runs is 60.6 ± 1.1 µg/mL and is within 15% of the nominal value of 53.3 µg/ mL, which is the mean of the theoretical values for three runs.

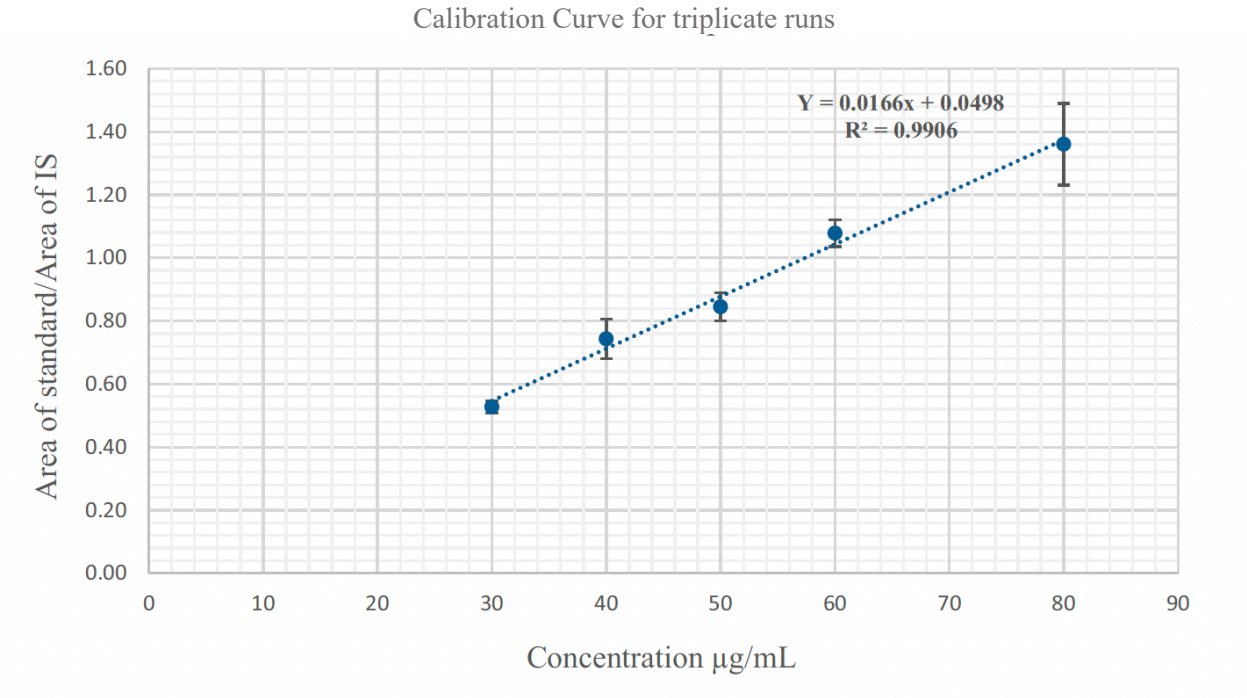

Figure 2.3. Average calibration curve from runs 1, 2, and 3 of the analysis.

2.5. Conclusion

DESI-MS allows the rapid and direct qualitative analysis of wide range of samples in their native environment, without any extraction, purification, and pretreatment, and under atmospheric pressure. The analyte of interest can be mass analyzed in a complex matrix such as chocolate by simply using the DESI-MS. Cannabis and cannabinoid detection is an interesting area of research nowadays, and many publications describe the usage of MS in this growing field. [48] [66] [67] [68] However, the quantitative analysis of cannabinoids from edible complex matrices with DESI-MS requires extractions, and it has not reported yet. Hence, the aim of our lab is to confirm the ability of DESI-MS towards this topic and elaborate techniques to advance this area of research.

A fast, reliable, and cost-effective analytical method has been developed and evaluated for the quantification of cannabinoid contents in cannabis-infused edibles. This method uses the advantages of QuEChERS method to remove the complex chocolate matrix and extract the cannabinoids in the organic solvent layer. The developed method has been successfully applied to the quantitation of THC cannabinoid from an edible chocolate.

For cannabinoid content analysis, the samples had cannabinoid content within ±15% of the stated value, where they were found under-labelled, which actually contained 13.7% more THC than stated. This fact can be due to the conversion of THCA, which is present in our extract in a fair amount, to THC by exposing to light, air, and heat.

The ambient technique of DESI-MS shows promises in accurate detection and measurement of smallest amount of sample, both quantitatively and qualitatively. One of the most important aspects of this work is that it can be applied to many vast and diverse cannabis related applications. It provides quantitative analysis of target composition for science and industry fields such as food, quality control, environmental, health- and safety-related material, forensics, medicinal, and pharmaceutical. We also believe that works and improvements into methods of detecting and quantifying cannabis will help law enforcement regulate its usage, and this particular analytical technique can be used for simple and legal defensible cannabis detection in contraband material; for instance, usage of this method as a detection technique in a mini and portable MS device [69] [70] [71] [72] [73] at airports, detection centers, correctional facilities, and roadside tests.

Chapter Three: Metabolomics Differences of Glycine max QTLs Resistant to Soybean Looper

Chapter 3 is a version of the published manuscript:

Yousefi-Taemeh, M., Lin, J., Ifa, D.R., Parrott, W., Kovinich, N. Metabolomics Differences of Glycine max QTLs Resistant to Soybean Looper. *Metabolites*. **2021**; 11 (10): 1-9.

3.1. Abstract

Quantitative trait loci (QTLs) E and M are major soybean alleles that confer resistance to leaf-chewing insects and are particularly effective in combination. Flavonoids and/or isoflavonoids are classes of plant secondary metabolites that previous studies agree are the causative agents of resistance of these QTLs. However, all previous studies have compared soybean genotypes that are of dissimilar genetic backgrounds, leaving it questionable what metabolites are a result of the QTL rather than the genetic background. Here, we conducted a non-targeted mass spectrometry approach without liquid chromatography to identify differences in metabolite levels among QTLs E, M, and both (EM) that were introgressed into the background of the susceptible variety Benning. Our results found that E and M mainly confer low-level, global differences in distinct sets of metabolites. The isoflavonoid daidzein was the only metabolite that demonstrated major increases, specifically in insect-treated M and EM. Interestingly, M confers increased daidzein levels in response to insect, whereas E restores M's depleted daidzein levels in the absence of insect. Since daidzein levels do not parallel levels of resistance, our data suggest a novel mechanism that the QTLs confer resistance to insects by mediating changes in hundreds of metabolites, which would be difficult for the insect to evolve tolerance. Collective global metabolite differences conferred by E and M might explain the increased resistance of EM.

3.2. Introduction

The use of crop protectants and fertilizers has helped maintain crop productivity, but these have also masked the fact that yield loss from insects continues to increase. [74] In the case of soybean, freshwater ecotoxicity has tripled, largely due to increased insecticide application, particularly ones that are more persistent in the soil and water. [75] Efforts to lower the cost of production, along with increased concerns over insecticide residues in the food chain and environment, underscore the need for insect-resistant crops. [76]

Soybean is one of the crops that is affected by defoliating insects, particularly in the Southeastern United States and in tropical South America. The use of soybean engineered with Bt (*Bacillus thuringiensis*) is a success story for plant resistance to insects. However, Bt is not

deployable in all areas and crops. [77] Case in point, soybean is a refuge for Bt corn and cotton in the United States, so Bt soybean cannot be commercialized in the USA without changes to Bt corn and cotton resistance management strategies. Thus, other sources of resistance are needed. Even in South America where Bt soybean is used [78], pyramiding other resistance genes with Bt is needed to obtain a more durable resistance.

Other resistance genes are available in the form of quantitative trait loci (QTLs) that confer resistance to defoliating insects in soybean. [79] Yet, almost nothing is known about the biochemical basis for such QTL-based resistance in soybean, or in most other crops. The first QTL was found on Linkage Group (LG) M (now chromosome 7) of a landrace, "Sodendaizu" (PI 229358). [80] [81] Since then, breeders have introgressed QTL-M (referred to henceforth as M) into diverse genetic backgrounds, showing its effectiveness is not genotype-dependent. [82] [83] Other groups have also mapped resistance to the same chromosomal region. [84] [85]

The second important QTL comes from LG E found in the landrace "Miyako White" (PI 227687) and is hence known as QTL-E (or E). [81] E is the same QTL initially identified by Terry et al. [86] To better study these QTLs and their interactions, they were bred into a set of near-isolines. [87] When tested under laboratory and field conditions, the near isoline containing both M and E shows agriculturally effective levels of resistance to a gamut of defoliating caterpillars. [87] Based on field trials, soybean without a resistance QTL reaches the economic threshold of 35% defoliation by eight days after caterpillars, which is when insecticide use would be warranted. This timeline also holds for the isoline carrying E by itself. The line carrying only M does not reach the economic threshold until the 10th day, while the line with both E and M takes 12.5 days to reach the threshold. [87] Nevertheless, despite 40 years of study, the chemical nature of this defoliator resistance remains an enigma.

Many of the original biochemical characterizations were done on soybean carrying E, with the resistance being attributed to various compounds at various times. Smith and Fischer determined that resistance was due to methanol-soluble compounds. [88] Glyceollins are isoflavonoid-derived phytoalexins that have well-established roles in protecting soybean from microbial pathogens. [89] [90] [91] Yet, Hart et al. ruled out glyceollins as a source of resistance

to leaf-chewing insects. [92] Caballero & Smith attributed resistance to coumestrol, phaseol, and afrormosin. [93] Sharma and Norris showed that a combination of daidzen, glyceollins, sojagol, and coumestrol, along with an unidentified compound, was involved in resistance. [94] In contrast, Liu et al. showed glyceollins, and not coumestrol, led to resistance. [95] [96] Alternatively, Piubelli et al. provided evidence that the resistance is due to rutin and genistin. [97] Hoffman-Campo et al. also implicated rutin in resistance. [98]

All of these studies implicate isoflavonoids and/or flavonoids as being responsible for the resistance of E, even if the results are contradictory and inconclusive when it comes to which particular compound confers resistance. Altogether, different results were obtained from a study based on transcripts upregulated upon insect feeding rather than on metabolomics. Wang et al. identified vegetative storage protein β (*GmVSPb*), NADPH:isoflavone reductase (*GmN:IFR*), and allene oxide synthase (*GmAOS1*) as genes providing resistance, but these do not co-map with any of the reported QTLs [99] [100], suggesting they are downstream in the response cascade.

The basis for M-mediated resistance is no clearer. Two genotypes containing M were found to both produce kaempferol 3-O-α-L-rhamnopyranosyl-(1→4)-[α-L-rhamnopyranosyl-(1→6)-β-D-galactopyranoside] and quercetin 3-O-β-D-glucopyranosyl-(1→2)-[α-L-rhamnopyranosyl-(1→6)-β-D-galactopyranoside]. In contrast, Zhao et al. associated the production of elevated genistein and glycitein with the increased resistance provided by M. [101] Recently, Gómez et al. found that compared with the control, a soybean cultivar with M had higher levels of the flavonoids kaempferol-3-O-L-rhamnopyranosyl-glucopyranoside, rutin (quercetin 3-O-rutinoside), quercetin-3,7-O-di-glucoside, quercetin-3-O-rhamnosylglycoside- 7-O-glucoside, quercetin-3-O-rhamnopyranosyl-glucopyranoside-rhamnopyranoside, and the isoflavonoids genistein-7-O-diglucosidedimalonyl, genistein-7-O-6-O-malonylglucoside, and daidzein 7-O-glucoside-malonate. [102] In a follow-up study, Gómez et al. isorhamnetin glycoconjugates in the resistant genotype, along with increased levels of proteinase inhibitors and flavonoids. [103]

All of these studies have been confounded by the use of different genotypic backgrounds for the QTLs being studied. Therefore, it has never been clear whether the presence of some compounds is simply due to the choice of genetic background, rather than being causative of

resistance. Thus, the goal of this work was to characterize metabolome differences of near isogenic lines containing QTLs E, M, or both (EM) that were introgressed into the background of the susceptible variety Benning in an effort to identify differences that are specifically a result of these QTLs. The use of near isogenic lines minimizes the effects of different genetic backgrounds and increases the chance that the observed effects are due to the QTLs.

3.3. Results

Mass spectrometric comparison of metabolites from soybean QTLs resistant to soybean looper

Principal component analysis (PCA) and orthogonal PLS-PA were unable to distinguish the genotypes or treatments based on the 13,950 unique peaks that were measured (Appendix Figure A.1). However, the genotypes were found to have significant differences based on their collective peak intensities (ANOVA, $p < 1.42 \times 10^{-11}$). Each insect-treated genotype was significantly different from all others (Tukey's post hoc, $p < 0.01$). Under mock treatment, all were significantly different except for QTL M compared to Benning.

Of the 13,950 unique peaks, 1521 and 957 peaks were significantly different (up- or down-accumulated) in at least one genotype compared to Benning upon insect and mock treatments, respectively (paired *t*-test, $p < 0.05$). EM demonstrated the greatest number of differences, with 1064 and 700 peaks different from those of Benning under insect and mock treatments, respectively (Figure 3.1). M had the second greatest number of differences, with 365 and 232 under insect and mock treatments. EM and M shared 39 differences under mock treatment and 15 in response to insect. In contrast, the number of peaks shared by EM and E increased from 20 to 43 in response to the insect treatment. A list of shared peaks is provided in (Appendix Table A.1).

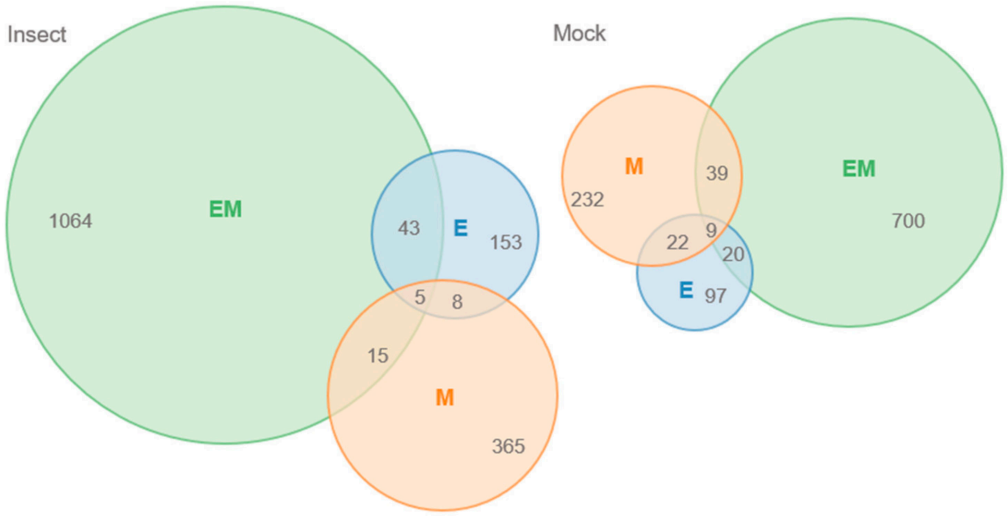

(**a**) (**b**)

Figure 3.1. Venn diagrams of the number of MS peaks from soybean QTLs that are significantly different in intensity from insect-susceptible parent Benning. (a) Treatment with soybean looper for 72 h. (b) No insect treatment.

A plot of those significantly different peaks revealed that relatively few (only 4.3% and 10.2% from insect- and mock-treated QTLs, respectively) differed in intensity by more than 1500 CPS compared to the peaks from Benning (Figure 3.2). Under insect treatment, only peaks corresponding to the isoflavonoid daidzein [*m/z* 277, $[M + Na]^+$] showed major increases compared to Benning (Figure 3.2a). This identity was confirmed by the spiking of samples with authentic standard. The elevated daidzein levels were found in EM and M, not in E. Under mock treatment, the most elevated peaks included an unknown at *m/z* 829, putative soyasaponin Ya (*m/z* 893), and soyasaponin Bd (*m/z* 978), which were most abundant in EM. Under mock treatment, most peaks that were shared by all three QTLs had reduced levels compared to those of Benning. These included the saponins ruscoponticoside C (*m/z* 707) and combreglucoside (*m/z* 664), an unknown compound at *m/z* 382, and the salicylate salicortin (*m/z* 226 $[M + H - 2H_2O]^+$). A subset of compounds that had major changes in intensity among the genotypes were selected for identification by MS/MS (Appendix Table A.2).

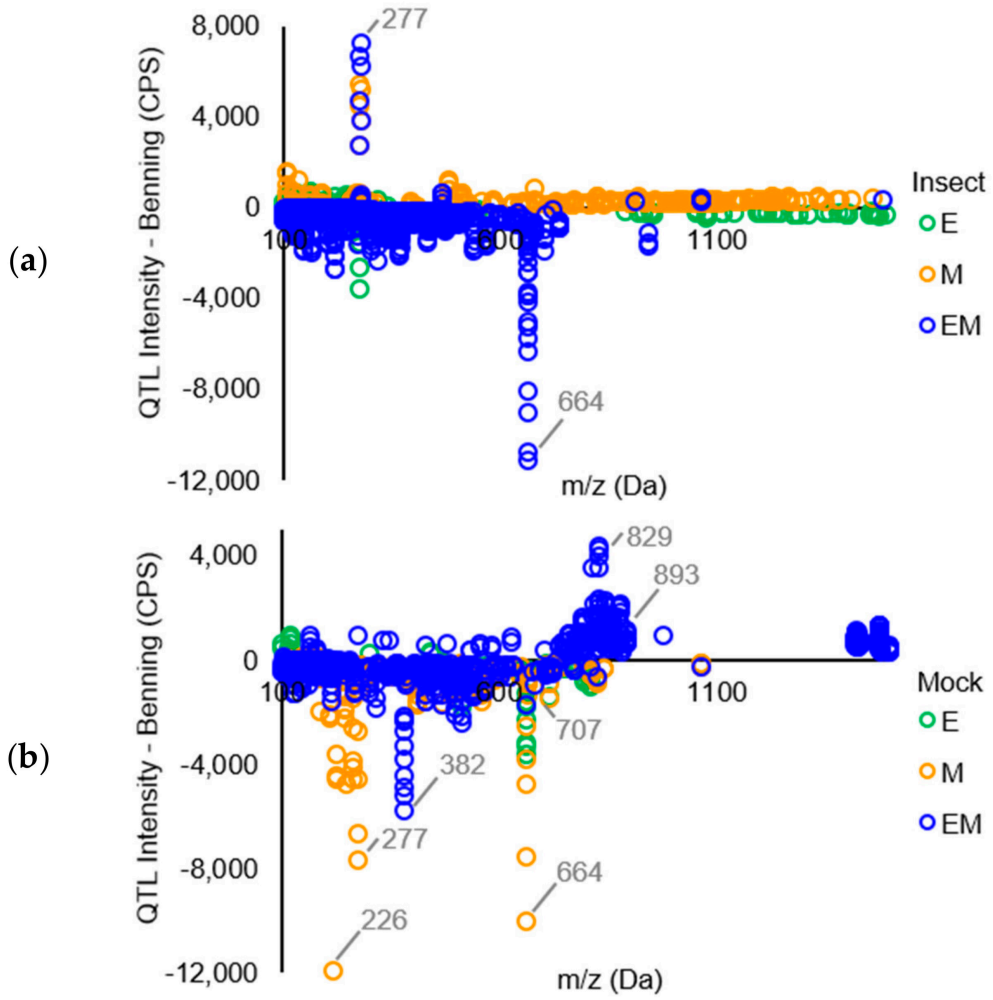

Figure 3.2. Comparison of average full scan mass spectra of soybean QTLs compared to Benning showing the increase or decrease of metabolites. Only mass spectra that were significantly different in intensity compared to Benning are shown. (a) Treatment with soybean looper for 72 h. (b) No insect treatment.

A graph of daidzein demonstrates that the levels decrease in Benning and E upon insect treatment. By contrast, levels are lower in mock M, but increase upon insect treatment. In EM, mock levels are similarly as high as Benning mock and do not decrease with insect treatment.

3.4. Discussion

The soybean QTLs E and M provide notable levels of resistance to leaf-chewing insects. [81] [87] [104] The amounts of flavonoids and isoflavones are known to increase in soybean leaves in response to defoliating insects. [105] While previous studies agree that flavonoid and/or

isoflavonoid metabolites are the causative agents of resistance, studies have always been on soybean genotypes that are of dissimilar genetic backgrounds. Thus, it has never been clear whether the presence of particular metabolites has been due to genetic background or specifically to the QTLs that provide resistance. Here, we compared the metabolite profiles of QTLs E, M, and both (EM) that have been introgressed into the background of the susceptible genotype Benning. Our non-targeted MS analysis generally found global, relatively low-level changes in metabolite composition compared to Benning whether the isolines were treated with insects or not (Figures 3.1 and 3.2). Thus, resistance could be due to differences in the abundance of a wide variety of metabolites, rather than the overaccumulation of just one or a few compounds, as was previously suggested. In this context, the enhanced resistance of EM over individual QTLs could result from the distinct sets of metabolites contributed by E and M.

Daidzein has been shown to be toxic to insects. [106] [107] [108] and was previously associated with insect resistance. [106] [107] [109] The importance of daidzein as a pesticide lies in its potential as an active compound in soybean chemical defenses against insect pests, particularly those from the Lepidoptera. Studies have shown that daidzein, along with other isoflavones like daidzin and formononetin, accumulates in soybean leaves in response to feeding by insects like Spodoptera litura. These isoflavones have been found to have antifeedant and/or antibiotic effects against pests like *Trichoplusia ni*, and in some cases, daidzein has been more effective than other compounds like glyceollins. Furthermore, analysis of insect frass indicated that daidzein remains intact and is not metabolized by the insect, while other isoflavones undergo processing in the insect gut. In addition, classical mosquito larval toxicity bioassays have identified daidzein and its derivatives as insecticidal. These findings support the notion that daidzein and other isoflavones play a significant role as active components in soybean's chemical defenses against insects. While the importance of daidzein as a pesticide is evident from these studies, it is crucial to consider that different compounds may have varying toxicity levels at different concentrations. Overall, daidzein's insecticidal potential is a valuable asset for the soybean industry in managing insect pests and ensuring crop protection. [107]

Since daidzein is the only metabolite that demonstrates major increases in M and EM compared to Benning (Figure 3.2), we focused on it for a more in-depth analysis. Benning

demonstrates relatively high levels of daidzein under mock treatment, yet levels exhibit major decreases upon insect treatment (Figure 3.3). The same was observed for E. Thus, in Benning and E, soybean looper may be able to suppress daidzein biosynthesis, enhance its degradation, and/or its conversion into glycosylated derivatives.

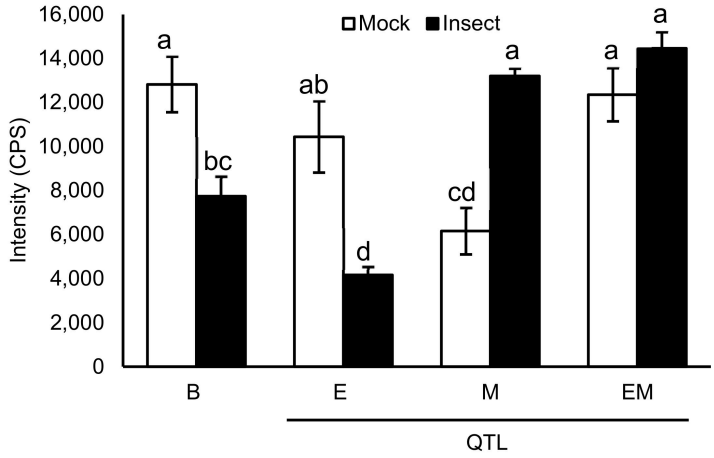

Figure 3.3. Average daidzein levels in mock and insect treated leaves of soybean QTLs and the insect-susceptible parent Benning. Different letters show significant differences by single factor ANOVA, Tukey post hoc test ($p < 0.05$, = 0.05). Error bars indicate SE (n = 3 biological replicates).

M has lower levels of daidzein compared to Benning under mock treatment. Yet, in contrast to Benning and E, daidzein levels increase upon insect treatment rather than decrease (Figure 3.3). This opposite response may suggest a signaling role for M, where M counteracts the suppressive mechanism of soybean looper seen in Benning and E.

E has lower levels of daidzein under mock and insect treatments, suggesting that the mechanism of resistance is independent of daidzein. Consistent with this, soybean varieties Enrei and Tamahomare are susceptible genotypes that have high levels of daidzein. [110] [111] E is a 2-Mb region on chromosome 15 that often co-segregates with the *Pb* locus for sharp-tipped trichomes (Figure 3.4). [112] Although there are earlier reports on the effect of pubescence traits on soybean resistance to insect [113] [114], Hulburt was the first to report that a sharp-trichome locus co-localizes with E. [115] Most soybean cultivars have blunt trichomes (*pb*) while the wild soybean, *Glycine soja*, almost universally has sharp trichomes. [116] Since some *G. soja* lines are more susceptible to defoliating insects than most *G. max* lines, it seems unlikely that the trichome tip alone governs resistance, despite the genomic collocation of the two traits. [112] Lambert and

Kilen showed that PI 227687's resistance is graft-transmissible, confirming that resistance in E is tissue-mobile metabolites or macromolecules. [117]

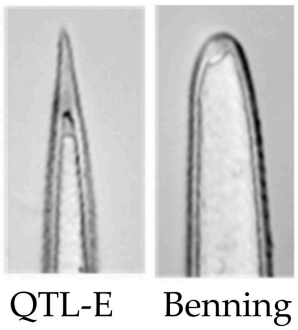

Figure 3.4. Trichomes of QTL E in the Benning background have sharp tip shape, whereas insect-susceptible Benning does not.

3.5. Materials and Methods

3.5.1. Chemicals

Methanol (HPLC grade, ≥99.9% purity) and water (HPLC grade) were purchased from Sigma-Aldrich. (St. Louis, MO, USA). Daidzein was obtained from Indofine Chemical Company (Hillsborough, NJ, USA).

3.5.2. Plant growth conditions

Plants of Benning, Benning M, Benning E, and Benning EM [87] were grown until the V5 growth stage [118] at 27 ^{O}C in an insecticide-free greenhouse under 16 h:8 h light:dark to prevent premature flowering. Each plant was grown in a 0.95 L styrofoam cup with three drainage holes punched in the bottom and filled with Fafard 3B potting mix (Conrad Fafard, Agawam, MA, USA). The pots were fertilized with approximately 75 Osmocote® 15-9-12 pellets (Scotts Miracle-Gro, Marysville, OH, USA) per cup at the V2 growth stage. At the V5 stage, three soybean looper neonate larvae were applied to each plant.

3.5.3. Insect treatments

The experimental design was a randomized complete block design with ten blocks. Each block consisted of the four genotypes under two treatments: thirty neonate soybean looper, *Chrysodeixis includens*, larvae (Benzon Research Inc., Carlisle, PA, USA) were added to one treatment, while the control treatment received no insects. At the 72-h timepoint after infestation, the first fully expanded trifoliolate leaf was collected from each plant. Leaves were flash frozen in liquid nitrogen and stored at -80 ^{O}C. Frozen leaves were homogenized by crushing and subsamples of the crushed, frozen leaves were lyophilized and ground to a powder using a bead mill.

3.5.4. Extraction and sample preparations

Fresh and freeze-dried leaf extracts were prepared and normalized by adding 25 μL of extraction solution (methanol and 80% methanol, respectively) per mg of tissue sample. The mixtures were shaken overnight at 100 rpm and then centrifuged at 12,000 x g for 30 min. The supernatants were transferred into new vials following another centrifugation at the speed of 12,000 x g for 30 min. The sample mixtures were passed through 0.2 μm filter and the extracted samples were kept in Eppendorf vials for further analyses.

Prior to injections in the ESI-MS system, a (1:25) dilution step was performed in acidic solution (80%methanol containing 1% formic acid), or basic solution (80%methanol containing 1% ammonium hydroxide) for positive and negative ion mode analyses, respectively.

The extracts of fresh and freeze-dried samples were analyzed in both positive and negative electrospray ionization (ESI) modes. As a result, the freeze-dried leaf extracts showed greater intensities for most peaks and was chosen over fresh samples for the next series of experiment. Next, samples previously discussed in Sections 3.5.2 and 3.5.3 were provided in biological triplicate (4 genotypes x 2 treatments x 3 replicates). For the positive and the negative ion mode analyses, samples were diluted to a 1:10 ratio, in acidic and basic solutions as explained before.

3.5.5. Metabolite analysis by ESI-MS

Direct infusion of diluted samples was performed in an LTQ linear ion trap mass spectrometer (Thermo Fisher Scientific, San Jose, CA, USA), which is controlled by Xcalibur 2.0 software and is equipped with an ESI ion source. The parameters for ESI-MS analysis were chosen

as follows: Nitrogen at 100 psi was used as the nebulizing gas for all the experiments. The flow rate, maximum ion trap injection time, and microscans were 10 μL min^{-1}, 20 ms, and 3 microscans per spectrum, respectively. The analyses were performed in full scan mode, in the range of *m/z* 150 to 1500. For the negative ion mode analyses, the ESI source parameters were as follows: spray voltage: -5 kV; capillary temperature: 250 ^{O}C, capillary voltage: -10 V, tube lens: -150 V, and sheath gas flow rate: 30. For the positive ion polarity analyses, the ESI source parameters were as follows: spray voltage: 5.5 kV; capillary temperature: 250 ^{O}C, capillary voltage: 30 V, tube lens: 150 V, and sheath gas flow rate: 10.

3.5.6. ESI-MS/MS and database search for putative compound identification

ESI-MS/MS analyses of the most significant signals among different genotypes and treatments were performed by the same MS instrumentation described in the previous section, to intentionally fragment molecules into smaller parts for structure elucidation. Comparison of unknown compound MS/MS spectra against databases containing reference or predicted MS/MS spectra, is a widely used method for putative metabolite identification. [119]

Each database employed in our study (Metlin [120], MassBank of North America—MoNA, https://mona.fiehnlab.ucdavis.edu (accessed on 21 June 2021), NIST-MS/MS library http://chemdata.nist.gov/mass-spc/msms-search/ (accessed on 21 June 2021) [121], and Saponins Mass Spectrometry Database [122]) has different mathematical/statistical approaches to rank the most probable compounds. The top ten compounds ranked were then manually inspected to identify the compound with highest number of fragment matches. In some cases, the compounds with higher scores (top rank) did not correspond to meaningful molecules, for instance they were high molecular weight compounds with multiple charges.

As a result of this search, lists of putative compound identification in positive and negative ion modes were created. The compounds were classified according to the confidence level as proposed by [123] (from level 0, unambiguous identification to level 4 unknown structure). Most of our findings reported in Appendix Table A.2 are in level 3 (most likely structure).

3.6. Conclusions

Two major QTLs have been identified that have alleles that make large contributions to resistance to defoliating insects in soybean. The combination of these alleles is especially effective at producing resistance, and now has been shown to result in hundreds of metabolites that are upregulated in response to insect feeding.

How these QTLs lead to production of multiple metabolites is unknown. What is clear now is that searching for a single or few insecticidal compounds synthesized by these QTLs may not provide insights into the source of insect resistance; instead, these results reveal that defoliator resistance may be due to a cocktail of hundreds of metabolites.

From a crop perspective, such resistance is desirable, as it is difficult for defoliators to develop simultaneous resistance to hundreds of different compounds. The ability to obtain multiple resistance factors from just two loci is attractive from a breeding perspective due to its simplicity. As more of the genes involved and their associated compounds are identified, it may be possible to fine-tune the resistance in soybean and use comparative genomics to create resistance in other legumes.

Chapter Four: Sublimation Application of 5-chloro-2-mercaptobenzothiazole (CMBT) Matrix for MALDI Mass Spectrometry Imaging of Mouse Kidney

Chapter 4 is a version of the published manuscript:

Yousefi-Taemeh, M., Duli, E., Dabija, L.G., Lemaire, M., Ifa, D.R. Sublimation application of 5-chloro-2-mercaptobenzothiazole (CMBT) matrix for MALDI mass spectrometry imaging of mouse kidney. *Rapid Commun Mass Spectrom*. **2023**. doi:10.1002/rcm.9594. **In press.**

4.1. Abstract

Sublimation is a solvent-free technique used to apply a uniform matrix coating over a large sample plate, improving the matrix's purity and enhancing the analyte signal. Although the 5-chloro-2- mercaptobenzothiazole (CMBT) matrix was introduced years ago, there are no reports of its application via sublimation. We investigated the experimental parameters that are optimal for CMBT matrix sublimation on mouse kidney samples. We also evaluated the stability of the sublimed CMBT matrix under a vacuum environment. Using kidneys samples prepared with a sublimated CMBT matrix, we conducted MALDI- MSI analysis of specific phospholipids: (phosphatidylcholine (PC) and phosphatidylglycerol (PG) in the positive ion mode and phosphatidylinositol (PI) in the negative ion mode. We also explored various spatial resolutions (50, 20, and 10 μm) and performed sequential MALDI-H&E staining. The CMBT matrix was applied to kidney samples using a sublimation apparatus connected to a vacuum pump to achieve a pressure of 0.05 Torr. The matrix was then subjected to different temperatures and sublimation times to determine the optimal conditions for matrix application. Subsequently, a Q-Exactive mass spectrometer equipped with a Spectroglyph MALDI ion source was employed for MALDI-MSI experiments. Standard protocols were followed for H&E staining after MALDI analysis. A matrix thickness of 0.15 mg/cm2 yielded high-quality images. The sublimated matrix exhibited minimal loss after approximately 20 hours of exposure to a vacuum of 7 Torr, indicating its stability under these conditions. Ion images were successfully obtained at spatial resolutions of 50, 20, and 10 μm. Furthermore, orthogonal histological information was obtained through sequential MALDI-H&E staining. We demonstrate that samples prepared for MALDI-MSI using sublimation to apply the CMBT matrix yield high-quality mass spectrometric images of mouse kidney sections. We also provided data on the impact of various experimental parameters on image quality (e.g., temperature, time, matrix thickness, and spatial resolution).

4.2. Introduction

4.2.1. MALDI imaging and matrix

Mass spectrometry imaging (MSI) techniques are classified based on how ions are generated from the sample. One approach is matrix-assisted laser desorption/ionization (MALDI)

mass spectrometry imaging (MSI): it uses laser irradiation to generate ions from discrete x and y locations, referred to as pixels, on a sample surface. [14] [15] MALDI-MSI is a powerful tool to determine the distribution of multiple compounds in a single measurement. Indeed, it can merge the mass spectrometer's *m/z* measurements with a surface sampling process that reveals the spatial distribution and identity of chemicals (when used in parallel with other techniques such as tandem mass spectrometry). [15] Because it allows for analyses of complex mixtures ranging from small drugs to large proteins, this technique has broad applicability to various fields, including proteomic studies, small molecule imaging, drug metabolism, disease pathology, synthetic polymers, and more. [15] [25]

Small organic compounds are used as matrices in MALDI-MSI experiments to assist with analyte desorption and ionization. [14] Several candidate compounds were studied since the introduction of MALDI-MSI. [25] Selecting the most optimal matrix is crucial when analyzing different compounds with MALDI-MSI. [25] Factors that should be considered include reproducibility, sensitivity, resolution over a wide mass range, and high signal intensity. [25]

Improving the resolution of images generated by MALDI-MSI is critical to gain novel biological insights. [27] Several parameters can influence the image resolution obtained with MALDI-MSI. These include tissue section preparation, matrix uniformity, matrix crystal size, laser spot size, and unwanted analyte delocalization during matrix deposition using matrix solutions. [27] The latter is particularly relevant when performing MALDI-MSI for lipids because of their low molecular weights and high solubility in organic solvents that are used to dissolve matrices.

Various matrix application methods are described for MALDI-MSI, such as micro-spotter, electrospray deposition, hand-held aerosol sprayers, or air brushers. [27] [28] [29] However, these methods all require dissolving the matrix in a water/organic solvent mixture, with the size of the droplets affecting the maximum achievable spatial resolution. [15] [27] Enhanced images may thus be generated with an approach that produces maximum matrix coverage of the sample without delocalizing the analyte. [15] Therefore, applying the matrix compound to the sample surface is critical to determine the spatial resolution, number, and intensity of ions detected. [15]

Automated sprayers are used to minimize operator-dependent variability in matrix crystal deposition. However, this approach requires multiple overlapping passes when applying the matrix to areas larger than the spray diameter, which may introduce another source of variation in ion intensity. [15] Uneven matrix crystal deposition can also compromise the detection sensitivity of the experiment. [30] To address these challenges, Hankin and colleagues introduced a solvent-free matrix deposition method that is inspired by the sublimation technique used by chemists. [27] It results in a uniform layer of matrix over a large sample plate, forms fine microcrystals, and increases the matrix's purity and the analyte signal; importantly, this method minimizes analyte delocalization during matrix application since it does not use solvents. [27]

4.2.2. CMBT matrix

The 5-chloro-2-mercaptobenzothiazole (CMBT) is a derivative of 2-mercaptobenzothiazole (MBT). It was first introduced as a new matrix for MALDI-MS at 337 nm laser radiation by Xu et al. in 1997. [124] They demonstrated that CMBT is suitable for analyzing a wide range of analytes, including peptides, muropeptides, low-mass proteins, glycolipids, oligosaccharides, and synthetic polymers. [124]

CMBT matrix were subsequently investigated when measuring various analytes. For example, CMBT has shown to be an effective matrix for the desorption and ionization of peptides and low- mass proteins, producing strong and stable signals for protonated analytes. [124] In contrast, protonated molecules are rarely detected when studying carbohydrates using CBMT, and cation adducts are abundant. [124] CMBT was successfully used as a cationizing matrix for the analysis of carbohydrates, even at low sample loading, indicating a remarkable sensitivity. [124]

CMBT has also been proposed to be effective for analyzing complex carbohydrates such as muropeptides, a structural component of the bacterial cell walls derived from peptidoglycan. [124] [125] The positive and negative ion polarities showed $[M+Na]^+$ and $[M-H]^-$ ions as the dominant species, respectively. [125] Yu et. al. tried various matrix preparation methods for analyzing intact glycoproteins and oligosaccharides, and the best results were achieved by depositing a small volume of CMBT as the first layer, followed by 2,5-dihydroxybenzoic acid (DHB) as a binary matrix system. [30]

Since the introduction of the CMBT matrix for MALDI-MS, many groups described matrix coating that require dissolution in a solvent mixture (e.g., CMBT in a mixture of ethanol:tetrahydrofuran:water (1:1:1) to make a solution of 10 g/L). [25] [124] The matrix mixture is then used either as a layer underneath other matrices, or it is mixed with analyte solution (that is, the matrix is co-crystalized with the analyte solution). [25] In another study, CMBT was dissolved in acetone/double distilled water (9:1) and the matrix solution was applied on the sample surface by a robotic aerosol sprayer. [20] In addition, CMBT was used in a study of gram-positive bacteria using MALDI-MS. [126] The matrix solution was deposited onto the cells after mixing in a solution of water:acetonitrile:methanol (1:1:1) containing 0.1% (v/v) formic acid. [126]

The application of matrix using robotic aerosol sprayers can affect adduct formation, which is caused by the presence of non-volatile salts introduced during the matrix application process. However, employing a sublimation method to apply the matrix can mitigate the formation of potassiated and sodiated adducts in the positive ion mode. [20]

This paper introduces the use of sublimation when applying a CMBT matrix for MALDI-MSI analysis. The impact of different temperatures and exposure times were explored to determine the optimal thickness of the matrix. The vacuum stability of the sublimated CMBT matrix was evaluated after 20 hours of exposure to the vacuum environment. This is important because the matrix layer must remain stable for extended acquisition periods to ensure signal integrity and prevent signal loss or variation during the imaging experiments. [20] [127] Ion images were acquired in the positive and negative ion modes to demonstrate the CMBT matrix performance after sublimation. Reproducibility of the method was assessed by analyzing samples in triplicates. Spatial resolution of MALDI-MSI of the sublimated CMBT matrix was examined at 50, 20 and 10 μm. Finally, we also examine if hematoxylin and eosin (H&E) staining of the same tissue section could be done reliably after removing the CMBT matrix once the MALDI-MSI analyses were done.

4.3. Materials and methods

4.3.1. Materials

The matrix, 5-Chloro-2-mercaptobenzothiazole (CMBT), was purchased from Sigma Aldrich (St. Louis, MO, USA). Indium tin oxide (ITO) coated slides were purchased from Delta Technologies (Loveland, CO, USA). HPLC-grade reagents were purchased from Sigma-Aldrich (Oakville, ON, Canada). Kidney samples were provided by the University of Toronto, Ontario, Canada. Mouse kidneys (n = 3 animals) were frozen and stored at a temperature of -80 °C until required for sectioning. Thin tissue sections (20 μm) were sliced using a Shandon Cryotome device, and thaw- mounted onto indium tin oxide slides (100Ω/m^2), for subsequent MALDI imaging analyses.

4.3.2. Matrix depositions

The ITO-coated glass slides containing sample sections were removed from the freezer and subjected to a drying process in a vacuum desiccator for 30 minutes. The matrix was then applied using a sublimation apparatus with a sublimation chamber, as depicted in Appendix Figure B.1. [27] [128] [129] The glass slide carrying the sample was attached to the flat-bottom condenser, which functioned as the sample holder, using copper tape to ensure consistent heat transfer. Approximately 300 mg of matrix powder was added to the matrix chamber, and the sample holder and the matrix chamber were assembled with an O-ring seal. The matrix powders in the chamber were located at a distance of 2 cm from the sample surface. The entire system was then connected to a vacuum pump. Once the vacuum pressure in the chamber reached 0.05 Torr, the condenser was filled with ice. The chamber was then submerged in heated oil, and the time was recorded. Subsequently, the matrix was heated, sublimed, and deposited onto the sample. After a specific time (between 1 to 10 minutes, as presented in Appendix Table B.1), the chamber was removed from the hot oil while still under a vacuum. After two additional minutes, the system was brought to ambient pressure, and the glass slide containing the sample was cautiously removed from the flat-bottom condenser.

4.3.3. MALDI analysis

The MALDI-MSI experiments were conducted using a Q-Exactive mass spectrometer (Thermo Fisher Scientific, San Jose, CA, USA) equipped with a Spectroglyph MALDI ion source (Spectroglyph LLC, Kennewick, WA, USA). All data were collected with a nominal mass resolution setting of 70,000 at *m/z* 400, a maximum injection time of 200 ms, and *m/z* ranges of 250–1,500 and 100-1,000 for the negative and positive ion polarities, respectively. Biological triplicate images were obtained at a spatial resolution of 50 μm in the positive and negative ion modes. Analytical triplicate images were collected at a spatial resolution of 20 and 10 μm in the negative ion mode. The laser (Nd:YLF, 349 nm) was employed to analyze samples at 20 and 50 μm spatial resolution at a repetition rate of 300 Hz and pulse energies of 7.5 μJ. An average of 60 shots per pixel were delivered with a measured laser spot diameter of 15 μm. For image analysis with 10 μm spatial resolution, the laser spot diameter was reduced to approximately 6.5 μm (Appendix Figure B.2). The laser was operated at a repetition rate of 500 Hz with pulse energies of 30 μJ, and an average of 100 laser shots per pixel were used. Ion images were generated using ImageInsight software (version: 0.1.0.1361, Spectroglyph LLC, WA).

4.3.4. Histochemistry and microscopy

To prepare the kidney tissue section for subsequent staining, the sublimated CMBT matrix was removed from the kidney tissue section by washing the slide with 95% ethanol for 30 seconds. The tissue section was then subjected to a standard hematoxylin and eosin (H&E) staining protocol [130], and the resulting H&E optical images of the tissue were recorded using an Omano microscope. Scanning electron microscopy was performed on the matrix coating using a Thermofisher Quanta 3D electron microscopy.

4.4. Results and Discussion

Sublimation is a physical process that involves the direct transition of a substance from the solid to the gas phase. The rate of sublimation can be increased by heat and reduced pressure. [27] Applying matrix by sublimation offers several advantages, particularly for compounds such as lipids that have partial to full solubility in common solvents used in matrix application. [27] Unlike solvent-based methods, sublimation is solvent-free, resulting in greater reproducibility and lower

costs. Additionally, sublimation generates high purity matrix coverage, which minimizes analyte delocalization due to solvent spraying. [27] The microcrystalline and highly pure nature of the coated matrix further enhances MALDI image processing. [27] Although sublimation has been previously reported as a method of matrix deposition for various matrices, it has not been used with the CMBT matrix. Therefore, this study focuses on investigating the experimental parameters of matrix sublimation for various coating thicknesses and examining the vacuum stability of the sublimated CMBT matrix under a mass spectrometry vacuum environment.

In MALDI-MSI, the choice of matrix and its optimal application conditions are empirical procedures. [25] For satisfactory MALDI-MSI performance, the amount of deposited matrix must be optimized. [127] The optimal matrix coating should be sufficiently thick to yield abundant ions following laser irradiation but thin enough to prevent suppression of analyte signals due to high-intensity signals from the matrix compound. [27]

4.4.1. Optimization of matrix coating

The matrix was applied onto tissue sections via sublimation using a custom-built sublimation apparatus (see Appendix Figure B.1). Approximately 300 mg of CMBT matrix were used at different temperatures and periods to achieve various coating thicknesses under a fixed vacuum pressure. The amount of sublimated matrix per unit area was calculated by measuring the density (mg/cm^2) differences before and after matrix coating. [20] The CMBT matrix was sublimed under a vacuum pressure of 0.05 Torr at temperatures ranging from 160 to 180 °C without decomposition, with parameters shown in Appendix Table B.1. The negative ion mode MALDI-MSI of the middle part of mouse kidney coronal sections using four different thicknesses (mg/cm^2) of CMBT matrix is illustrated in Appendix Figure B.3, with details in Appendix Table B.1. The results showed that the *m/z* images obtained by CMBT matrix thicknesses of 0.9 and 1.8 mg/cm^2 were not able to show distinguishable features and good- quality images due to excessive matrix coating, whereas images obtained by less matrix coating (0.15 and 0.4 mg/cm^2) showed more features and better image quality. Coronal mouse kidney sections (20 μm) were coated with CMBT matrix using the sublimation method described and imaged in both polarities in triplicate. The parameters of 0.05 Torr pressure, 165 °C temperature, 1.5 minutes, and matrix thickness density of around 0.15 mg/cm^2 were chosen for these analyses.

4.4.2. Vacuum stability and homogeneity

Matrix's vacuum stability (low volatility) is a critical requirement for its use in vacuum MALDI- MSI experimentation, which may require lengthy acquisition times (hours). [20] [127] Maintaining the stability of the matrix layer is essential to preserve sample integrity and prevent signal loss or variation during imaging experiments. [20] [127] In this study, the vacuum stability of the CMBT matrix was evaluated by quantifying the amount of matrix loss after 20 hours of exposure to a vacuum environment of 7 Torr.

To assess the vacuum stability of the CMBT matrix, an ITO slide coated with a homogeneous layer of matrix (0.1511 mg/cm^2) via sublimation was introduced to the vacuum environment. After 20 hours of exposure, the amount of matrix coating was measured to be 0.1508 mg/cm^2, and the difference was calculated as "matrix loss". The sublimed CMBT matrix was found to exhibit negligible matrix loss after around 20 hours of exposure to a vacuum of 7 Torr, indicating its vacuum stability.

Furthermore, microscopic images of the matrix layer were obtained before and after introducing the sample slide coated with the CMBT matrix to the vacuum environment for MALDI-MSI analysis. Figure 4.1 shows a coronal section (20 μm thickness) of a mouse kidney coated with CMBT matrix (0.1511 mg/cm^2 thickness) by sublimation application. The microscopic inspection of the CMBT layer on the sample slide surface after matrix sublimation revealed a homogenous crystalline and high sample surface coverage with a uniform layer of the sublimed matrix over the entire sample and ITO slide area. The post-imaging matrix layer also showed no signs of the matrix falling off or cracking of the matrix layer after the laser irradiations hit it. These findings suggest that the sublimed CMBT matrix meets the critical requirement of vacuum stability for use in vacuum MALDI-MSI experimentation, and sublimation may be a promising application method for this matrix candidate for further studies.

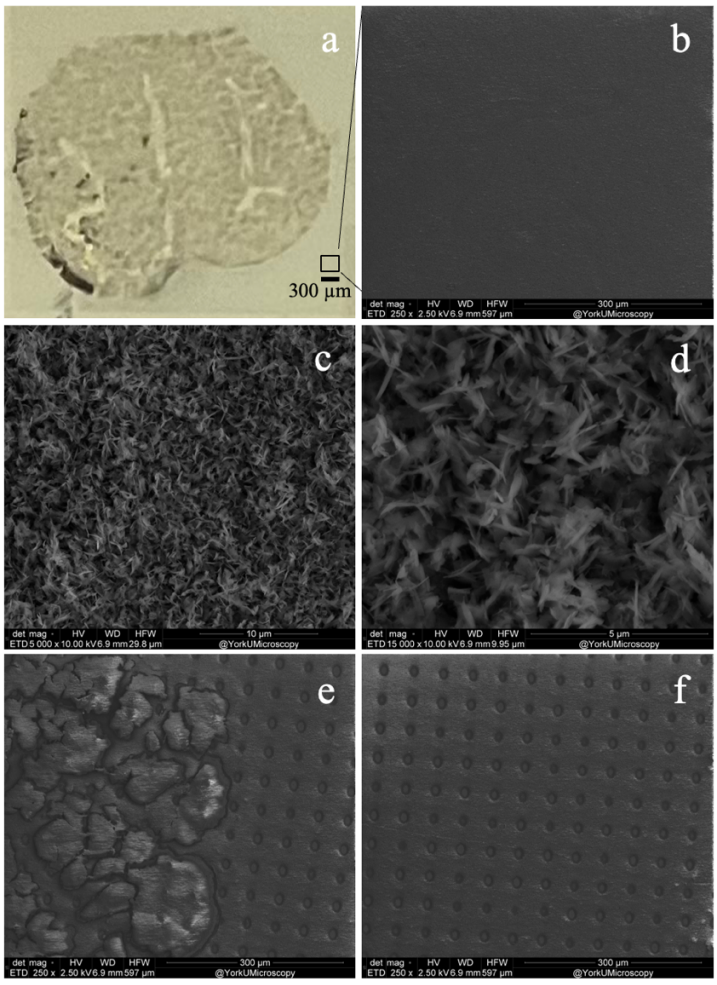

Figure 4.1. Microscopic images of a coronal section (20 µm thickness) of a mouse kidney before and after MALDI-MSI. The kidney tissue was coated with CMBT matrix using sublimation application, resulting in a thickness of 0.1511 mg/cm^2. (a) presents a photograph of the kidney tissue coated with CMBT matrix by sublimation. (b), (c), and (d) display Scanning Electron Microscopy images of the CMBT crystals that were deposited onto the ITO glass slide containing the kidney tissue section. These images show the matrix coating at magnifications of 250x, 5000x, and 15000x, respectively, before irradiation by laser for MALDI-MSI analysis. (e) and (f) show Scanning Electron Microscopy images of the ITO slide containing the kidney tissue section and sublimated CMBT matrix after lase irradiation during MALDI-MSI experimentation. Each spot represents an average of 60 laser shots on the sample covered with the matrix layer, with a spatial resolution of 50 µm.

4.4.3. Phospholipid identification

The present study investigated the spatial distribution of various classes of lipids in mouse kidneys using sublimated CMBT matrix for MALDI-MSI in the positive and negative ion modes. The ion images were created according to the mass-to-charge ratio (*m/z*) of compounds previously

described in the literature. [20] [131] [132] Table 4.1 outlines the tentative identification of each compound, the adduct type, and the parts per million error for lipids imaged in both ion polarities.

Various lipid classes, including phosphatidylcholine (PC) and phosphatidylglycerol (PG) in the positive ion mode and phosphatidylinositol (PI) in the negative ion mode, were imaged, and their spatial distribution was mapped on the mouse kidneys (Figure 4.2 & 4.3). As shown in Figure 4.2 for kidney-1, PC (34:2) (*m/z* 758.5703, $[M+H]^+$), PC (34:1) (*m/z* 760.5843, $[M+H]^+$), PC (36:4) (*m/z* 782.5708, $[M+H]^+$), PC (36:3) (*m/z* 784.5819, $[M+H]^+$), PC (36:2) (*m/z* 786.6012, $[M+H]^+$), PG (38:4) (*m/z* 799.5518, $[M+H]^+$), PC (38:6) (*m/z* 806.5708, $[M+H]^+$), PC (38:5) (*m/z* 808.5816, $[M+H]^+$), and PG (38:4) (*m/z* 820.5270, $[M+Na]^+$), were analyzed in triplicate, using sublimation application of CMBT matrix in the positive ion mode. Figure 4.3 displays the analysis of phosphatidylinositols, such as PI (38:4) (*m/z* 885.5513, $[M-H]^-$), PI (38:3) (*m/z* 887.5606, $[M-H]^-$), PI (40:7) (*m/z* 907.5381, $[M-H]^-$), and PI (40:6) (*m/z* 909.5450, $[M-H]^-$) for kidney-1, which were analyzed in triplicate using sublimation application of CMBT matrix in the negative ion mode. The observed *m/z* of phospholipids for kidney-2 and kidney-3 are also shown in Figures 4.2 and 4.3. All lipid images were mapped within the 5 ppm mass error range of their corresponding exact mass.

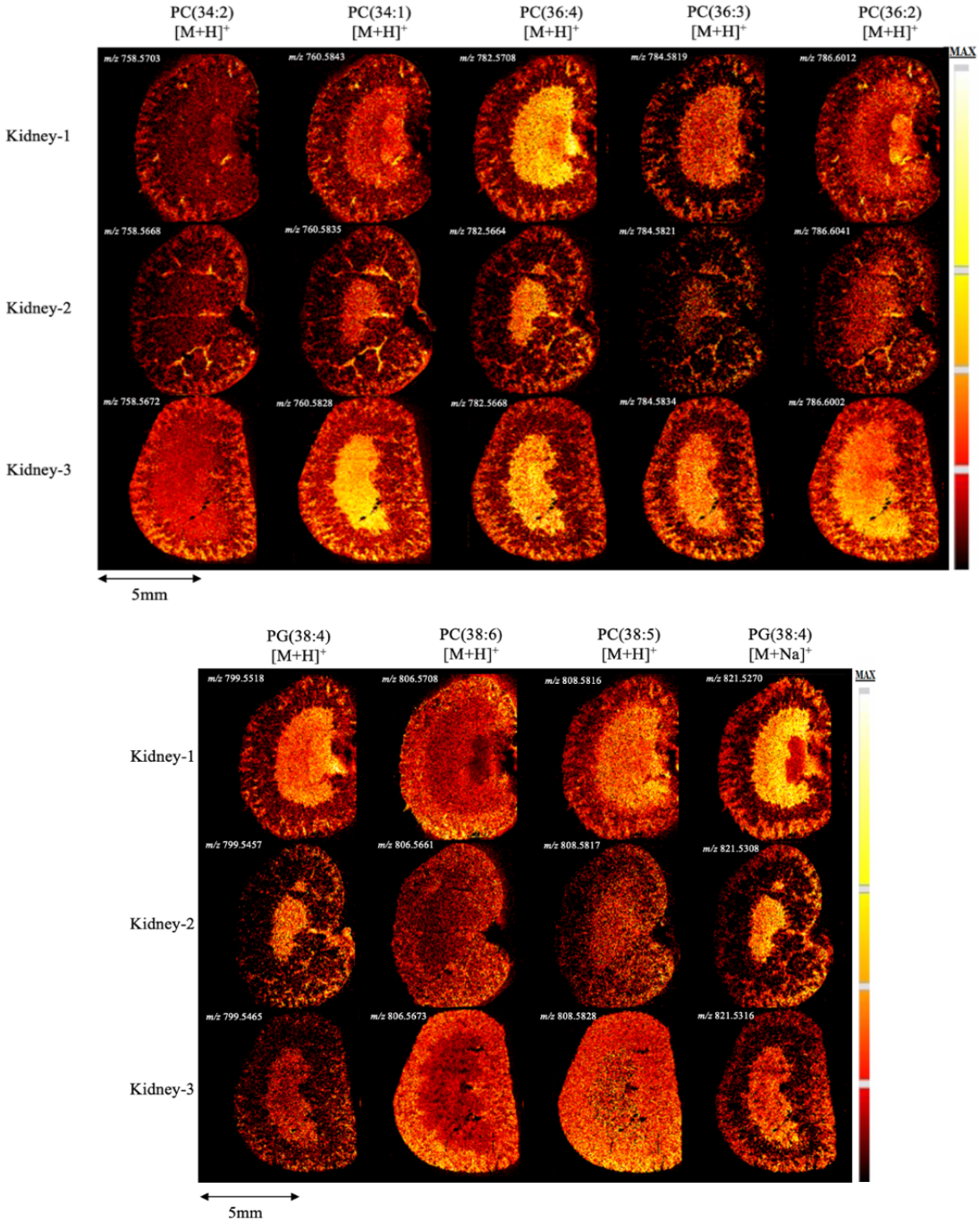

Figure 4.2. The results of a positive ion mode MALDI-MSI analysis of kidney phospholipids, tentatively identified as phosphatidylcholine (PC) and phosphatidylglycerol (PG), using sublimated CMBT matrix. The analysis was conducted on biological triplicates at a spatial resolution of 50 µm. The naming convention used for identifying the phospholipids is based on the number of carbons and the degree of unsaturation. For instance, PC(34:2) indicates a phosphatidylcholine molecule with 34 carbon atoms and 2 double bonds. The brighter regions in the figure correspond to higher signal intensity of the m/z of interest. Due to the differences in the tissue sections of each replicate, the morphological features and localization of each *m/z* might vary across replicates

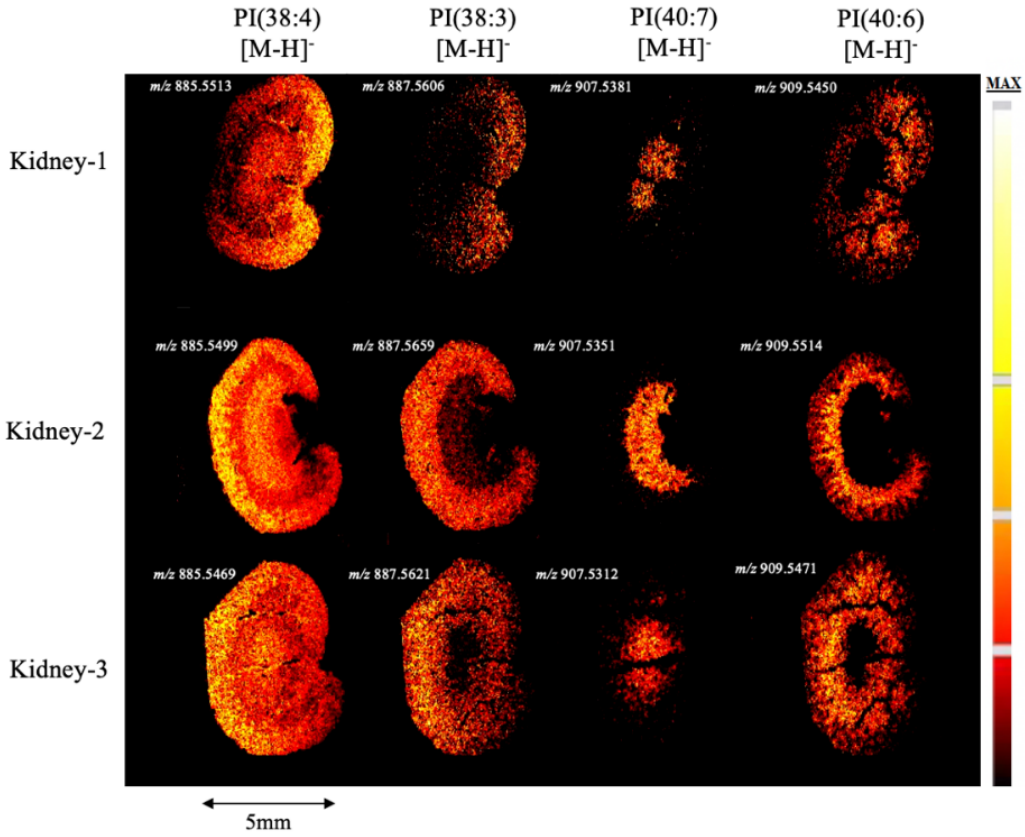

Figure 4.3. The results of negative ion mode MALDI-MSI analysis of kidney phospholipids using sublimated CMBT matrix. The compounds were tentatively identified as Phosphatidylinositol (PI), and their spatial distribution was observed on biological triplicates at 50 µm spatial resolution. For example, PI(38:4) refers to PI(number of carbons: degree of unsaturation). The color scheme indicates the intensity of the *m/z* signal, with brighter regions representing higher signal intensity. It should be noted that due to differences in the tissue sections of each replicate, the morphological features and localization of each m/z may vary across replicates.

In order to assess the performance of sublimated CMBT matrix in both positive and negative ion modes, averaged mass spectra from three biological replicates of coronal mouse kidney tissue sections were obtained. These mass spectra are presented in Appendix Figure B.4. Additionally, Appendix Table B.2 shows the signal-to-noise ratio (S/N) values for the biological triplicates in the positive and negative ion modes. The variability in S/N values is attributed to the different distributions of the compounds present in different histological cuts. However, even though some of the S/N values were low (ranging from 5 to 10), they were still considered acceptable for mapping the ions.

4.4.4. Spatial resolution

The analysis of single cells has become an important approach for studying biological variability and differential susceptibility to disease. [133] There has been growing interest in molecular profiling of a single cell. This is due to cells' morphological, physiological, and pathological heterogeneity, which can affect their molecular profile. [134] Mass spectrometry imaging is a powerful technique that can provide spatially resolved information about the distribution of compounds in cells and tissue sections in a single analysis. [134] The required spatial resolution for MSI of single cells depends on the size of the cell, which can range from 5 to 150 µm in diameter, with an average size of about 20 µm for human cells. [134]

To assess the effect of higher spatial resolution on the quality of the resulting ion maps, using sublimated CMBT, higher spatial resolution MALDI-MSI analyses were performed on transverse kidney sections (5.5 x 5 mm) to reduce the acquisition time. Analytical triplicate analyses were conducted at 10 and 20 µm spatial resolutions, and some of the resulting phosphatidylinositol ion maps are shown in Figures 4.4 and 4.5.

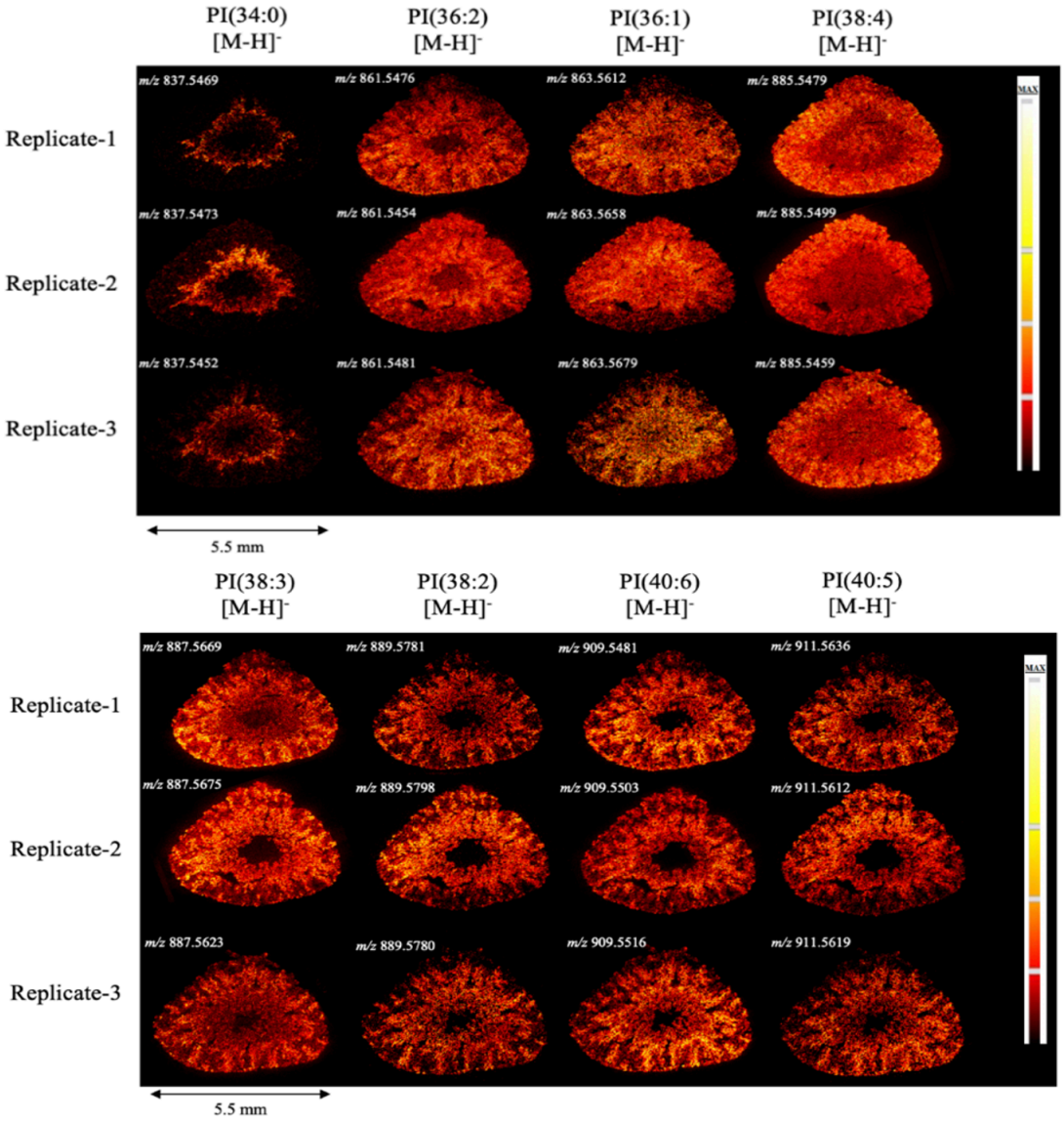

Figure 4.4. The results of negative ion mode MALDI-MSI analysis of kidney PI phospholipids with sublimated CMBT matrix, conducted on analytical triplicates and at a spatial resolution of 20 µm. The PI phospholipids were identified based on the tentative assignment of their molecular formula. The brighter regions in the images indicate higher signal intensity of the *m/z* of interest. The results of this analysis contribute to the optimization of the spatial resolution required for MALDI-MSI of sublimated CMBT, especially in the context of single-cell analysis.

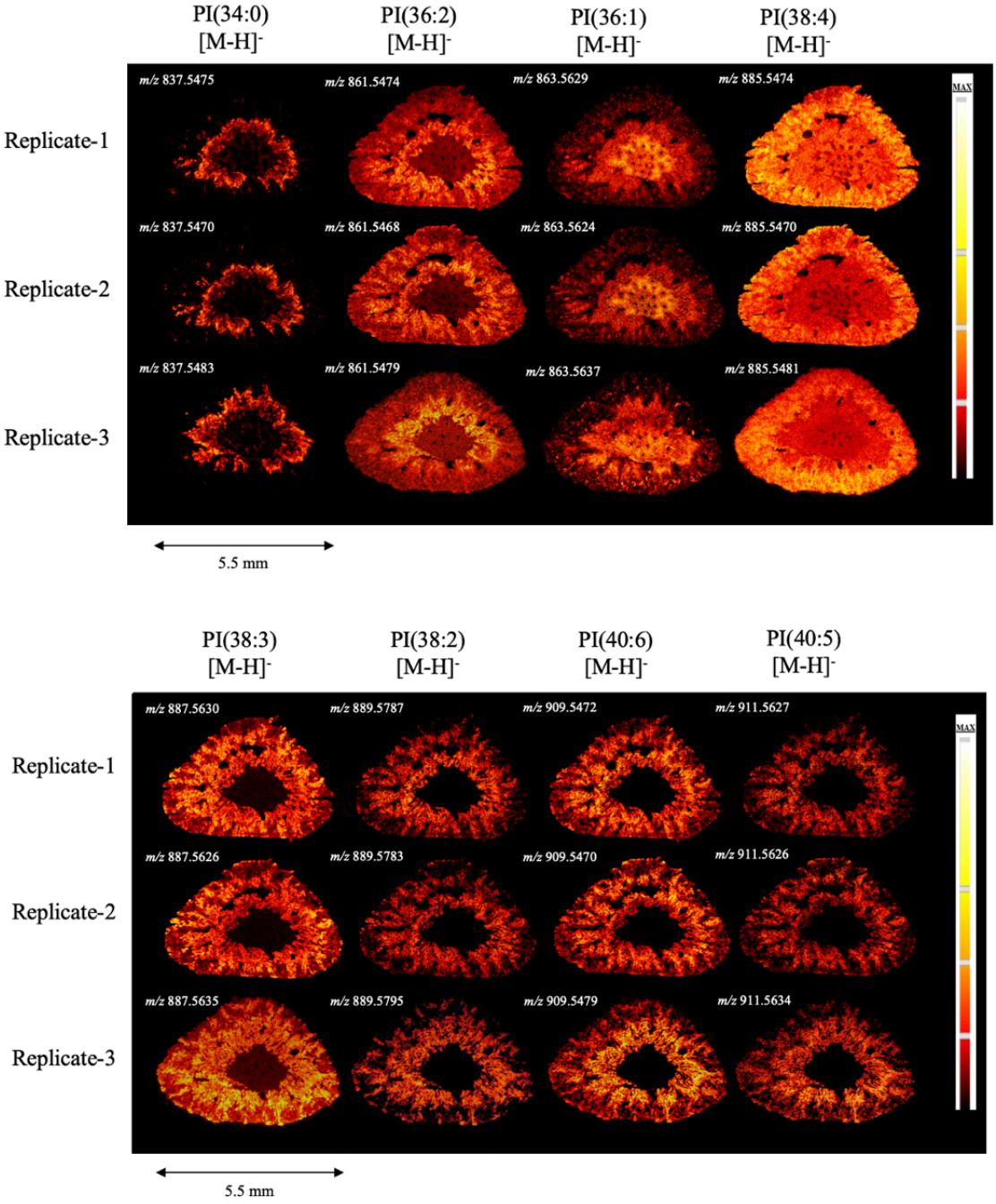

Figure 4.5. The results of negative ion mode MALDI-MSI analysis of kidney PI phospholipids using sublimated CMBT matrix at 10 µm spatial resolution. Analytical triplicate analyses were performed to obtain the ion maps, which reveal the spatial distribution of the *m/z* values of interest. The brighter regions in the ion maps correspond to higher signal intensity of the specific *m/z* value. The higher spatial resolution allows for a more detailed and precise analysis of the distribution of the compounds in the tissue sections, which is particularly important for the study of single cells and their heterogeneity.

Appendix Figure B.2 depicts electron microscopy images of laser spot sizes at 50 µm, 20 µm, and 10 µm spatial resolutions for MALDI-MSI analyses. At 50 µm and 20 µm spatial resolutions, the laser spot diameter averaged around 15 µm. Achieving a spatial resolution of 10 µm depends on several experimental parameters, such as laser spot size and matrix homogeneity without lateral analyte migration. [135] In order to obtain this resolution, the laser spot diameter was reduced to 6.5 µm (Appendix Figure B.2). It is worth noting that imaging a transverse section of the kidney at a 10 µm spatial resolution took approximately 20 hours, while a 20 µm spatial resolution took only 5 hours. As such, further studies and considerations should be considered to justify the longer acquisition time and larger data file size required for 10 µm spatial resolution analysis. In addition, if single-cell analysis is intended, further optimization of tissue thickness and laser potency is needed to avoid the collection of ions from different layers of cells.

4.4.5. Histological Staining after MALDI Analysis

To achieve orthogonal histological information that complements the chemical data acquired from MALDI-MSI, a hematoxylin and eosin (H&E) staining was performed on one of the transverse kidney sections used as an analytical replicate. After the MALDI-MSI analysis, the CMBT matrix was removed from the slide using 95% ethanol for 30 seconds. [14] The standard H&E staining protocol was then applied to the section. [130] Figure 4.6 displays microscopic images of the stained section. The sequential analysis of MALDI-MSI and H&E staining provided relatively good images. Although some cracking is visible in the stained section (Figure 4.6 d), as previously reported by Eberlin et al. [14], the image still offers valuable morphological information.

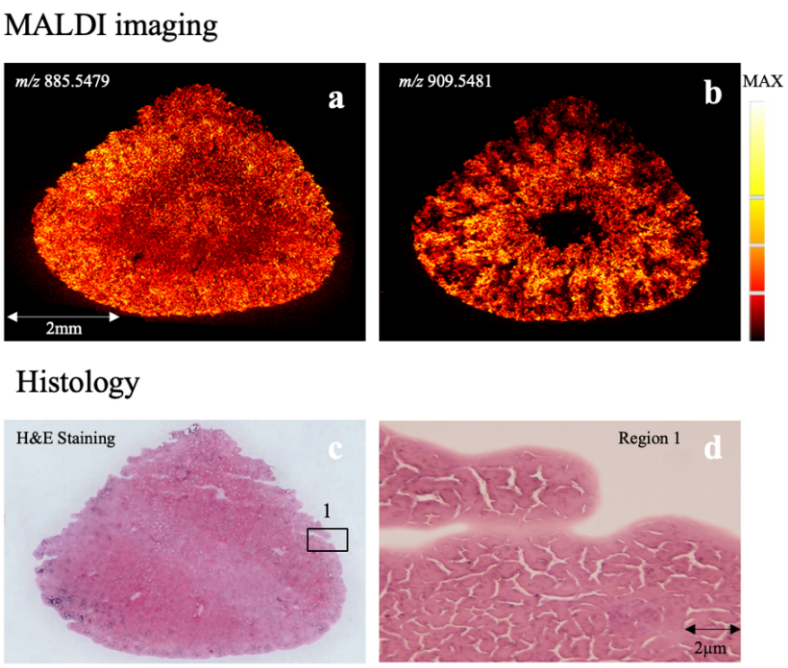

Figure 4.6. The results of the MALDI-MSI and H&E staining analysis of a mouse kidney transverse section. The distribution of a) *m/z* 885.5479, PI (38:4) and b) *m/z* 909.5481, PI (40:6) are shown after MALDI-MSI analysis in the negative ion mode at 20 µm resolution. c) exhibits the optical image of the whole transverse section after removing the CMBT matrix and H&E staining. Lastly, d) is a high-magnification view of a morphological region of the same tissue section after H&E staining. The results suggest that CMBT MALDI-MSI and H&E staining can be combined to provide complementary chemical and morphological information.

4.5. Conclusion

In this study, we have demonstrated the effectiveness of sublimated CMBT matrix for MALDI- MSI analysis of kidney tissue samples. We carefully optimized the parameters of the sublimation process, including pressure, temperature, time, and matrix thickness, to achieve high-quality mass spectrometric images. We also evaluated the performance of the sublimated CMBT matrix at 50, 20, and 10 µm spatial resolution analyses. Although a spatial resolution of 10 µm can yield ion images of high quality, it should be acknowledged that imaging a transverse kidney section at this resolution requires a significant amount of time, approximately 20 hours. Therefore, when considering using this resolution for future studies and analysis, it is important to consider the extended acquisition time and larger data file size and justify their necessity. In addition, we demonstrated the sequential analysis of MALDI-MSI and H&E staining, which provides both

chemical and histological information about the tissue. Overall, our findings suggest that sublimated CMBT matrix may be a useful sample preparation method for MALDI-MSI analysis, and we believe that our optimized sublimation parameters could guide experiments for other tissue types and analyte classes for improved imaging results.

Table 4.1. Tentative identification of phospholipids, adduct types, observed and calculated masses, and mass error (ppm) for *m/z* ions detected using MALDI-MSI of kidney sections with sublimated CMBT matrix in the positive and negative ion modes (ppm: parts per PC: phosphatidylcholines; PG: PI: phosphatidylinositol).

			Kidney-1			Kidney-2			Kidney-3		
	Compound	**Adduct**	**Observed mass**	**Exact mass**	**ppm mass error**	**Observed mass**	**Exact mass**	**ppm mass error**	**Observed mass**	**Exact mass**	**ppm mass error**
Figure 2	PC(34:2)	$[M+H]^+$	758.5703	758.5699	0.5273	758.5668	758.5699	-4.0866	758.5672	758.5699	-3.5593
	PC(34:1)	$[M+H]^+$	760.5843	760.5856	-1.7092	760.5835	760.5856	-2.7610	760.5828	760.5856	-3.6813
	PC(36:4)	$[M+H]^+$	782.5708	782.5699	1.1500	782.5664	782.5699	-4.4724	782.5668	782.5699	-3.9613
	PC(36:3)	$[M+H]^+$	784.5819	784.5856	-4.7158	784.5821	784.5856	-4.4609	784.5834	784.5856	-2.8040
	PC(36:2)	$[M+H]^+$	786.6012	786.6012	0.0000	786.6041	786.6012	3.6867	786.6002	786.6012	-1.2712
	PG(38:4)	$[M+H]^+$	799.5518	799.5489	3.6270	799.5457	799.5489	-4.0022	799.5465	799.5489	-3.0016
	PC(38:6)	$[M+H]^+$	806.5708	806.5699	1.1158	806.5661	806.5699	-4.7113	806.5673	806.5699	-3.2235
	PC(38:5)	$[M+H]^+$	808.5816	808.5856	-4.9469	808.5817	808.5856	-4.8232	808.5828	808.5856	-3.4628
	PG(38:4)	[M+Na]+	821.5270	821.5308	-4.6255	821.5291	821.5308	-2.0693	821.5316	821.5308	0.9737
Figure 3	PI(38:4)	$[M-H]^-$	885.5513	885.5493	2.2584	885.5499	885.5493	0.6775	885.5469	885.5493	-2.7101
	PI(38:3)	$[M-H]^-$	887.5606	887.5649	-4.8447	887.5659	887.5649	1.1266	887.5621	887.5649	-3.1546
	PI(40:7)	$[M-H]^-$	907.5381	907.5336	4.9584	907.5351	907.5336	1.6528	907.5312	907.5336	-2.6445
	PI(40:6)	$[M-H]^-$	909.5450	909.5493	-4.7276	909.5514	909.5493	2.3088	909.5471	909.5493	-2.4187
			Replicate-1			**Replicate-2**			**Replicate-3**		
	Compound	**Adduct**	**Observed mass**	**Exact mass**	**ppm mass error**	**Observed mass**	**Exact mass**	**ppm mass error**	**Observed mass**	**Exact mass**	**ppm mass error**
Figure 4	PI(34:0)	$[M-H]^-$	837.5469	837.5493	-2.8655	837.5473	837.5493	-2.3879	837.5452	837.5493	-4.8952
	PI(36:2)	$[M-H]^-$	861.5476	861.5493	-1.9731	861.5454	861.5493	-4.5267	861.5481	861.5493	-1.3928
	PI(36:1)	$[M-H]^-$	863.5612	863.5649	-4.2845	863.5658	863.5649	1.0421	863.5679	863.5649	3.4739
	PI(38:4)	$[M-H]^-$	885.5479	885.5493	-1.5809	885.5499	885.5493	0.6775	885.5459	885.5493	-3.8394
	PI(38:3)	$[M-H]^-$	887.5669	887.5649	2.2533	887.5675	887.5649	2.9293	887.5623	887.5649	-2.9293
	PI(38:2)	$[M-H]^-$	889.5781	889.5806	-2.8103	889.5798	889.5806	-0.8993	889.5780	889.5806	-2.9227
	PI(40:6)	$[M-H]^-$	909.5481	909.5493	-1.3193	909.5503	909.5493	1.0994	909.5516	909.5493	2.5287
	PI(40:5)	$[M-H]^-$	911.5636	911.5649	-1.4261	911.5612	911.5649	-4.0589	911.5619	911.5649	-3.2910
Figure 5	PI(34:0)	$[M-H]^-$	837.5475	837.5493	-2.1491	837.5470	837.5493	-2.7461	837.5483	837.5493	-1.1939
	PI(36:2)	$[M-H]^-$	861.5474	861.5493	-2.2053	861.5468	861.5493	-2.9017	861.5479	861.5493	-1.6249
	PI(38:1)	$[M-H]^-$	863.5629	863.5649	-2.3159	863.5624	863.5649	-2.8949	863.5637	863.5649	-1.3895
	PI(38:4)	$[M-H]^-$	885.5474	885.5493	-2.1455	885.5470	885.5493	-2.5972	885.5481	885.5493	-1.3550
	PI(38:3)	$[M-H]^-$	887.5630	887.5649	-2.1406	887.5626	887.5649	-2.5913	887.5635	887.5649	-1.5773
	PI(38:2)	$[M-H]^-$	889.5787	889.5806	-2.1358	889.5783	889.5806	-2.5854	889.5795	889.5806	-1.2365
	PI(40:6)	$[M-H]^-$	909.5472	909.5493	-2.3088	909.5470	909.5493	-2.5287	909.5479	909.5493	-1.5392
	PI(40:5)	$[M-H]^-$	911.5627	911.5649	-2.4134	911.5626	911.5649	-2.5231	911.5634	911.5649	-1.6455

Chapter Five: Assessment of MALDI Matrices for Phosphoinositide Detection and Visualization in Mouse Kidney Models Through Matrix Assisted Laser Desorption Ionization (MALDI) Imaging Techniques

Chapter 5 represents a partial version of the manuscript that is currently being prepared for publication:

Maryam Yousefi-Taemeh, Laurentiu G. Dabija, Ergi Duli, Mathieu Lemaire, Demian R. Ifa. **In preparation.**

5.1. Abstract

Phosphatidylinositols (PIs) and their phosphorylated derivatives, known as phosphoinositides, play vital roles in various cellular processes. Abnormalities in phosphoinositides have been associated with a range of diseases. Accurately determining and tracking phosphoinositide levels in tissues is crucial for understanding their contributions to cellular processes and disease development.

One powerful technique for mapping the spatial distribution of molecules in biological samples is matrix-assisted laser desorption/ionization mass spectrometry imaging (MALDI-MSI). This technique allows for the simultaneous detection and analysis of multiple lipid classes, making it invaluable for unbiased lipidomic studies. However, detecting phosphoinositides can be challenging due to their relatively low abundance in tissues. When utilizing MALDI-MSI, the choice of matrix and instrument tuning significantly affects the study outcomes, particularly when investigating molecules with low relative abundance.

This study focuses on selecting the matrix type and optimizing its thickness to enhance the detection of phosphoinositides in mouse kidney tissues using MALDI-MSI. Various matrices, including 9AA, DAN, CMBT, and DHA, were evaluated, and their thicknesses were varied to improve ionization efficiency. The results demonstrated that 9AA, DAN, and DHA matrices produced high-intensity images of PI distributions within kidney sections, while CMBT yielded lower intensity images. Although detecting some low-abundance phosphoinositides proved challenging, it was achievable using CMBT and 9AA matrices. The findings indicate that utilizing a matrix mixture of DAN, 9AA, and CMBT has the potential to improve phosphoinositide mapping by increasing signal intensity. These findings provide valuable insights for future research on the involvement of phosphoinositides in kidney pathophysiology and facilitate disease pathology studies using MALDI-MSI.

5.2. Introduction

Among various metabolites, lipids are of particular interest and are extensively studied due to their vital roles in numerous aspects of living systems. [39] They serve as structural components, energy storage molecules, involved in biochemical processes, membrane permeability, functional lipid biosynthesis, and molecular recognition processes beyond genes and proteins. [39] Phospholipids are a significant group of lipids, and among them, phosphatidylinositols (PIs) are found in relatively small amounts in eukaryotic cell membranes. PIs are acidic phospholipids that are linked to a myo-inositol head group. [40] After binding to the phospholipid, the cyclic inositol is left with five free hydroxyl moieties around it, from which three are readily available for phosphorylation. [40] As a result, the combination of seven phosphorylated derivatives known as phosphoinositides, a group of low abundance phospholipids, can be formed that are known to be fundamental in different structural and instructional roles, including protein interaction and regulation, membrane transport, cytoskeletal function, plasma membrane signalling and etc. [40] [41] [136] As such, the following phosphoinositides, including phosphatidylinositol phosphate (PIP), phosphatidylinositol bisphosphate (PIP2), and phosphatidylinositol trisphosphate (PIP3), are fundamental in various cellular processes.

The distribution of phosphoinositides exhibits significant heterogeneity at the cellular level, with each phosphoinositide species being most prominent on specific organelle membranes. [137] Furthermore, variations in phosphoinositide species concentrations and acyl chain abundance are observed between organs and within an organ, reflecting different microenvironments' unique metabolic and functional demands. [138]

Abnormalities in phosphatidylinositols and phosphoinositides, including their relative kinase activities and levels, have been associated with various diseases, such as human nervous system diseases, cancer, inflammation, thrombosis-related diseases, immune system diseases, and others. [41] [138] [42] [43] [44] [45] To gain a comprehensive understanding of the roles of phosphoinositides in cellular processes and disease pathogenesis, accurate determination and tracking of phosphoinositide levels in various tissues are crucial. Traditional methods, such as

grinding organs and analyzing lipid extracts, are time-consuming, solvent-intensive, and may lead to sample alteration. Additionally, these methods do not provide spatial distribution information.

Mass Spectrometry Imaging (MSI) has emerged as a promising and powerful tool for mapping the spatial distribution of molecules on biological sample surfaces. [13] [14] In this technique, numerous chemical compounds can be detected and spatially mass resolved concurrently based on their mass-to-charge ratio (*m/z*). As a result of data obtained from MSI, the cause of certain diseases can be unraveled by studying the metabolite expressions and biomarker measurements from disease versus healthy tissue comparisons. [13]

In recent years, MSI techniques, such as MALDI (Matrix-Assisted Laser Desorption Ionization), have allowed the generation of *m/z* distribution images for PIs and other lipid species. [46] [139] [140] Unlike traditional methods such as lipid extractions that are time-consuming, require solvents, and may lead to the loss or reduction of certain lipid classes, MALDI-MSI allows for the simultaneous detection and analysis of multiple lipid classes in their natural biological context. This characteristic makes MALDI-MSI a valuable tool for lipidomic studies in both preclinical and clinical settings.

As previously mentioned in section 1.6 of this dissertation, phospholipids tend to ionize in one of the two forms: either as a phosphate anion (which is the case for PIs) or nitrogen-centered cations during the MALDI process. [46] The intensity of PI compounds generated in MS experiments relates to the quantity of molecules present in a tissue sample. [46] Phosphatidylinositols are not as numerous as other phospholipids. The most abundant PI in many tissues is PI(18:0/20:4), with a signal observed at *m/z* 885.5 in the negative ion mode. [46] Polyphosphoinositol lipids or phosphoinositides (PIP, PIP_2, PIP_3) are products of PI kinases and have crucial intracellular roles. [46] However, their abundance is so low that detecting them with MSI requires method optimizations and developments.

As stated in section 1.4.2.1, MALDI utilizes a matrix, a small organic compound, to assist in the desorption of analytes from the sample surface and their subsequent ionization. [20] Choosing the right matrix is crucial for the successful application of MALDI-MSI. The

characteristics and thickness of the matrix compound have a direct influence on the signal intensity of the detected analytes. [20]

In the literature, several matrices have been suggested as compatible with lipids or phosphatidylinositols (PIs) in general. However, despite these reports, a single matrix has not emerged as the definitive choice for achieving optimal results in the untargeted analysis of PIs, PIPs, PIP2s, and PIP3s across diverse experimental settings. Consequently, this study serves as a pioneer effort to establish a framework for fine-tuning the selection of matrix type and thickness, as well as developing enhanced methodologies for MALDI-MSI analysis of kidney samples. The primary objective is to enhance sensitivity in the detection of phosphatidylinositol and phosphoinositide species, thereby contributing to a more comprehensive understanding of their involvement in kidney pathophysiology. Regarding MALDI imaging, the most widely employed matrices for phospholipids include 5-Chloro-2-mercaptobenzothiazole (CMBT), 1,5-Diaminonapthalene (DAN), and 9-aminoacridine (9-AA), and 2,5-Dihydroxyacetophenone (DHA). [43] [44] [20] [124]

This study aims to evaluate the capabilities of MALDI-MSI under various matrix types and thickness conditions for the detection of phosphatidylinositols and phosphoinositides in mouse kidney models. The label-free data obtained through this approach has the potential to contribute to the spatially resolved analysis and further our understanding of the involvement of phosphoinositides in various disease pathologies. By optimizing the matrix type and thickness, this research aims to enhance the sensitivity of MALDI-MSI for the detection of these important lipid compounds in healthy and diseased states, thereby facilitating future disease pathology research.

5.3. Materials and Methods

5.3.1. Materials

All matrix compounds were purchased from Sigma Aldrich (St. Louis, MO, USA). Indium tin oxide (ITO) coated slides were purchased from Delta Technologies (Loveland, CO, USA).

HPLC-grade reagents were purchased from Sigma-Aldrich (Oakville, ON, Canada). Kidney samples were provided by the University of Toronto, Ontario, Canada. Mouse kidneys (n = 3 animals) were frozen and stored at a temperature of -80 °C until required for sectioning. Thin tissue sections (20 μm) were sliced using a Shandon Cryotome device, and thaw-mounted onto indium tin oxide slides (100Ω/m^2), for subsequent MALDI imaging analyses.

5.3.2. Matrix depositions

The ITO-coated glass slides containing sample sections were removed from the freezer and subjected to a drying process in a vacuum desiccator for 30 minutes. Each matrix was then applied using a sublimation apparatus with a sublimation chamber, as previously shown in section 1.4.2.1. [141] In brief, the sample glass slide was securely attached to the flat-bottom condenser using copper tape, ensuring consistent heat transfer. A matrix chamber was filled with approximately 300 mg of matrix powder, and the sample holder and chamber were sealed with an O-ring. The system was connected to a vacuum pump, reaching a pressure of 0.05 Torr. The condenser was cooled with ice while the chamber was submerged in heated oil. Following a specific time interval (1 to 10 minutes), the matrix was heated, sublimed, and deposited onto the sample. The system was then brought to ambient pressure, and the sample glass slide was carefully detached from the condenser. A range of matrix thicknesses were achieved by varying the sublimation temperature and time periods.

5.3.3. MALDI analysis

MALDI-MSI experiments were performed utilizing a Q-Exactive mass spectrometer (Thermo Fisher Scientific, San Jose, CA, USA) equipped with a Spectroglyph MALDI ion source (Spectroglyph LLC, Kennewick, WA, USA). Data acquisition parameters included a nominal mass resolution setting of 70,000 at *m/z* 400, a maximum injection time of 200 ms, and specific *m/z* range of *m/z* 250 – 1200 for negative ion polarity. MALDI-MSI experiments were conducted to acquire ion images of different matrix thicknesses. Triplicate analyses were performed for each matrix, selecting the most promising result within each group of thicknesses. All experiments were carried out at a spatial resolution of 50 μm.

The laser (Nd:YLF, 349 nm) employed for analysis operated at different repetition rates, pulse energies, and shot numbers per pixel depending on the matrix type. The laser was operated at a repetition rate of 300 Hz with pulse energies of 7.5 μJ for DAN and CMBT, as well as 25 and 42 μJ for DHA and 9AA, respectively. An average of 60 laser shots per pixel were delivered. Ion images were generated using ImageInsight software (version: 0.1.0.1361, Spectroglyph LLC, WA).

5.4. Results and Discussion

In this study, we conducted MALDI-MSI analyses of mouse kidney models using well-established matrices known for lipid detection, namely 9AA, DAN, CMBT, and DHA. [43] [20] The optimization of matrix application on the sample surface was performed through sublimation. Multiple thicknesses of each matrix were examined and documented in Appendix Table C.1. Each matrix required specific temperature, pressure, and time parameters due to their distinct structures and characteristics. A consistent pressure of 0.05 Torr was maintained across all trials. To achieve varying thicknesses of the same matrix, the pressure and temperature remained constant while the sublimation time was adjusted. Subsequently, laser was employed to generate ions, which ionized specific compounds within the kidney tissue sections for mass analysis. [142]
To ensure efficient analysis while capturing representative information, the selection of the most promising result within each group of thicknesses was achieved from the central region of each kidney sample, which encompasses the renal cortex, medulla, and pelvis. This approach aimed to provide a comprehensive assessment of the targeted area while minimizing the analysis time. A list of reported PI, PIP, PIP2, and PIP3 compounds were gathered from the literature and the Avanti Polar Lipids website (Appendix Table C.2). [143] The detectability of PI, PIP, PIP2, and PIP3 categories was assessed through the investigation of various matrix types and thicknesses.

The PI molecular species are typically identified as $[M-H]^-$ ions and are predominantly observed within the *m/z* range of 800-950 under the experimental conditions employed. Among these molecular species, PI diacyl (18:0/20:4) at *m/z* 885.5493 in negative ion mode is the most prevalent. The ability to detect this specific PI molecular species is crucial, and any condition that fails to detect it is deemed unacceptable.

Figure C.1 (Appendix) illustrates the detectability or absence of PI compounds across diverse matrices and thickness variations. Optimal matrix thicknesses were determined based on the quality (intensity) of the obtained images. Among the tested matrix coating thicknesses, the DAN matrix exhibited the best images when utilizing a matrix coating range of 0.1 to 0.25 mg/cm². The DHA matrix yielded satisfactory images for matrix coatings ranging from 0.2 to 0.35 mg/cm². In the case of the CMBT and 9AA matrices, coating thicknesses of 0.15 and 0.1 mg/cm² respectively were deemed optimal.

Next, triplicate MALDI-MSI analyses were conducted on transverse cut kidney tissues, employing each matrix compound at its selected thickness. The distribution of the PI compounds is visualized in Figures 5.1-5.4. Figure 5.1 illustrates the m/z distribution of PI compounds using the DAN matrix. With the exception of one compound, DAN successfully visualized the distribution of all other PIs, exhibiting predominantly good image intensities and distinct morphological features of the kidney. Figure 5.2 demonstrates the mapping results obtained with the CMBT matrix, which captured the distribution of most PIs, albeit with a few missing compounds. However, the intensities of the m/z peaks and image quality were not as favorable as those achieved with the DAN matrix. Nevertheless, discernible morphological aspects of the kidney were still observed. Similarly, Figure 5.3 depicts the PI distributions within the kidney section using the 9AA matrix. Remarkably, 9AA proved to be the only matrix capable of successfully capturing the distribution of all targeted PIs, albeit with a few compounds exhibiting lower analyte intensities. Lastly, Figure 5.4 showcases the utilization of the DHA matrix, which resulted in high-intensity images for all but three PIs that remained undetected. Based on these findings, it is evident that 9AA, DAN, and DHA matrices yielded high signal intensity images of PI distributions within kidney sections. Notably, 9AA matrix successfully visualized all PIs in the list, whereas CMBT resulted in lower intensity images for the targeted PIs.

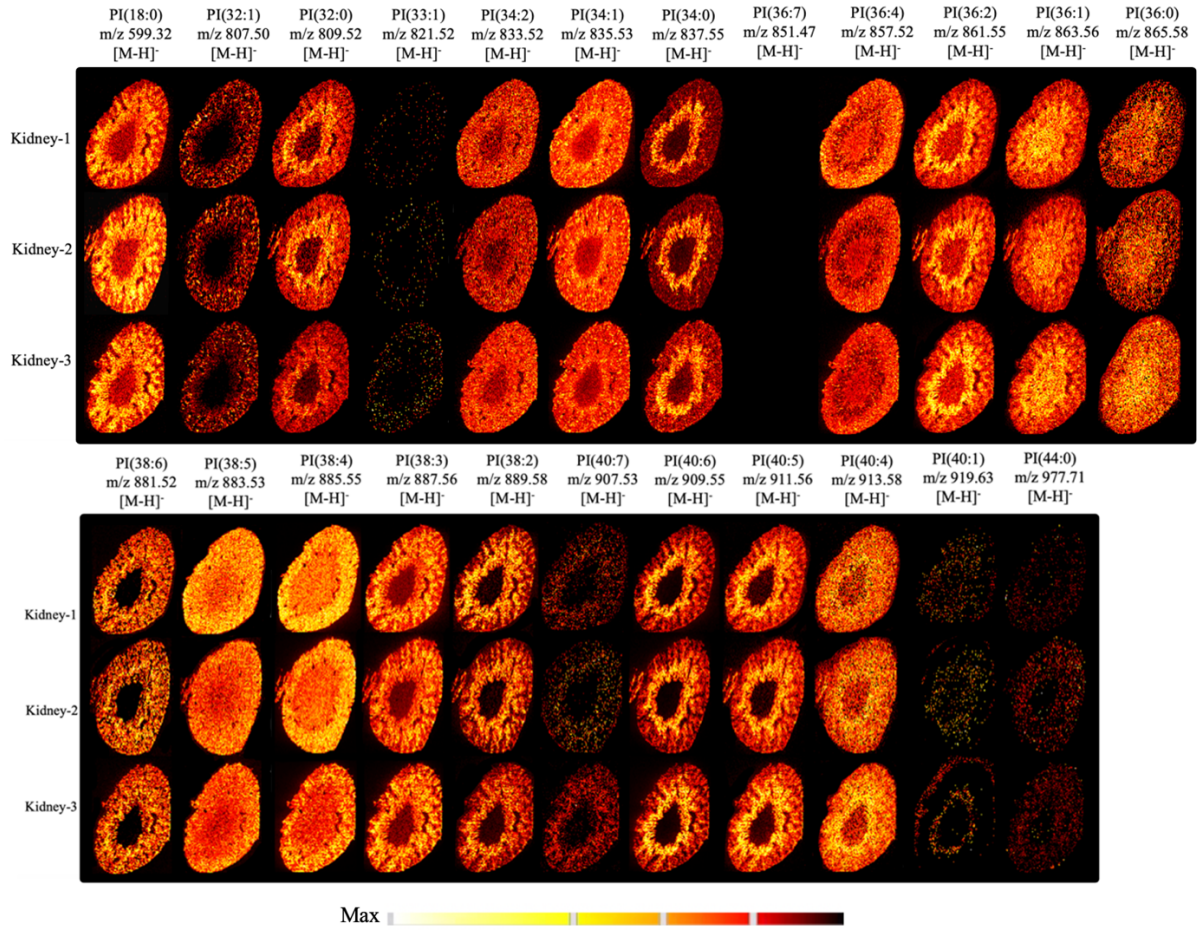

Figure 5.1. The m/z distribution of PI compounds using the DAN matrix in negative ion mode MALDI-MSI. With the exception of one compound, DAN successfully visualized the distribution of all other PIs, exhibiting predominantly good image intensities and distinct morphological features of the kidney.

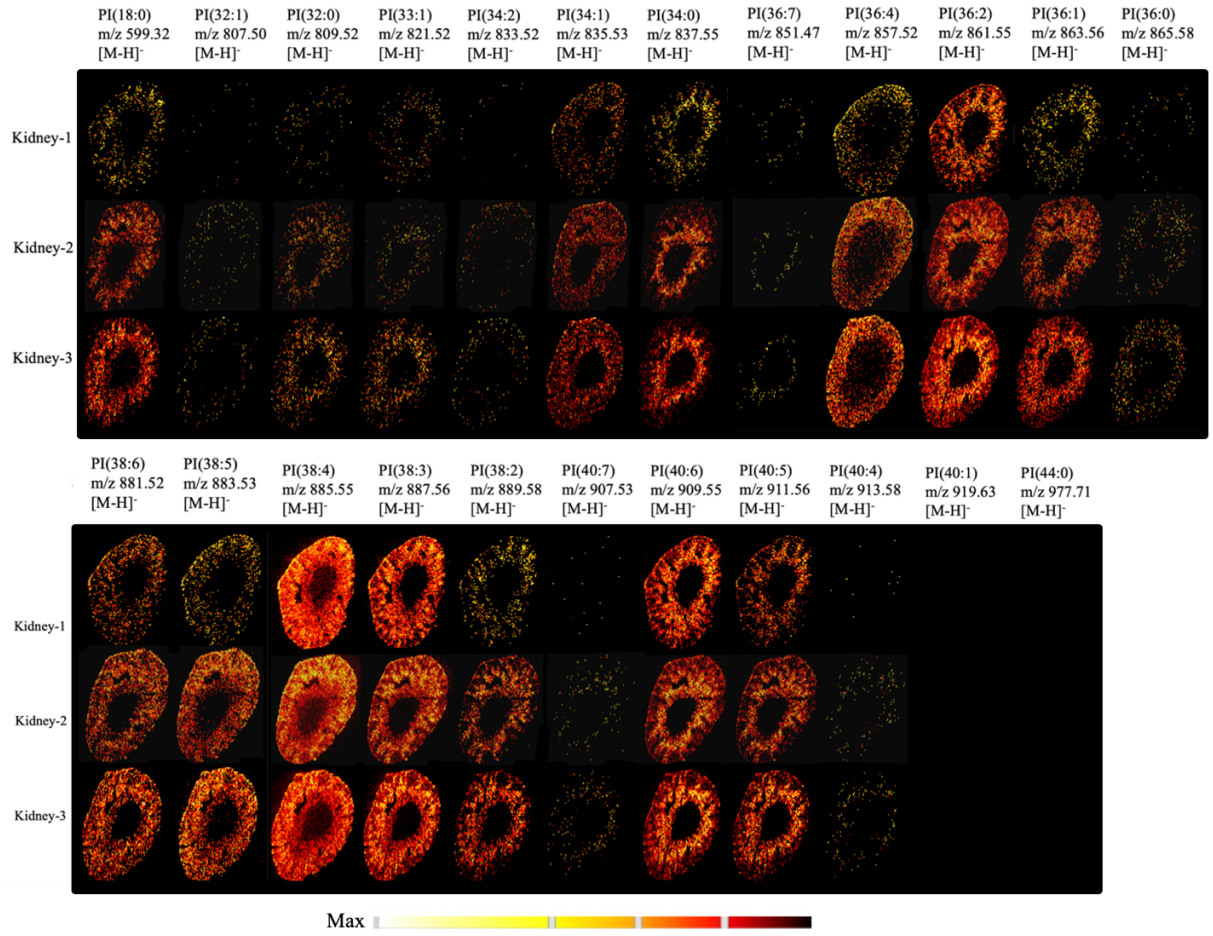

Figure 5.2. The m/z distribution of PI compounds using the CMBT matrix in negative ion mode MALDI-MSI. The mapping results obtained with the CMBT matrix revealed the distribution of most PIs, albeit with a few compounds missing. However, it is worth noting that the intensities of the m/z peaks and image quality were not as favorable as those achieved with other matrices. Despite this, discernible morphological aspects of the kidney were still observed.

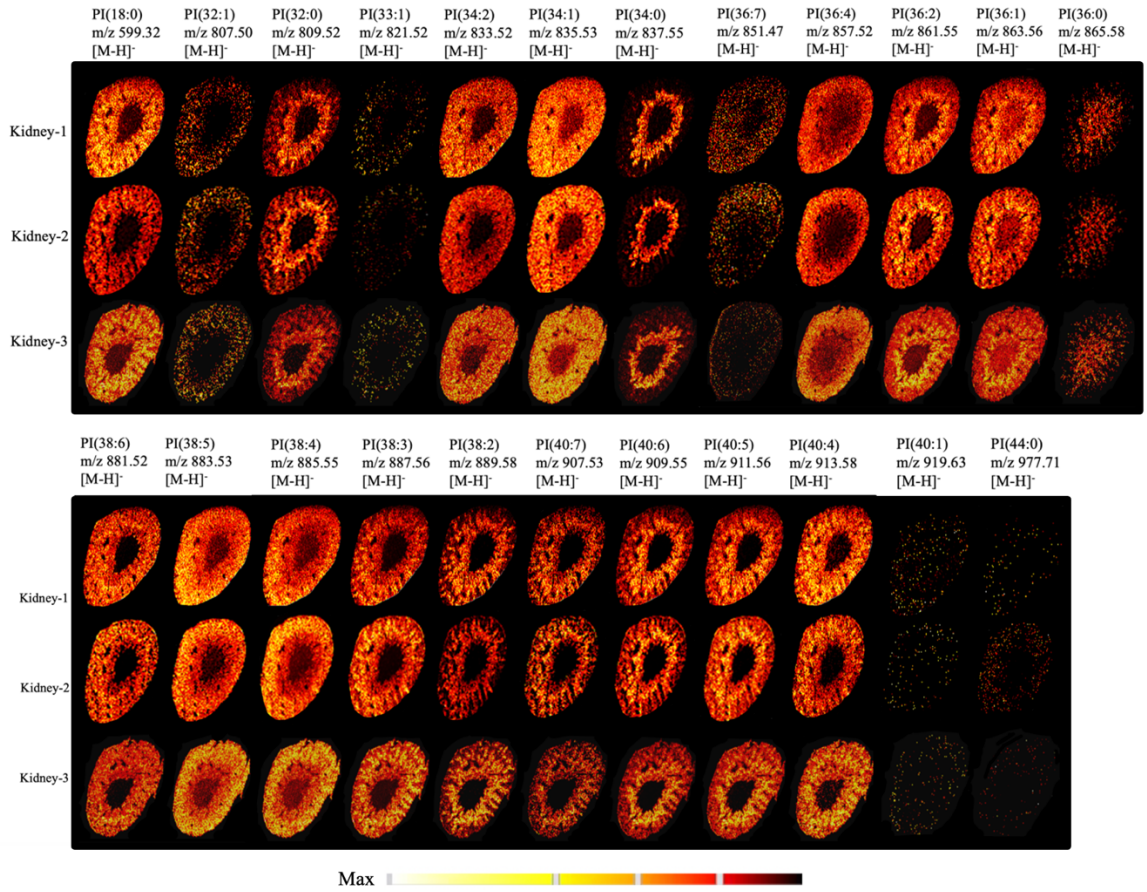

Figure 5.3. The m/z distribution of PI compounds using the 9AA matrix in negative ion mode MALDI-MSI. Remarkably, 9AA proved to be the only matrix capable of successfully capturing the distribution of all targeted PIs. However, it is worth noting that a few compounds exhibited lower analyte intensities despite being detected.

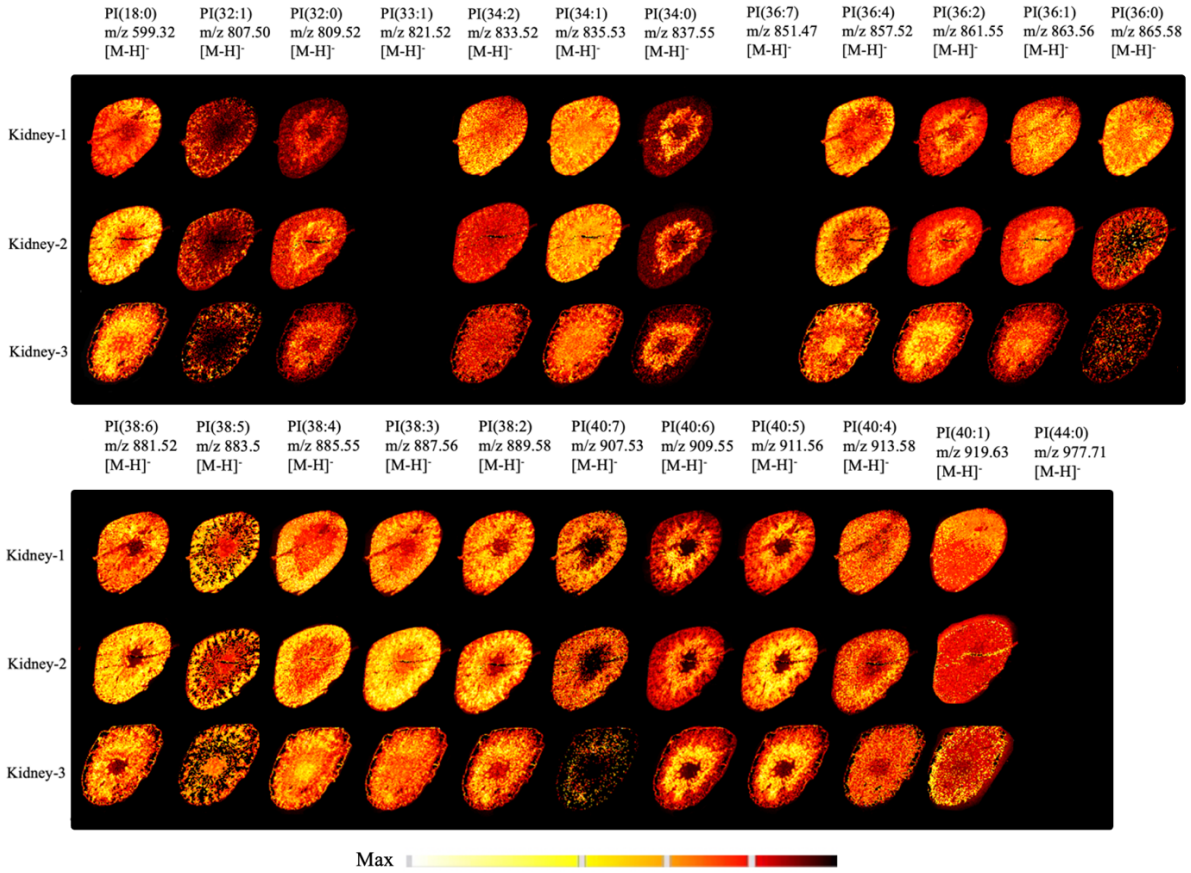

Figure 5.4. The m/z distribution of PI compounds using the DHA matrix in negative ion mode MALDI-MSI. The DHA matrix yielded high-intensity images for most PIs; however, three PIs remained undetected.

After evaluating the detection capabilities of the matrices for PI compounds, the *m/z* distribution of all phosphoinositides (PIP, PIP_2, and PIP_3) was also mapped. Phosphoinositides are known to be present in low abundance in tissue, posing a challenge for their detection using mass spectrometry imaging. The choice of matrix and instrument tuning will have a substantial impact on the results of studies when the molecules of interest are present in low relative abundance. [144] Therefore, the primary focus of this work was to prioritize detection, even with low intensity, with the goal of improving and achieving higher intensity results.

Surprisingly, as illustrated in Figure 5.5, the results revealed that the CMBT matrix, despite resulting in lower intensity PI mappings, was able to detect four phosphoinositides: PIP(34:1) with *m/z* 887.4686, PIP_2(36:2) with *m/z* 1021.4820, PIP_3(38:4) with *m/z* 1125.4483, and PIP_3(38:3) with *m/z* 1127.4639. It should be noted that the intensities of these compounds were relatively low.

Furthermore, the 9AA matrix successfully detected one PIP compound, PIP(38:4) with *m/z* 965.5156, with relatively good quality and intensity. In contrast, neither the DAN matrix nor the DHA matrix were able to detect any of the phosphoinositides from the list.

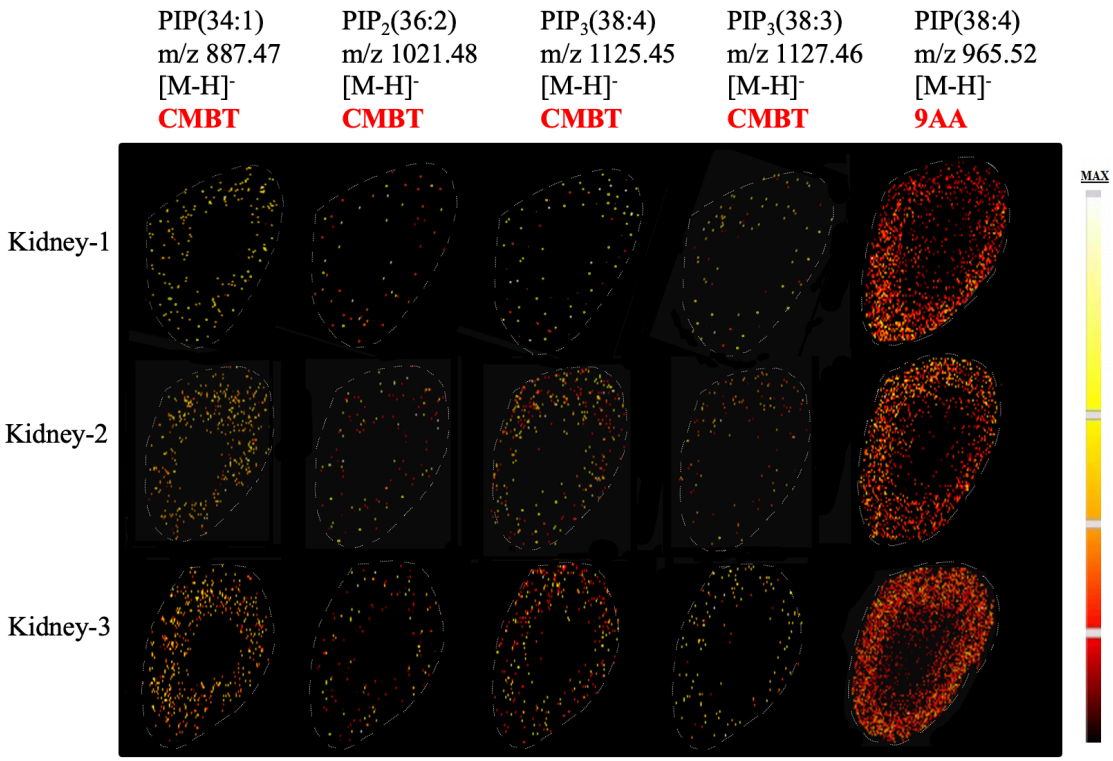

Figure 5.5. The m/z distribution of detected phosphoinositides (PIP, PIP2, and PIP3) using negative ion mode MALDI-MSI. Surprisingly, the results demonstrated that the CMBT matrix, despite yielding lower intensity PI mappings, was able to detect four phosphoinositides, albeit with relatively low intensities. Additionally, the 9AA matrix successfully detected one PIP compound, demonstrating relatively good quality and intensity.

These findings indicate that both CMBT and 9AA matrices hold promise for achieving phosphoinositide mappings. Conversely, although DAN matrix produced high-intensity images for PI m/z distribution, it was unable to detect these low-abundance compounds. On the other hand, DHA matrix yielded high-intensity images for PIs; however, its well-known instability and rapid sublimation under vacuum conditions present challenges. [144] [139] Previous studies have reported that using DHA matrix for long-duration MSI applications, such as high-resolution MSI analysis, was unsuccessful due to matrix evaporation during the analysis, resulting in inadequate matrix compounds remaining on the sample for effective analyte desorption and ionization.

In order to advance our goal of utilizing MALDI-MSI for the discovery of potential markers related to PI and phosphoinositide-related pathogenesis, further development is necessary to map additional phosphoinositide compounds with higher intensity. To accomplish this, we have decided to continue the project by utilizing combinations of matrix compounds that have demonstrated optimal results. For instance, DAN matrix produced high-quality PIs, and CMBT and 9AA matrices were also able to cover some of the phosphoinositides. Therefore, our future work will involve combining these three matrices and employing matrix mixtures for MALDI-MSI of PIs and phosphoinositides. However, due to the poor stability observed under high vacuum conditions, the DHA matrix has been excluded from further study.

5.5. Conclusion

In conclusion, this study demonstrates the optimization of matrix type and thickness for enhanced detection of PIs and phosphoinositides in mouse kidney tissues using MALDI-MSI. The results highlight the importance of selecting the appropriate matrix and optimizing its thickness to improve ionization efficiency and enhance signal intensity.

Among the matrices evaluated, 9AA, DAN, and DHA were found to produce high-intensity images of phosphatidylinositols (PIs) within kidney sections, while CMBT yielded lower intensity images. Although detecting some low-abundance phosphoinositides proved challenging, it was achievable using CMBT and 9AA matrices. The findings suggest that a matrix mixture of DAN, 9AA, and CMBT might have the potential to improve phosphoinositide mapping by increasing signal intensity.

This optimization of matrix type and thickness in MALDI-MSI analysis provides valuable insights for future research on the involvement of phosphoinositides in kidney pathophysiology and facilitates disease pathology studies. The spatial distribution of phosphoinositides and their variations in different organs and within organs can be crucial for understanding their contributions to cellular processes and disease development. The use of MALDI-MSI for lipidomic studies, including phosphoinositide analysis, offers several advantages over traditional methods. It allows for simultaneous detection and analysis of multiple lipid classes, minimizes the risk of sample

alteration, and provides spatial distribution information. By fine-tuning the matrix type and thickness, MALDI-MSI can enhance the sensitivity and accuracy of phosphoinositide detection in healthy and diseased states, enabling comprehensive analysis and furthering our understanding of their roles in various disease pathologies.

Overall, this study contributes to the advancement of phosphoinositide research and the application of MALDI-MSI in lipidomics. It establishes a framework for optimizing matrix conditions in MALDI-MSI analysis and provides a basis for future studies investigating the involvement of phosphoinositides in cellular processes and disease pathogenesis. The insights gained from this research have the potential to drive advancements in the field and contribute to the development of new diagnostic and therapeutic approaches for diseases associated with phosphoinositide abnormalities.

Chapter Six: Conclusion and Future Works

The works presented in this dissertation highlight the power and versatility of mass spectrometry (MS) techniques in revolutionizing our analytical capabilities for complex mixtures across various scientific disciplines. Through the exploration of modern applications of MS, including electrospray ionization (ESI), tandem mass spectrometry (MS/MS), and mass spectrometry imaging (MSI) techniques such as matrix-assisted laser desorption/ionization (MALDI) and desorption electrospray ionization (DESI), we have strengthened our knowledge and practical experience in utilizing these methodologies. With the objective of developing methods to profile, separate, detect, map, and quantify targeted and untargeted analytes from complex matrices, we focused on specific applications within the MS field.

In Chapter 2, we focused on developing and validating an analytical method utilizing DESI-MS for the detection, characterization, and quantification of cannabinoids in cannabis-infused chocolate. The legalization of marijuana in Canada and select states in the United States has significantly increased the demand for precise analytical techniques in cannabis-related applications, particularly in forensic and pharmaceutical analysis. This method offers a cost-effective, reliable, and time-efficient approach for analyzing complex matrices such as edibles. The study assessed the quantitative analysis of tetrahydrocannabinol (THC) in cannabis-infused chocolate using thin-layer chromatography (TLC)-DESI-MS and the QuEChERS extraction method. Both techniques proved to be cost-effective and capable of delivering rapid results. The QuEChERS method effectively eliminated matrix components from the chocolate, enabling accurate THC analysis. TLC separation combined with DESI-MS provided a robust and selective method for identifying and quantifying THC in complex matrices.

Future research in this field can expand the method to analyze a wider range of cannabinoids and their derivatives in different cannabis-infused products. This expansion would address the growing demand for reliable and efficient analytical tools in the cannabis industry. Additionally, efforts can be made to optimize the extraction and separation processes to enhance the method's sensitivity and selectivity. Furthermore, research can focus on the challenges related

to accurately labeling cannabis-infused products. Developing analytical methods that verify the claimed cannabinoid content in edibles will ensure consumer safety and mitigate potential health risks. Studying the stability and degradation of cannabinoids in various matrices, including edibles, would contribute to understanding their shelf life and quality control.

Chapter 3 centered on investigating the biochemical basis of quantitative trait loci (QTLs) E and M, which confer resistance to leaf-chewing insects in soybean. Previous studies have identified flavonoids and isoflavonoids as the potential causative agents of resistance, but there has been uncertainty about whether these metabolites are a result of the QTLs or the genetic background. The current research used a non-targeted mass spectrometry approach to compare the metabolite profiles of QTLs E, M, and both (EM) introgressed into the susceptible variety Benning. The results revealed that E and M primarily confer low-level, global differences in distinct sets of metabolites. Among the metabolites analyzed, daidzein was the only compound that showed significant increases, specifically in insect-treated M and EM genotypes. Interestingly, M increased daidzein levels in response to insect feeding, while E restored M's depleted daidzein levels in the absence of insects. However, daidzein levels did not directly correlate with levels of resistance, suggesting a novel mechanism by which the QTLs confer resistance through mediating changes in numerous metabolites. This mechanism may make it challenging for insects to evolve tolerance.

For future work, it would be valuable to further explore the specific metabolites that contribute to resistance in soybean QTLs E and M. In-depth analysis of other metabolites showing significant changes and their potential roles in resistance mechanisms should be undertaken. Additionally, investigating the signaling pathways and molecular mechanisms underlying the observed changes in metabolite levels would provide a deeper understanding of how these QTLs confer resistance.

In Chapter 4, we successfully investigated the application of the 5-chloro-2-mercaptobenzothiazole (CMBT) matrix through sublimation as a solvent-free technique for sample preparation in MALDI-MSI analysis of mouse kidney tissue samples. We optimized the sublimation parameters and achieved high-quality mass spectrometric images. The sublimated

CMBT matrix demonstrated stability under vacuum conditions and allowed for ion imaging at different spatial resolutions. We also demonstrated the sequential analysis of MALDI-MSI and H&E staining, providing both chemical and histological information about the tissue. Overall, the sublimated CMBT matrix proved to be an effective sample preparation method for MALDI-MSI analysis.

And lastly, in Chapter 5, we aimed to optimize the matrix type and thickness for the detection of phosphatidylinositols and phosphoinositides in mouse kidney tissues using MALDI-MSI. The disruption of PIs and phosphoinositides in mammalian tissue has been associated with the impairment of normal cellular functions and the onset of various diseases. Understanding the molecular species changes in phosphoinositides can provide valuable insights into disease progression and facilitate the development of strategies for early detection and treatment. The optimized matrix conditions identified in this study provide valuable insights for future research on the involvement of phosphoinositides in kidney pathophysiology and facilitate disease pathology studies using MALDI-MSI. Various matrices, including 9AA, DAN, CMBT, and DHA, were evaluated, and their thicknesses were varied to enhance ionization efficiency. The results demonstrated that 9AA, DAN, and DHA matrices produced high-intensity images of phosphatidylinositols (PIs) within kidney sections, while CMBT yielded lower intensity images. Although detecting some low-abundance phosphoinositides proved challenging, it was achievable using CMBT and 9AA matrices. The findings suggest that a matrix mixture of DAN, 9AA, and CMBT may have the potential to improve phosphoinositide mapping by increasing signal intensity. However, there are several avenues for future work and improvements in this area. First, further optimization of matrix composition may be explored to enhance the detection sensitivity of low-abundance phosphoinositides. Additionally, the study can be expanded to investigate phosphoinositide distributions in other tissues or disease models to gain a comprehensive understanding of their roles in various cellular processes and disease pathogenesis. The findings contribute to the advancement of lipidomics research and provide a foundation for future studies in this field.

Moving forward with using data obtained from Chapters 4 and 5, further investigations will be warranted to uncover the underlying mechanisms involved in the context of DGKE

nephropathy, a rare pediatric kidney disease and the pathophysiological significance of phosphoinositide alterations in collaboration with Dr. Mathieu Lemaire from the University of Toronto, Department of Pediatrics. The aim will be to contribute to a better understanding of the pathophysiology of this disease, leading to improved clinical care and the development of targeted therapeutic approaches.

The proposed future work will include conducting MALDI-MSI and LC-MS analyses of mouse kidney models, comparing wild type and knockout samples. The goal will be to differentiate the compound composition in different kidney samples, particularly in relation to phosphoinositides. Successful discoveries in these analyses will be followed by characterization and quantification experiments to gain deeper insights into the nephropathy. Additionally, the potential associations between phosphoinositide abnormalities and other diseases, such as nervous system diseases, cancer, inflammation, thrombosis-related diseases, immune system diseases, and acute renal inefficiency in infancy, can be explored using the obtained data. Furthermore, the characterization of the phosphoinositide landscape in the kidneys, with a specific focus on glomeruli, will be crucial. This can be achieved through MALDI-MSI and higher resolution imaging techniques, enabling the visualization and assessment of phosphoinositide levels in various tissues.

Bibliography

[1] G. Münzenberg, "Development of mass spectrometers from Thomson and Aston to present," *International Journal of Mass Spectrometry,* Vols. 349-350, pp. 9-18, 2013.

[2] J. J. Thomson, "Cathode Rays (Reprinted from Philosophical Magazine Series 5, vol 44, pg 293-316, 1897)," *Philosophical magazine,* vol. 90, pp. 25-29, 2010.

[3] K. Wien, "100 Years of Ion Beams: Willy Wien's Canal Rays," *Brazilian Journal of Physics,* vol. 29, no. 3, pp. 401-414, 1999.

[4] J. M. Wiseman, D. R. Ifa, Q. Song and R. G. Cooks, "Tissue Imaging at Atmospheric Pressure Using Desorption Electrospray Ionization (DESI) Mass Spectrometry," *Angewandte Chemie,* vol. 118, no. 43, pp. 7346-7350, 2006.

[5] H. H. Willard, L. L. Merritt, J. A. Dean and F. A. Settle, Instrumental methods of analysis (7th ed.), California: Wadsworth Publishing Co., 1988.

[6] C. S. Ho, C. K. Lam, M. M. Chan, R. K. Cheung, L. K. Law, L. W. Lit, K. F. Ng, M. M. Suen and H. L. Tai, "Electrospray Ionisation Mass Spectrometry: Principles and Clinical Applications," *The Clinical biochemist. Reviews,* vol. 24, no. 1, pp. 3-12, 2003.

[7] J. W. Robinson, E. M. Frame and G. M. Frame, Undergraduate instrumental analysis (6th ed.), New York: Marcel Dekker, 2005.

[8] A. Zhang, X. Zhou, H. Zhao, S. Zou, C. W. Ma, Q. Liu, H. Sun, L. Liu and X. Wang, "Metabolomics and proteomics technologies to explore the herbal preparation affecting metabolic disorders using high resolution mass spectrometry," *Molecular BioSystems,* vol. 13, pp. 320-329, 2017.

[9] J. B. Fenn, "Electrospray wings for molecular elephants (Nobel lecture)," *Angewandte Chemie,* vol. 42, pp. 3871-3894, 2003.

[10] J. B. Fenn, M. Mann, C. K. Meng, S. F. Wong and C. M. Whitehouse, "Electrospray Ionization for Mass Spectrometry of Large Biomolecules," *American Association for the Advancement of Science,* vol. 246, no. 4926, pp. 64-71, 1989.

[11] S. Banerjee and s. Mazumdar, "Electrospray Ionization Mass Spectrometry: A Technique to Access the Information beyond the Molecular Weight of the Analyte," *International Journal of Analytical Chemistry,* vol. 2012, pp. 1-40, 2012.

[12] L. Konermann, E. Ahadi, A. D. Rodriguez and S. Vahidi, "Unraveling the Mechanism of Electrospray Ionization," *Analytical Chemistry,* vol. 85, no. 1, pp. 2-9, 2013.

[13] D. Gode and D. A. Volmer, "Lipid imaging by mass spectrometry – a review," *Analyst,* vol. 138, pp. 1289-1315, 2013.

[14] L. S. Eberlin, X. Liu, C. R. Ferreira, S. Santagata, N. Y. Agar and G. R. Cooks, "Desorption Electrospray Ionization then MALDI Mass Spectrometry Imaging of Lipid and Protein Distributions in Single Tissue Sections," *Analytical chemistry,* vol. 83, no. 22, pp. 8366-8371, 2011.

[15] D. S. Cornett, M. L. Reyzer, P. Chaurand and R. M. Caprioli, "MALDI imaging mass spectrometry: molecular snapshots of biochemical systems," *NATURE METHODS,* vol. 4, no. 10, pp. 828-833, 2007.

[16] M.-Z. Huang, S.-C. Cheng, Y.-T. Cho and J. Shiea, "Ambient ionization mass spectrometry: A tutorial," *Analytica Chimica Acta,* vol. 702, no. 1, pp. 1-15, 2011.

[17] Z. Takáts, J. M. Wiseman and R. G. Cook, "Ambient mass spectrometry using desorption electrospray ionization (DESI): Instrumentation, mechanisms and applications in forensics, chemistry, and biology," *Journal of Mass Spectrometry,* vol. 40, no. 10, pp. 1261-1275, 2005.

[18] Z. Takáts, J. M. Wiseman, B. Gologan and G. R. Cooks, "Mass Spectrometry Sampling Under Ambient Conditions with Desorption Electrospray Ionization," *Science,* vol. 306, pp. 471-473, 2004.

[19] M. E. Monge, G. A. Harris, P. Dwivedi and F. M. Fernández, "Mass Spectrometry: Recent Advances in Direct Open Air Surface Sampling/Ionization," *Chemical Reviews,* vol. 113, no. 4, pp. 2269-2308, 2013.

[20] W. J. Perry, N. H. Patterson, B. M. Prentice, E. K. Neumann, R. M. Caprioli and J. M. Spraggins, "Uncovering matrix effects on lipid analyses in MALDI imaging mass spectrometry experiments," *Journal of Mass Spectrometry,* vol. 55, pp. 1-11, 2019.

[21] F. Hillenkamp, M. Karas, R. C. Beavis and B. T. Chait, "Matrix-Assisted Laser Desorption/lonization Mass Spectrometry of Biopolymers," *Analytical Chemistry,* vol. 63, no. 24, pp. 1193-1203, 1991.

[22] T. C. Rohner, D. Staab and M. Stoeckli, "MALDI mass spectrometric imaging of biological tissue sections," *Mechanisms of Ageing and Development,* vol. 126, pp. 177-185, 2005.

[23] P. Chaurand, S. A. Schwartz, M. L. Reyzer and R. M. Caprioli, "Imaging Mass Spectrometry: Principles and Potentials," *Toxicologic Pathology,* vol. 33, no. 1, pp. 92-101, 2005.

[24] M. Stoeckli, P. Chaurand, D. E. Hallahan and R. M. Caprioli, "Imaging mass spectrometry: A new technology for the analysis of protein expression in mammalian tissues," *Nature Medicine,* vol. 7, no. 4, pp. 493-496, 2001.

[25] A. Pfenninger, M. Karas, B. Finke, B. Stahl and G. Sawatzki, "Matrix optimization for matrix-assisted laser desorption/ionization mass spectrometry of oligosaccharides from human milk," *Journal of Mass Spectrometry,* vol. 34, no. 2, pp. 98-104, 1999.

[26] R. Fernández, J. Garate, L. Martín-Saiz, I. Galetich and J. A. Fernández, "Matrix Sublimation Device for MALDI Mass Spectrometry Imaging," *Analytical Chemistry,* vol. 91, pp. 803-807, 2019.

[27] J. A. Hankin, R. M. Barkley and R. C. Murphy, "Sublimation as a Method of Matrix Application for Mass Spectrometric Imaging," *Journal of the American Society for Mass Spectrometry,* vol. 18, no. 9, pp. 1646-1652, 2007.

[28] H.-R. Aerni, D. S. Cornett and R. M. Caprioli, "Automated Acoustic Matrix Deposition for MALDI Sample Preparation," *Analytical Chemistry,* vol. 78, no. 3, pp. 827-834, 2006.

[29] J. C. Jurchen, S. S. Rubakhin and J. V. Sweedler, "MALDI-MS Imaging of features smaller than the size of the laser beam," *Journal of the American Society for Mass Spectrometry,* vol. 16, no. 10, pp. 1654-1659, 2005.

[30] T. Yu, Y. Luo and K. Yang, "Rapid characterization of N-linked glycosylation site using non-specific protease digestion of gel-separated glycoproteins and matrix-assisted laser

desorption/ ionization tandem time-of-flight mass spectrometry," *EUROPEAN JOURNAL OF MASS SPECTROMETRY,* vol. 17, no. 6, pp. 573-579, 2011.

[31] M. Karas, D. Bachmann, U. Bahr and F. Hillenkamp, "Matrix-assisted ultraviolet laser desorption of non-volatile compounds," *International Journal of Mass Spectrometry and Ion Processes,* vol. 78, no. 24, pp. 53-68, 1987.

[32] E. Lehmann, R. Knochenmuss and R. Zenobi, "Ionization mechanisms in matrix-assisted laser desorption/ionization mass spectrometry: contribution of pre-formed ions," *Rapid Communications in Mass Spectrometry,* vol. 11, no. 14, pp. 1483-1492, 1997.

[33] R. Zenobi and R. Knochenmuss, "Ion formation in MALDI mass spectrometry," *Mass Spectrometry Reviews,* vol. 17, no. 5, pp. 337-366, 1998.

[34] Y. J. Bae, Y. S. Shin, J. H. Moon and M. S. Kim, "Degree of Ionization in MALDI of Peptides: Thermal Explanation for the Gas-Phase Ion Formation," *Journal of The American Society for Mass Spectrometry,* vol. 23, no. 8, pp. 1326-1335, 2012.

[35] M. Karas, M. Glückmann and J. Schäfer, "Ionization in matrix-assisted laser desorption/ionization: singly charged molecular ions are the lucky survivors," *Journal of Mass Spectrometry,* vol. 35, no. 1, pp. 1-12, 2000.

[36] T. W. Jaskolla and M. Karas, "Compelling Evidence for Lucky Survivor and Gas Phase Protonation: The Unified MALDI Analyte Protonation Mechanism," *Journal of the American Society for Mass Spectrometry,* vol. 22, no. 6, pp. 976-988, 2011.

[37] Thermo Electron Corporation, "Finnigan™ LTQ™ Hardware Manual, Revision B," pp. 1-206, 2005.

[38] Thermo Fisher Scientific, "Exactive series operating manual," pp. 1-258, 2017.

[39] C. Zhao, P. Xie, T. Yong, H. Wang, A. C. K. Chung and Z. Cai, "MALDI-MS Imaging Reveals Asymmetric Spatial Distribution of Lipid Metabolites from Bisphenol S-Induced Nephrotoxicity," *Analytical Chemistry,* vol. 90, no. 5, pp. 3196-3204, 2018.

[40] B. H. Falkenburger, J. B. Jensen, E. J. Dickson, B.-C. Suh and B. Hille, "Phosphoinositides: lipid regulators of membrane proteins," *The Journal of Physiology,* pp. 3179-3185, 2010.

[41] P. Raghu, A. Joseph, H. Krishnan, P. Singh and S. Saha, "Phosphoinositides: Regulators of Nervous System Function in Health and Disease," *Frontiers in Molecular Neuroscience,* vol. 12, pp. 1-26, 2019.

[42] D. Kong and T. Yamori, "ZSTK474 is an ATP-competitive inhibitor of class I phosphatidylinositol 3 kinase isoforms," *Cancer Science,* vol. 98, no. 10, pp. 1638-1642, 2007.

[43] H. Enomoto, S. Takeda and H. Hatta, "Spatial Analysis of Phosphatidylinositol Molecular Species in Pork Chop Tissues Using Matrix-assisted Laser Desorption/ionization-Mass Spectrometry Imaging," *Journal of Oleo Science,* vol. 70, no. 7, pp. 979-987, 2021.

[44] M. Kawashima, M. Tokiwa, T. Nishimura, Y. Kawata, M. Sugimoto, T. R. Kataoka, T. Sakurai, K. Iwaisako, E. Suzuki, M. Hagiwara, A. L. Harris and M. Toi, "High-resolution imaging mass spectrometry combined with transcriptomic analysis identified a link between fatty acid composition of phosphatidylinositols and the immune checkpoint pathway at the primary tumour site of breast cancer," *British Journal of Cancer ,* vol. 122, pp. 245-257, 2020.

[45] R. M. Epand, V. So, W. Jennings, B. Khadka, R. S. Gupta and M. Lemaire, "Diacylglycerol Kinase-ε: Properties and Biological Roles," *Frontiers in Cell and Developmental Biology,* vol. 4, no. 112, pp. 1-18, 2016.

[46] K. A. Zemski Berry, J. A. Hankin, R. M. Barkley, J. M. Spraggins, R. M. Caprioli and R. C. Murphy, "MALDI Imaging of Lipid Biochemistry in Tissues by Mass Spectrometry," *Chemical Reviews,* vol. 111, no. 10, p. 6491–6512, 2011.

[47] D. G. Barrus, K. L. Capogrossi, S. C. Cates, C. K. Gourdet, N. C. Peiper, S. P. Novak, T. W. Lefever and J. L. Wiley, "Tasty THC: Promises and Challenges of Cannabis Edibles," Methods Report (RTI Press, Publication No. OP-0035-1611), Research Triangle Park, NC, 2016.

[48] M. Wang, Y.-H. Wang, B. Avula, M. M. Radwan, A. S. Wanas, Z. Mehmedic, J. v. Antwerp, M. A. ElSohly and I. A. Khan, "Quantitative Determination of Cannabinoids in Cannabis and Cannabis Products Using Ultra-High-Performance Supercritical Fluid Chromatography and Diode Array/Mass Spectrometric Detection," *Journal of Forensic Sciences,* vol. 62, no. 3, pp. 602-611, 2016.

[49] "Government of Canada, Department of justice," [Online]. Available: http://www.justice.gc.ca/eng/cj-jp/cannabis/. [Accessed 31 October 2018].

[50] X. Wang, M. J. Telepchak, J. Searfoss and D. Mackowsky, "Determination of Cannabinoid Content and Pesticide Residues in Cannabis Edibles and Beverages," *LCGC ,* vol. 30, no. 6, pp. 16-21, 2017.

[51] J. Cochran, A. Rigdon, J. Kowalski, G. Fagras, J. H. Dahl and D. Laine, "Evaluation of Modified QuEChERS for Pesticide Analysis in Cannabis," *LCGC,* vol. 35, no. 5, pp. 8-22, 2017.

[52] A. G. Harrison and R. J. Cotter, "Methods of ionization," *Methods in Enzymology,* vol. 193, pp. 3-37, 1990.

[53] A. Leghissa, Z. L. Hildenbrand and K. A. Schug, "Choosing Analytical Tools to Assess Complex Cannabis-Infused Matrices," *Cannabis Science and Technology,* vol. 1, no. 1, pp. 24-35, 2018.

[54] D. E. Raynie, "General Application of QuEChERS Extraction in the Isolation of Cannabinoids," *Cannabis Science and Technology,* vol. 1, no. 1, pp. 58-60, 2018.

[55] J. F. García-Reyes, A. U. Jackson, A. Molina-Díaz and G. R. Cooks, "Desorption Electrospray Ionization Mass Spectrometry for Trace Analysis of Agrochemicals in Food," *Analytical Chemistry,* vol. 81, no. 2, pp. 820-829, 2009.

[56] S. C. Nanita and L. G. Kaldon, "Emerging flow injection mass spectrometry methods for high-throughput quantitative analysis," *Analytical and Bioanalytical Chemistry,* vol. 408, no. 1, pp. 23-33, 2016.

[57] Q. Meng, B. Buchanan, J. Zuccolo, M.-M. Poulin, J. Gabriele and D. C. Baranowski, "A reliable and validated LC-MS/MS method for the simultaneous quantification of 4 cannabinoids in 40 consumer products," *Plos One,* vol. 13, no. 5, pp. 1-16, 2018.

[58] N. E. Manicke, T. Kistler, D. R. Ifa, G. Cooks and Z. Ouyang, "High-throughput quantitative analysis by desorption electrospray ionization mass spectrometry," *Journal of the American Society for Mass Spectrometry,* vol. 20, no. 2, pp. 321-325, 2009.

[59] C. B. Lietz, E. Gemperline and L. Li, "Qualitative and quantitative mass spectrometry imaging of drugs and metabolites," *Advanced Drug Delivery Reviews,* vol. 65, no. 8, pp. 1074-1085, 2013.

[60] A. Badu-Tawiah and G. R. Cooks, "Enhanced ion signals in desorption electrospray ionization using surfactant spray solutions," *Journal of the American Society for Mass Spectrometry,* vol. 21, no. 8, pp. 1423-1431, 2010.

[61] T. J. Kauppila, N. Talaty, T. Kuuranne, T. Kotiaho, R. Kostiainen and G. R. Cooks, "Rapid analysis of metabolites and drugs of abuse from urine samples by desorption electrospray ionization-mass spectrometry," *Analyst,* vol. 132, no. 9, pp. 868-875, 2007.

[62] G. J. Van Berkel, B. A. Tomkins and V. Kertesz, "Thin-Layer Chromatography/Desorption Electrospray Ionization Mass Spectrometry: Investigation of Goldenseal Alkaloids," *Analytical Chemistry,* vol. 79, no. 7, pp. 2778-2789, 2007.

[63] P. Sharma, P. Murthy and S. M. Bharath, "Chemistry, Metabolism, and Toxicology of Cannabis: Clinical Implications," *Iranian Journal of Psychiatry,* vol. 7, no. 4, pp. 149-156, 2012.

[64] D. R. Ifa, N. E. Manicke, A. L. Dill and G. R. Cooks, "Latent Fingerprint Chemical Imaging by Mass Spectrometry," *Science,* vol. 321, no. 5890, p. 805, 2008.

[65] B. C. Smith, "Inter-lab variation in the cannabis industry, Part I: problem and causes," Cannabis Science and Technology, 2019. [Online]. Available: http://www.cannabissciencetech.com/authors/brian-c-smith. [Accessed 8 May 2019].

[66] A. M. Stolker, J. van Schoonhoven, A. J. de Vries, I. Bobeldijk-Pastorova, W. H. Vaes and R. van den Berg, "Determination of cannabinoids in cannabis products using liquid chromatography–ion trap mass spectrometry," *Journal of Chromatography A,* vol. 1058, no. 1-2, pp. 143-151, 2004.

[67] J. Broséus, F. Anglada and P. Esseiva, "The differentiation of fibre- and drug type Cannabis seedlings by gas chromatography/mass spectrometry and chemometric tools," *Forensic Science International,* vol. 200, no. 1-3, pp. 87-92, 2010.

[68] C. Citti, G. Ciccarella, D. Braghiroli, C. Parenti, M. A. Vandelli and G. Cannazza, "Medicinal cannabis: Principal cannabinoids concentration and their stability evaluated by a high performance liquid chromatography coupled to diode array and quadrupole time of flight mass spectrometry method," *Journal of Pharmaceutical and Biomedical Analysis,* vol. 128, pp. 201-209, 2016.

[69] M. C. Gizzi, A. M. Bruno, C. C. Mulligan and C. R. Curtis, "The fourth amendment and the potential use of field-portable mass spectrometry systems in law enforcement," *Journal of Crime and Justice,* vol. 42, no. 3, pp. 316-330, 2019.

[70] C. C. Mulligan, N. Talaty and G. R. Cooks, "Desorption electrospray ionization with a portable mass spectrometer: in situ analysis of ambient surfaces," *Chemical Communications,* no. 16, pp. 1709-1711, 2006.

[71] A. Keil, N. Talaty, C. Janfelt, R. J. Noll, L. Gao, Z. Ouyang and G. R. Cooks, "Ambient Mass Spectrometry with a Handheld Mass Spectrometer at High Pressure," *Analytical Chemistry,* vol. 79, no. 20, pp. 7734-7739, 2007.

[72] Z. E. Lawton, A. Traub, W. L. Fatigante, J. Mancias, A. E. O'Leary, S. E. Hall, J. R. Wieland, H. Oberacher, M. C. Gizzi and C. C. Mulligan, "Analytical Validation of a

Portable Mass Spectrometer Featuring Interchangeable, Ambient Ionization Sources for High Throughput Forensic Evidence Screening," *Journal of the American Society for Mass Spectrometry,* vol. 28, no. 6, pp. 1048-1059, 2017.

[73] A. M. Bruno, S. R. Cleary, A. E. O'Leary, M. C. Gizzi and C. C. Mulligan, "Balancing the utility and legality of implementing portable mass spectrometers coupled with ambient ionization in routine law enforcement activities," *Analytical Methods,* vol. 9, no. 34, pp. 5015-5022, 2017.

[74] R. Peshin and A. K. Dhawan, "Integrated Pest Management: Innovation-Development Process," Berlin/Heidelberg, Germany, Springer Science & Business Media, 2009, pp. 83-87.

[75] Y. Yang and S. Suh, "Changes in environmental impacts of major crops in the US," *Environmental Research Letters,* vol. 10, p. 094016, 2015.

[76] C. Mitchell, R. M. Brennan, J. Graham and A. J. Karley, "Plant Defense against Herbivorous Pests: Exploiting Resistance and Tolerance Traits for Sustainable Crop Protection," *Frontiers in Plant Science,* vol. 7, pp. 1-8, 2017.

[77] F. Huang, D. A. Andow and L. L. Buschman, "Success of the high-dose/refuge resistance management strategy after 15 years of Bt crop use in North America," *Entomologia Experimentalis et Applicata,* vol. 140, no. 1, pp. 1-16, 2011.

[78] N. Storer, G. D. Thompson and G. P. Head, "Application of pyramided traits against Lepidoptera in insect resistance management for Bt crops," *GM Crops and Food,* vol. 3, no. 3, pp. 154-162, 2012.

[79] W. Parrott, D. Walker, S. Zhu, R. H. Boerma and J. All, "Genomics of Insect-Soybean Interactions," in *Genetics and Genomics of Soybean*, Berlin/Heidelberg, Germany, Springer, 2008, pp. 269-291.

[80] B. G. Rector, J. N. All, W. A. Parrott and H. R. Boerma, "Identification of molecular markers linked to quantitative trait loci for soybean resistance to corn earworm," *Theoretical and Applied Genetics,* vol. 96, pp. 786-790, 1998.

[81] B. G. Rector, J. N. All, W. A. Parrott and H. R. Boerma, "Quantitative Trait Loci for Antibiosis Resistance to Corn Earworm in Soybean," *Cell Biology and Molecular Genetic,* vol. 40, no. 1, pp. 233-238, 2000.

[82] A. L. Lourenção, M. A. Miranda, J. C. Pereira and G. Ambrosano, "Resistência de soja a insetos: X. Comportamento de cultivares e linhagens em relação a percevejos e desfolhadores," *Anais da Sociedade Entomológica do Brasil,* vol. 26, pp. 543-550, 1997.

[83] J. M. Narvel, D. R. Walker, B. G. Rector, J. N. All, W. A. Parrott and R. H. Boerma, "A Retrospective DNA Marker Assessment of the Development of Insect Resistant Soybean," *Crop Science,* vol. 41, no. 6, pp. 1931-1939, 2001.

[84] K. Komatsu, M. Takahashi and Y. Nakazawa, "Antibiosis Resistance of QTL Introgressive Soybean Lines to Common Cutworm (Spodoptera litura Fabricius)," *Crop Science,* vol. 48, no. 2, pp. 527-532, 2008.

[85] N. Oki, K. Komatsu, T. Sayama, M. Ishimoto, M. Takahashi and M. Takahashi, "Genetic analysis of antixenosis resistance to the common cutworm (Spodoptera litura Fabricius) and its relationship with pubescence characteristics in soybean (Glycine max (L.) Merr.)," *Breeding Science,* vol. 61, no. 5, pp. 608-617, 2012.

[86] L. I. Terry, K. Chase, T. Jarvik, J. Orf, L. Mansur and K. G. Lark, "Soybean Quantitative Trait Loci for Resistance to Insects," *Crop Science,* vol. 40, no. 2, pp. 375-382, 2000.

[87] M. A. Ortega, L. A. Lail, D. E. Wood, J. N. All, Z. Li, R. H. Boerma and W. A. Parrott, "Registration of Two Soybean Germplasm Lines Containing Leaf-Chewing Insect Resistance QTLs from PI 229358 and PI 227687 Introgressed into 'Benning'," *Journal of Plant Registrations,* vol. 11, no. 2, pp. 185-191, 2017.

[88] M. C. Smith and N. H. Fischer, "Chemical Factors of an Insect Resistant Soybean Genotype Affecting Growth and Survival of the Soybean Looper," *Entomologia Experimentalis et Applicata,* vol. 33, no. 3, pp. 343-345, 1983.

[89] A. Jahan, B. Harris, M. Lowery, A. M. Infante, R. J. Percifield and N. Kovinich, "Glyceollin Transcription Factor GmMYB29A2 Regulates Soybean Resistance to Phytophthora sojae," *Plant Physiology,* vol. 183, no. 2, pp. 530-546, 2020.

[90] A. V. Lygin, C. B. Hill, O. V. Zernova, L. Crull, J. M. Widholm, G. L. Hartman and V. V. Lozovaya, "Response of Soybean Pathogens to Glyceollin," *Phytopathology,* vol. 100, no. 9, pp. 897-903, 2010.

[91] J. A. Veech, "Phytoalexins and their Role in the Resistance of Plants to Nematodes," *The Journal of Nematology,* vol. 14, no. 1, pp. 2-9, 1982.

[92] S. V. Hart, M. Kogan and J. D. Paxton, "Effect of soybean phytoalexins on the herbivorous insects mexican bean beetle and soybean looper," *Journal of Chemical Ecology,* vol. 9, pp. 657-672, 1983.

[93] P. Caballero and M. C. Smith, "ISOFLAVONES FROM AN INSECT-RESISTANT VARIETY OF SOYBEAN AND THE MOLECULAR STRUCTURE OF AFRORMOSIN," *Journal of Natural Products,* vol. 49, no. 6, pp. 1126-1129, 1986.

[94] H. C. Sharma and D. M. Norris, "Chemical basis of resistance in soya bean to cabbage looper, Trichoplusia ni," *Journal of the Science of Food and Agriculture,* vol. 55, no. 3, pp. 353-364, 1991.

[95] S. Liu, D. M. Norris, E. E. Hartwig and M. Xu, "Inducible Phytoalexins in Juvenile Soybean Genotypes Predict Soybean Looper Resistance in the Fully Developed Plants," *Plant Physiology,* vol. 100, no. 3, pp. 1479-1485, 1992.

[96] S. Liu, D. M. Norris and M. Xu, "Insect Resistance and Glyceollin Concentration in Seedling Soybeans Support Resistance Ratings of Fully Developed Plants," *Journal of Economic Entomology,* vol. 86, no. 2, pp. 401-406, 1993.

[97] G. C. Piubelli, C. B. Hoffmann-Campo, F. Moscardi, S. H. Miyakubo and M. C. De Oliveira, "Are Chemical Compounds Important for Soybean Resistance to Anticarsia gemmatalis?," *Journal of Chemical Ecology,* vol. 31, pp. 1509-1525, 2005.

[98] C. B. Hoffmann-Campo, J. A. Ramos Neto, M. C. De Oliveira and L. J. Oliveira, "Detrimental effect of rutin on Anticarsia gemmatalis," *Base de Dados da Pesquisa Agropecuária (BDPA) ,* vol. 41, pp. 1453-1459, 2006.

[99] Y. Wang, H. Wang, R. Fan, Q. Yang and D. Yu, "Transcriptome analysis of soybean lines reveals transcript diversity and genes involved in the response to common cutworm (Spodoptera litura Fabricius) feeding," *Plant, Cell and Environment,* vol. 37, no. 9, pp. 2086-2101, 2014.

[100] Y. Wang, H. Wang, Y. Ma, W. Yang, Q. Yang and D. Yu, "Identification of soybean herbivory-regulated genes and a transgenic investigation of their potential in insect resistance," *Plant Cell, Tissue and Organ Culture,* vol. 123, pp. 321-340, 2015.

[101] G. Zhao, Z. Jiang, D. Li, Y. Han, H. Hu, L. Wu, Y. Wang, Y. Gao, W. Teng, Y. Li, G. Zeng, F. Meng and W. Li, "Molecular loci associated with seed isoflavone content may underlie resistance to soybean pod borer (Leguminivora glycinivorella)," *Plant Breeding,* vol. 134, no. 1, pp. 78-84, 2015.

[102] J. D. Gómez, C. E. Vital, M. G. Oliveira and H. J. Ramos, "Broad range flavonoid profiling by LC/MS of soybean genotypes contrasting for resistance to Anticarsia gemmatalis (Lepidoptera: Noctuidae)," *Plos One,* vol. 13, pp. 1-24, 2018.

[103] J. D. Gómez, V. J. Pinheiro, J. C. Silva, J. V. Romero, Y. Meriño-Cabrera, F. S. Coutinho, A. L. Lourenção, J. E. Serrão, C. E. Vital, E. P. Fontes, M. G. Oliveira and H. J. Ramos, "Broad range flavonoid profiling by LC/MS of soybean genotypes contrasting for resistance to Anticarsia gemmatalis (Lepidoptera: Noctuidae)," *Plant Physiology and Biochemistry,* vol. 155, pp. 196-212, 2020.

[104] C. R. Yesudas, H. Sharma and D. A. Lightfoot, "Identification of QTL in soybean underlying resistance to herbivory by Japanese beetles (Popillia japonica, Newman)," *Theoretical and Applied Genetics,* vol. 121, pp. 353-362, 2010.

[105] B. F. O'Neil, A. R. Zangerl, O. Dermody, D. D. Bilgin, C. L. Casteel, J. A. Zavala, E. H. DeLucia and M. R. Berenbaum, "Impact of Elevated Levels of Atmospheric CO2 and Herbivory on Flavonoids of Soybean (Glycine max Linnaeus)," *Journal of Chemical Ecology,* vol. 36, pp. 35-45, 2010.

[106] W. T. Hay, R. W. Behle, M. A. Berhow, A. C. Miller and G. W. Selling, "Biopesticide synergy when combining plant flavonoids and entomopathogenic baculovirus," *Scientific Reports,* vol. 10, pp. 1-9, 2020.

[107] J. D. Hohenstein, M. E. Studham, A. Klein, N. Kovinich, K. Barry, Y.-J. Lee and G. C. MacIntosh, "Transcriptional and Chemical Changes in Soybean Leaves in Response to Long-Term Aphid Colonization," *Frontiers in Plant Science,* vol. 10, pp. 1-18, 2019.

[108] S. Kikuta, "The Cytotoxic Effect of Genistein, a Soybean Isoflavone, against Cultured Tribolium Cells," *Insects,* vol. 11, no. 4, p. 241, 2020.

[109] I. Sabljic, J. A. Barneto, K. B. Balestrasse, J. A. Zavala and E. A. Pagano, "Role of reactive oxygen species and isoflavonoids in soybean resistance to the attack of the southern green stink bug," *Peer J,* vol. 8, p. e9956, 2020.

[110] S. Murakami, R. Nakata, T. Aboshi, N. Yoshinaga, M. Teraishi, Y. Okumoto, A. Ishihara, H. Morisaka, A. Huffaker, E. A. Schmelz and N. Mori, "Insect-Induced Daidzein, Formononetin and Their Conjugates in Soybean Leaves," *Metabolites,* vol. 4, no. 3, pp. 532-546, 2014.

[111] R. Nakata, Y. Kimura, K. Aoki, N. Yoshinaga, M. Teraishi, Y. Okumoto, A. Huffaker, E. A. Schmelz and N. Mori, "Inducible De Novo Biosynthesis of Isoflavonoids in Soybean Leaves by Spodoptera litura Derived Elicitors: Tracer Techniques Aided by High Resolution LCMS," *Journal of Chemical Ecology,* vol. 42, pp. 1226-1236, 2016.

[112] D. J. Hulburt, R. H. Boerma and J. N. All, "Effect of Pubescence Tip on Soybean Resistance to Lepidopteran Insects," *Journal of Economic Entomology,* vol. 97, no. 2, pp. 621-627, 2004.

[113] E. Hollowell and H. Johnson, "Correlation between rough-hairy pubescence in soybean and freedom from injury by Empoasca fabae," *Phytopathology,* vol. 24, p. 12, 1934.

[114] H. Kanno, "Role of Leaf Pubescence in Soybean Resistance to the False Melon Beetle, Atrachya menetriesi FALDERMANN (Coleoptera: Chrysomelidae)," *Applied Entomology and Zoology,* vol. 31, no. 4, pp. 597-603, 1996.

[115] D. Hulburt, Identifying Additional Insect Resistance Quantitative Trait Loci in Soybean Using Simple Sequence Repeats. Master's Thesis, Athens, GA, USA: University of Georgia, 2002.

[116] C. L. Ting, "Genetic Studies on the Wild and Cultivated Soybeans," *Agronomy Journal,* vol. 38, no. 5, pp. 381-393, 1946.

[117] L. Lambert and T. C. Kilen, "Insect Resistance Factor in Soybean PI's 229358 and 227687 Demonstrated by Grafting," *Crop Science,* vol. 24, no. 1, pp. 163-165, 1984.

[118] W. R. Fehr, C. E. Caviness, D. T. Burmood and J. S. Pennington, "Stage of Development Descriptions for Soybeans, Glycine Max (L.) Merrill," *Crop Science,* vol. 11, no. 6, pp. 929-931, 1971.

[119] F. Allen, R. Greiner and D. Wishart, "Competitive fragmentation modeling of ESI-MS/MS spectra for putative metabolite identification," *Metabolomics,* vol. 11, pp. 98-110, 2015.

[120] C. A. Smith, G. O. Maille, E. J. Want, C. Qin, S. A. Trauger, T. R. Brandon, D. E. Custodio, R. Abagyan and G. Siuzdak, "METLIN: A Metabolite Mass Spectral Database," *Therapeutic Drug Monitoring,* vol. 27, no. 6, pp. 747-751, 2005.

[121] National Institute of Standards and Technology. EPA/NIH Mass Spectral Library, Gaithersburg, MD, USA: National Institute of Standards and Technology, 2014.

[122] F.-Q. Huang, X. Dong, X. Yin, Y. Fan, Y. Fan, C. Mao and W. Zhou, "A mass spectrometry database for identification of saponins in plants," *Journal of Chromatography A,* vol. 1625, p. 461296, 2020.

[123] I. Blaženovic, T. Kind, J. Ji and O. Fiehn, "Software Tools and Approaches for Compound Identification of LC-MS/MS Data in Metabolomics," *Metabolites,* vol. 8, no. 2, p. 31, 2018.

[124] N. Xu, Z.-H. Huang, J. T. Watson and D. A. Gagecor, "Mercaptobenzothiazoles: A new class of matrices for laser desorption ionization mass spectrometry," *Journal of the American Society for Mass Spectrometry,* vol. 8, no. 2, pp. 116-124, 1997.

[125] N. Xu, Z.-H. Huang, B. L. M. de Jonge and D. A. Gage, "Structural Characterization of Peptidoglycan Muropeptides by Matrix-Assisted Laser Desorption Ionization Mass Spectrometry and Postsource Decay Analysis," *Analytical Biochemistry,* vol. 248, no. 1, pp. 7-14, 1997.

[126] D. J. Evason, M. A. Claydon and D. B. Gordon, "Exploring the Limits of Bacterial Identification by Intact Cell-Mass Spectrometry," *Journal of the American Society for Mass Spectrometry ,* vol. 12, no. 1, pp. 49-54, 2001.

[127] W. Tang, A. Gordon, F. Wang, Y. Chen and B. Li, "Hydralazine as a Versatile and Universal Matrix for High-Molecular Coverage and Dual-Polarity Matrix-Assisted Laser Desorption/ Ionization Mass Spectrometry Imaging," *Analytical Chemistry,* vol. 93, no. 26, pp. 9083-9093, 2021.

[128] S. Caughlin, D. H. Park, K. K.-C. Yeung, D. F. Cechetto and S. N. Whitehead, "Sublimation of DAN Matrix for the Detection and Visualization of Gangliosides in Rat Brain Tissue for MALDI Imaging Mass Spectrometry," *Journal of Visualized Experiments,* no. 121, 2017.

[129] P. Chaurand, D. S. Cornett, P. M. Angel and R. M. Caprioli, "From Whole-body Sections Down to Cellular Level, Multiscale Imaging of Phospholipids by MALDI Mass Spectrometry," *Molecular & Cellular Proteomics,* vol. 10, no. 2, 2011.

[130] R. D. Cardiff, C. H. Miller and R. J. Munn, "Manual Hematoxylin and Eosin Staining of Mouse Tissue Sections," *Cold Spring Harbor Protocols,* no. 6, 2014.

[131] E. Moreno-Gordaliza, D. Esteban-Fernández, A. Lázaro, B. Humanes, S. Aboulmagd, A. Tejedor, M. W. Linscheid and M. M. Gómez-Gómez, "MALDI-LTQ-Orbitrap mass spectrometry imaging for lipidomic analysis in kidney under cisplatin chemotherapy," *Talanta,* vol. 164, pp. 16-26, 2017.

[132] B. Brügger, G. Erben, R. Sandhoff, F. T. Wieland and W. D. Lehmann, "Quantitative analysis of biological membrane lipids at the low picomole level by nano-electrospray ionization tandem mass spectrometry," *Proceedings of the National Academy of Sciences,* vol. 94, no. 6, pp. 2339-2344, 1997.

[133] S. S. Rubakhin, E. V. Romanova, P. Nemes and J. V. Sweedler, "Profiling metabolites and peptides in single cells," *Nature Methods,* vol. 8, pp. S20-S29, 2011.

[134] X. Zhu, T. Xu, C. Peng and S. Wu, "Advances in MALDI Mass Spectrometry Imaging Single Cell and Tissues," *Frontiers in Chemistry,* vol. 9, 2022.

[135] A. Thomas, J. L. Charbonneau, E. Fournaise and P. Chaurand, "Sublimation of New Matrix Candidates for High Spatial Resolution Imaging Mass Spectrometry of Lipids: Enhanced Information in Both Positive and Negative Polarities after 1,5-Diaminonapthalene Deposition," *Analytical Chemistry,* vol. 84, no. 4, pp. 2048-2054, 2012.

[136] A. Traynor-Kaplan, M. Kruse, E. J. Dickson, G. Dai, O. Vivas, H. Yu, D. Whittington and B. Hille, "Fatty-acyl chain profiles of cellular phosphoinositides," *Biochimica et Biophysica Acta (BBA) - Molecular and Cell Biology of Lipids,* vol. 1862, no. 5, pp. 513-522, 2017.

[137] O. Idevall-Hagren and P. De Camilli, "Detection and manipulation of phosphoinositides," *Biochimica et Biophysica Acta (BBA) - Molecular and Cell Biology of Lipids,* vol. 1851, no. 6, pp. 736-745, 2015.

[138] W. Szlasa, I. Zendran, A. Zalesińska, M. Tarek and J. Kulbacka, "Lipid composition of the cancer cell membrane," *Journal of Bioenergetics and Biomembranes,* vol. 52, pp. 321-342, 2020.

[139] K. Shrivas, T. Hayasaka, N. Goto-Inoue, Y. Sugiura, N. Zaima and M. Setou, "Ionic Matrix for Enhanced MALDI Imaging Mass Spectrometry for Identification of Phospholipids in Mouse Liver and Cerebellum Tissue Sections," *Analytical Chemistry ,* vol. 82, no. 21, pp. 8800-8806, 2010.

[140] R. C. Murphy, J. A. Hankin and R. M. Barkley, "Imaging of lipid species by MALDI mass spectrometry," *Journal of Lipid Research,* vol. 50, pp. S317-S322, 2009.

[141] M. Yousefi-Taemeh, E. Duli, L. G. Dabija, M. Lemaire and D. R. Ifa, "Sublimation application of 5-chloro-2-mercaptobenzothiazole (CMBT) matrix for MALDI mass spectrometry imaging (MSI) of mouse kidney," *Rapid communications,* 2023.

[142] H. Ruh, T. Salonikios, J. Fuchser, M. Schwartz, C. Sticht, C. Hochheim, B. Wirnitzer, N. Gretz and C. Hopf, "MALDI imaging MS reveals candidate lipid markers of polycystic kidney disease," *Journal of Lipid Research,* vol. 54, pp. 2785-2794, 2013.

[143] "Avanti Polar Lipids," [Online]. Available: https://avantilipids.com/. [Accessed 10 August 2022].

[144] H.-Y. J. Wang, S. N. Jackson and A. S. Woods, "Direct MALDI-MS Analysis of Cardiolipin from Rat Organs Sections," *Journal of the American Society for Mass Spectrometry,* vol. 18, no. 3, pp. 567-577, 2007.

APPENDICES

Appendix A. Supplementary materials for chapter 3

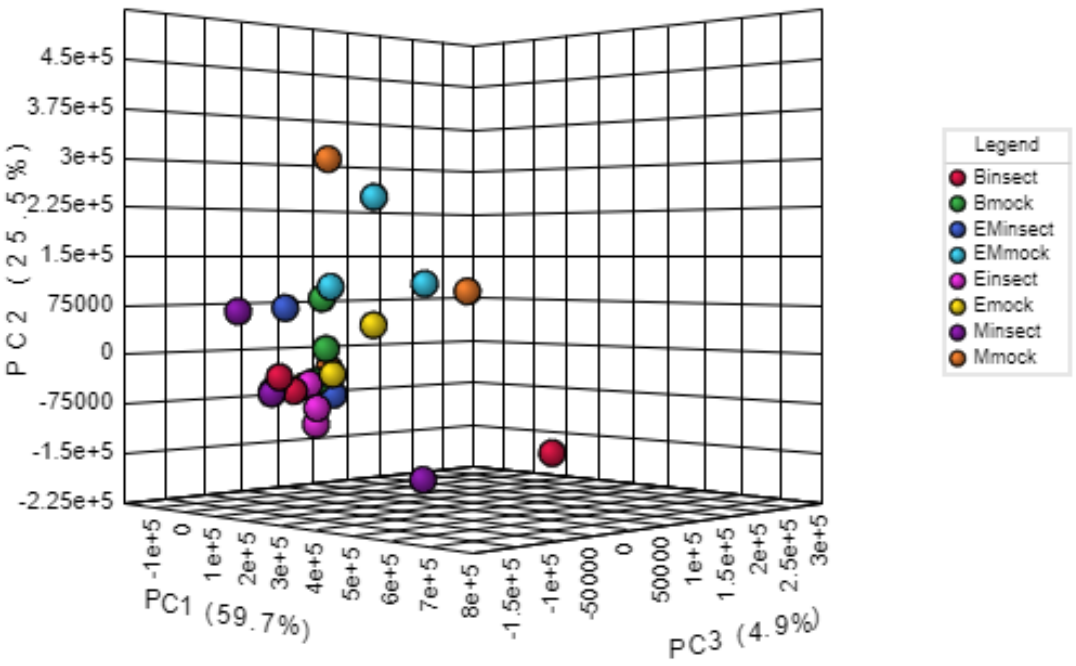

Figure A.1: Principal component (PCA) analysis of soybean genotypes harboring insect resistance QTLs E, M, and EM compared to the introgressed susceptible parent Benning. The analysis was based on 13,950 unique peaks identified by mass spectroscopy and was conducted using Metaboanalyst 5.0 (https://dev.metaboanalyst.ca/) filtering based on relative standard deviation (RSD).

Table A.1: MS peaks from insect-resistant QTLs that were significantly different from insect-susceptible parent Benning.[a] (The complete version of Table A.1 is available online at **https://www.mdpi.com/article/10.3390/metabo11100710/s1**.)

Treatment	Mock							Insect						
QTL	E	M	EM	E&M	E&EM	M&EM	E&M&EM	E	M	EM	E&M	E&EM	M&EM	E&M&EM
m/z [M+H]+	707.1	707.1	707.1	707.1	707.1	707.1	707.1	277	277	277	277	277	277	277
	707	707	707	707	707	707	707	276.9	276.9	276.9	276.9	276.9	276.9	276.9
	706.9	706.9	706.9	706.9	706.9	706.9	706.9	276.8	276.8	276.8	276.8	276.8	276.8	276.8
	664.8	664.8	664.8	664.8	664.8	664.8	664.8	276.7	276.7	276.7	276.7	276.7	276.7	276.7
	544	544	544	544	544	544	544	108.6	108.6	108.6	108.6	108.6	108.6	108.6
	514.9	514.9	514.9	514.9	514.9	514.9	514.9	1216.3	1216.3	339.5	1216.3	339.5	1064.6	
	244.8	244.8	244.8	244.8	244.8	244.8	244.8	121.3	121.3	326.7	121.3	326.7	1064.5	
	226.7	226.7	226.7	226.7	226.7	226.7	226.7	108.5	108.5	299.5	108.5	299.5	1064.4	
	226.6	226.6	226.6	226.6	226.6	226.6	226.6	339.5	1064.6	262.6		262.6	278	
	812.2	812.2	721.1	812.2	721.1	825.1		326.7	1064.5	246.3		246.3	277.2	
	810.9	810.9	541.7	810.9	541.7	725		299.5	1064.4	246.2		246.2	277.1	
	703.1	703.1	531.2	703.1	531.2	709		262.6	278	246.1		246.1	216.7	
	703	703	531.1	703	531.1	708.9		246.3	277.2	246		246	128.4	
	664.9	664.9	515.2	664.9	515.2	603.2		246.2	277.1	245.5		245.5	108.7	
	664.7	664.7	515.1	664.7	515.1	603.1		246.1	216.7	245.4		245.4	108.4	
	663.8	663.8	515	663.8	515	531		246	128.4	244.5		244.5		
	663.7	663.7	469.8	663.7	469.8	514.8		245.5	108.7	238.8		238.8		
	663.6	663.6	455.1	663.6	455.1	512.1		245.4	108.4	229.3		229.3		
	649.2	649.2	455	649.2	455	500		244.5	1462	217.2		217.2		
	649.1	649.1	384.2	649.1	384.2	499.9		238.8	1411.5	202.7		202.7		
	542.9	542.9	825.1	542.9		499.4		229.3	1385.9	202.6		202.6		
	495.1	495.1	725	495.1		499.3		217.2	1377.7	199.5		199.5		
	721.1	825.1	709			483.2		202.7	1350.8	199		199		
	541.7	725	708.9			483.1		202.6	1338	198.9		198.9		
	531.2	709	603.2			482.9		199.5	1337.9	198.7		198.7		
	531.1	708.9	603.1			469.1		199	1334.7	198.5		198.5		
	515.2	603.2	531			366.3		198.9	1334.6	197.5		197.5		
	515.1	603.1	514.8			366.2		198.7	1304.1	169.2		169.2		
	515	531	512.1			366.1		198.5	1304	168.8		168.8		
	469.8	514.8	500			366		197.5	1286.3	163.3		163.3		
	455.1	512.1	499.9			365.9		169.2	1286.2	140.8		140.8		
	455	500	499.4			349.8		168.8	1272.3	129.1		129.1		
	384.2	499.9	499.3			246.3		163.3	1272.2	129		129		

[a]Paired students T-test, $P<0.05$

Table A.2: Peak annotation and levels of confidence. (The full version of Table A.2 is available online at **https://www.mdpi.com/article/10.3390/metabo11100710/s1**.)

Appendix B. Supplementary materials for chapter 4

Figure B.1: The matrix sublimation apparatus. This system was constructed following the guidelines outlined in references [4], [13], and [14].

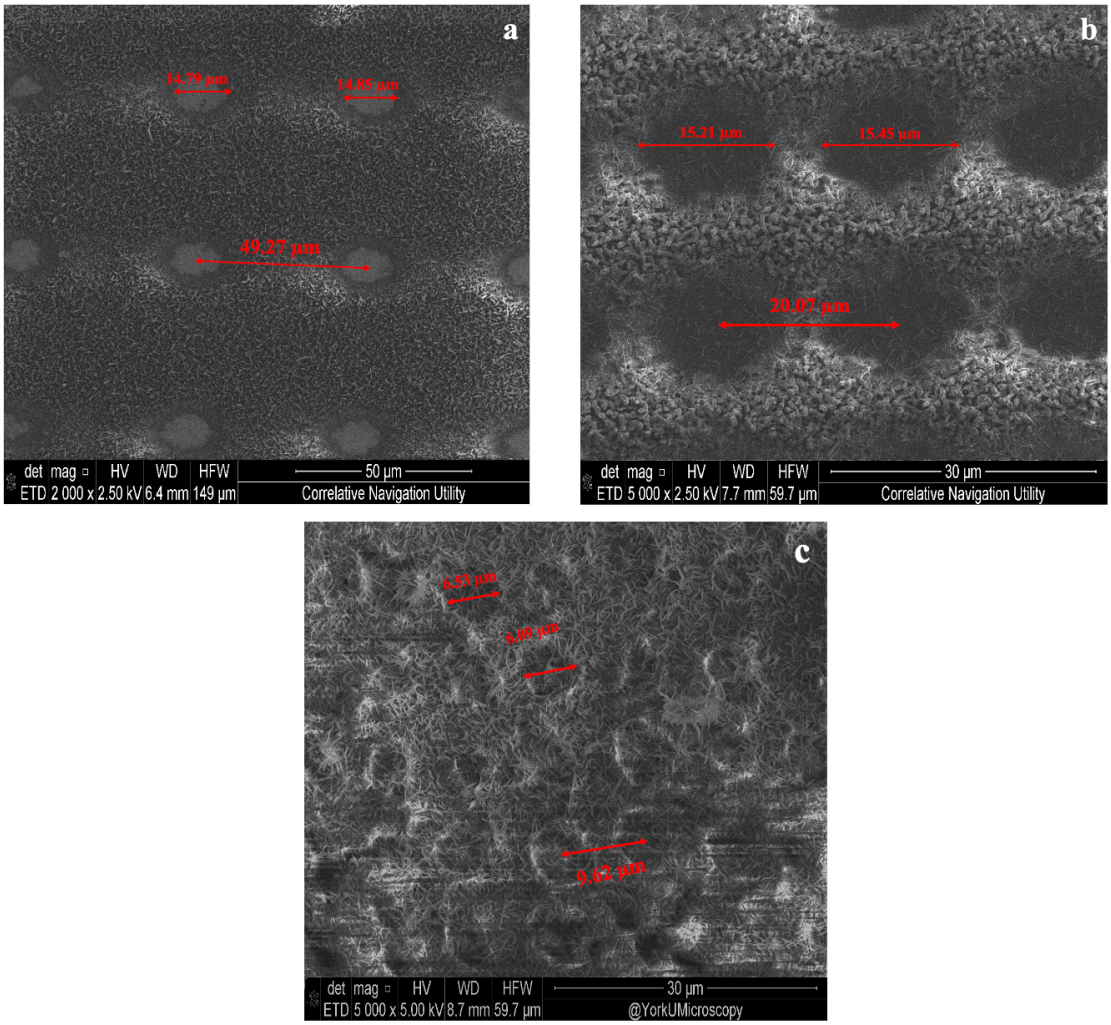

Figure B.2: Electron microscopy images were obtained to determine the laser spot sizes for MALDI-MSI analysis at (a) 50 µm, (b) 20 µm, and (c) 10 µm spatial resolutions. The average laser spot size for MALDI-MSI at 50 and 20 µm spatial resolutions was found to be approximately 15 µm. At a spatial resolution of 10 µm, the laser spot size is around 6.5 µm.

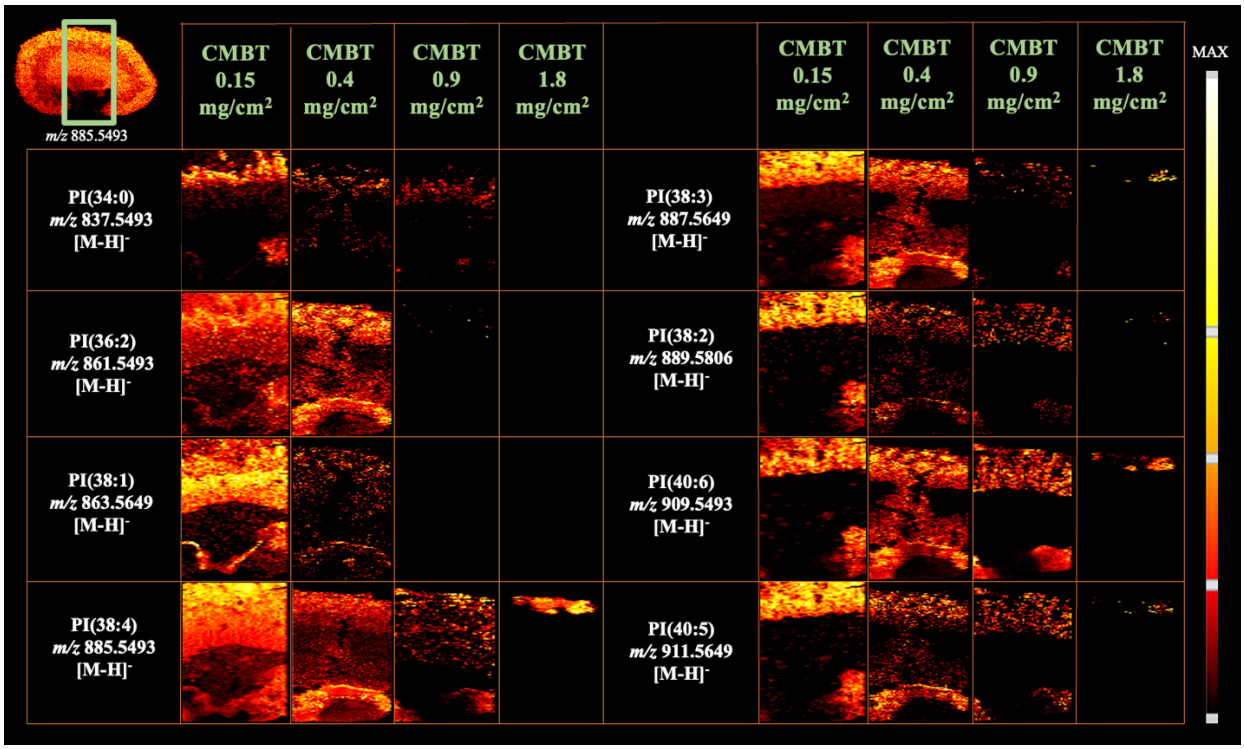

Figure B.3: Negative ion mode MALDI-MS imaging of coronal sections of mice kidney was performed using various thicknesses (mg/cm^2) of CMBT matrix as described in Appendix Table B.1. The green rectangle shows the area used for the comparison of various thicknesses. Here, some of the most important PIs are shown. It is important to note that the thickness of the matrix layer can significantly affect the quality and quantity of ions detected in MALDI-MSI. If the matrix layer is too thin, very few ions are detected, while if it is too thick, only matrix ions are detected. As a result, *m/z* images obtained using CMBT matrix thicknesses of 0.9 and 1.8 mg/cm^2 did not show distinguishable features and resulted in poor quality images due to excessive matrix coating. Conversely, *m/z* images obtained with less CMBT matrix coating of 0.15 and 0.4 mg/cm^2 showed more features and produced better quality images.

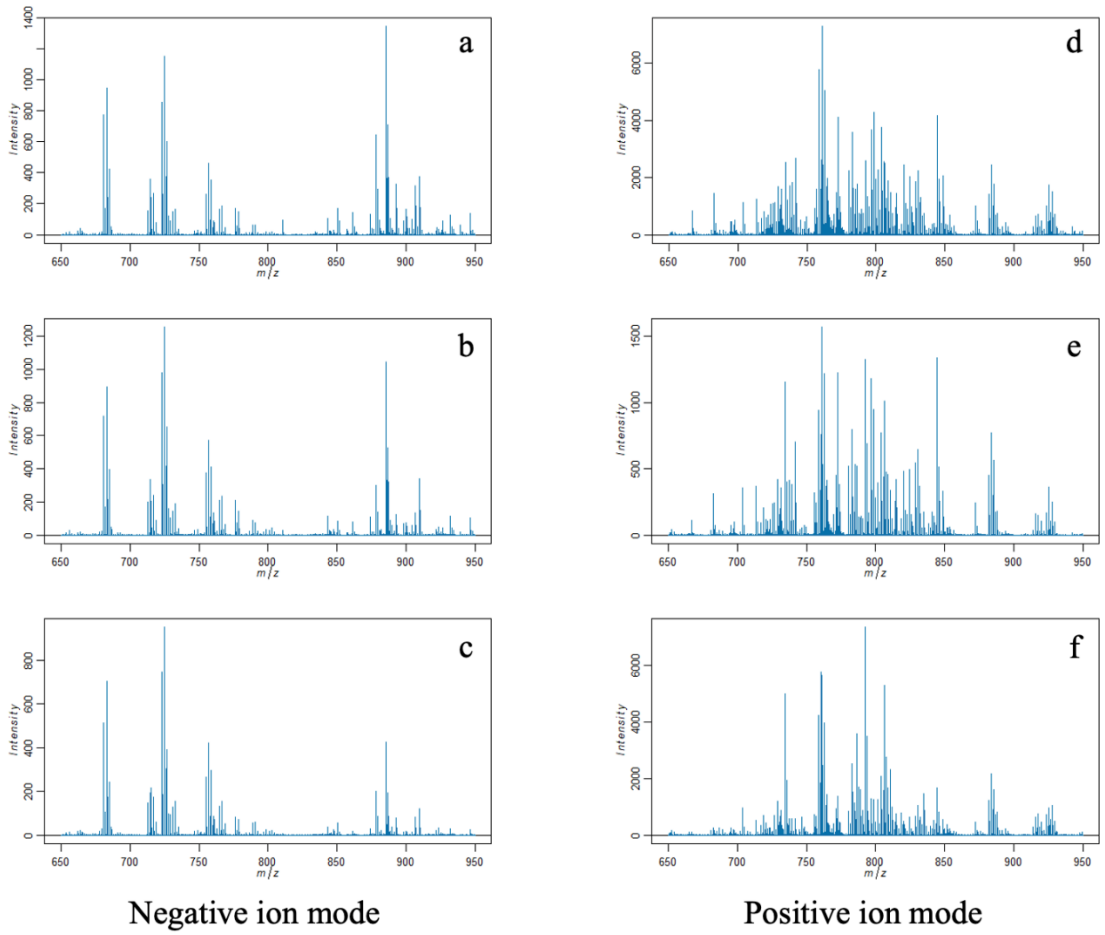

Figure B.4: Average mass spectra were obtained in both negative (a, b, & c) and positive (d, e, & f) ionization modes after CMBT matrix sublimation and MALDI image acquisition from biological triplicate coronal kidney tissue sections. In order to improve the clarity of the phospholipid region, a mass range of 650-950 *m/z* was selected for both positive mode and negative modes.

Table B.1: The estimated pressure, temperature, and time conditions necessary to achieve various CMBT matrix densities for coating the sample section before conducting MALDI-MSI analysis.

Matrix (mg)	Pressure (Torr)	Temperature (°C)	Time (minutes: seconds)	Thickness (mg/cm²)
~300	0.05	180	06:00	4.11
~300	0.05	180	03:30	1.10
~300	0.05	180	02:15	0.41
~300	0.05	180	01:45	0.35
~300	0.05	180	01:00	0.12
~300	0.05	175	08:40	1.95
~300	0.05	175	08:35	1.83
~300	0.05	175	08:30	1.23
~300	0.05	175	03:00	0.98
~300	0.05	175	02:00	0.33
~300	0.05	175	01:30	0.19
~300	0.05	175	01:20	0.12
~300	0.05	175	01:10	0.11
~300	0.05	175	01:00	0.10
~300	0.05	170	10:00	3.90
~300	0.05	170	09:00	2.19
~300	0.05	165	01:30	0.16
~300	0.05	165	01:15	0.11
Replicates				
~300	0.05	165	01:30	0.15
~300	0.05	165	01:30	0.15
~300	0.05	165	01:30	0.16
~300	0.05	165	01:30	0.15
~300	0.05	165	01.30	0.16

Table B.2: The calculated signal-to-noise ratio values for the biological triplicate MALDI-MSI of coronal kidney sections coated with CMBT matrix, as shown in Figure 4.2 and 4.3 for positive and negative ion polarities, respectively.

			Kidney-1		Kidney-2		Kidney-3	
	Compound	Adduct	Observed mass m/z	S/N	Observed mass m/z	S/N	Observed mass m/z	S/N
Figure 2	PC(34:2)	$[M+H]^+$	758.5703	240.2	758.5668	129.0	758.5672	488.5
	PC(34:1)	$[M+H]^+$	760.5843	422.9	760.5835	160.5	760.5828	802.0
	PC(36:4)	$[M+H]^+$	782.5708	556.1	782.5664	147.0	782.5668	465.9
	PC(36:3)	$[M+H]^+$	784.5819	112.6	784.5821	31.0	784.5834	177.3
	PC(36:2)	$[M+H]^+$	786.6012	248.5	786.6041	101.0	786.6002	455.2
	PG(38:4)	$[M+H]^+$	799.5518	270.0	799.5457	61.5	799.5465	59.7
	PC(38:6)	$[M+H]^+$	806.5708	290.7	806.5661	156.3	806.5673	504.1
	PC(38:5)	$[M+H]^+$	808.5816	262.7	808.5817	84.0	808.5828	245.5
	PG(38:4)	$[M+Na]^+$	821.5270	181.3	821.5291	36.2	821.5316	29.4
Figure 3	PI(38:4)	$[M-H]^-$	885.5513	232.3	885.5499	147.5	885.5469	134.0
	PI(38:3)	$[M-H]^-$	887.5606	62.2	887.5659	44.6	887.5621	24.4
	PI(40:7)	$[M-H]^-$	907.5381	35.7	907.5351	8.3	907.5312	5.6
	PI(40:6)	$[M-H]^-$	909.5450	62.1	909.5514	50.6	909.5471	18.2

Appendix C: Supplementary materials for chapter 5

Table C.1. Multiple matrix types and various coating densities were investigated to determine the optimal matrix thickness for achieving higher intensity phosphatidylinositol (PI) images in MALDI-MSI analysis.

Matrix	Thickness
9AA	0.08
9AA	0.094
9AA	0.33
9AA	0.48
9AA	0.74
CMBT	0.135
CMBT	0.33
CMBT	0.4
CMBT	0.9
CMBT	1.8
DAN	0.11
DAN	0.17
DAN	0.22
DAN	0.26
DAN	0.36
DAN	0.437
DAN	0.475

Table C.2: Below is a comprehensive list of phosphatidylinositols and phosphoinositides, along with their respective formulae, exact masses, potential charges and adduct types, as well as the anticipated m/z (mass-to-charge ratio) values.

Type	Chain unsaturation	Molecular formula	Exact mass	Charge	Adduct type	Negative ion mode m/z	Reference
PI	08:0/08:0 PI	C25H47O13P	586.2754	-1	[M-H]-	585.2676	Avanti polar lipids
	18:0/OH PI	C27H53O12P	600.327468	-1	[M-H]-	599.319643	Lipidmaps
	16:0/16:1 PI	C41H77O13P	808.510183	-1	[M-H]-	807.502358	HMDB
	16:0/16:0 PI	C41H79O13P	810.5258	-1	[M-H]-	809.518	Avanti polar lipids
	15:0/18:1 PI	C42H79O13P	822.5258	-1	[M-H]-	821.518	Avanti polar lipids
	16:0/18:2 PI	C43H79O13P	834.525832	-1	[M-H]-	833.518008	HMDB
	16:1/18:1 PI	C43H79O13P	834.525832	-1	[M-H]-	833.518008	HMDB
	16:0/18:1 PI	C43H81O13P	836.5415	-1	[M-H]-	835.5336	Avanti polar lipids
	16:0/18:0 PI	C43H83O13P	838.557133	-1	[M-H]-	837.549308	HMDB
	14:1/22:6 PI	C45H73O13P	852.478883	-1	[M-H]-	851.471058	Lipidmaps
	16:0/20:4 PI	C45H79O13P	858.525832	-1	[M-H]-	857.518008	PubChem
	18:1/18:1 PI	C45H83O13P	862.557133	-1	[M-H]-	861.549308	Avanti polar lipids
	18:0/18:1 PI	C45H85O13P	864.572783	-1	[M-H]-	863.564957	HMDB
	18:0/18:0 PI	C45H87O13P	866.5884	-1	[M-H]-	865.5806	Avanti polar lipids
	16:0/22:6 PI	C47H79O13P	882.525832	-1	[M-H]-	881.518008	Lipidmaps
	18:0/20:5 PI	C47H81O13P	884.541483	-1	[M-H]-	883.533658	Mass Bank Record
	18:0/20:4 PI	C47H83O13P	886.5571	-1	[M-H]-	885.5493	Avanti polar lipids
	18:0/20:3 PI	C47H85O13P	888.572783	-1	[M-H]-	887.564957	PubChem
	18:0/20:2 PI	C47H87O13P	890.588433	-1	[M-H]-	889.580608	HMDB
	18:1/22:6 PI	C49H81O13P	908.541483	-1	[M-H]-	907.533658	Lipidmaps
	18:0/22:6 PI	C49H83O13P	910.557133	-1	[M-H]-	909.549308	PubChem
	18:0/22:5 PI	C49H85O13P	912.572783	-1	[M-H]-	911.564957	PubChem
	18:0/22:4 PI	C49H87O13P	914.588433	-1	[M-H]-	913.580608	HMDB
	18:0/22:1 PI	C49H93O13P	920.635383	-1	[M-H]-	919.627558	Lipidmaps
	22:0/22:0 PI	C53H103O13P	978.713633	-1	[M-H]-	977.705807	HMDB
PIP	08:0/08:0 PIP	C25H48O16P2	666.2418	-1	[M-H]-	665.234	Avanti polar lipids
				-2	[M-2H]-2	664.2261/2= 332.1131	
	16:1/18:0 PIP	C41H78O16P2	888.476516	-1	[M-H]-	887.468691	PubChem
				-2	[M-2H]-2	886.460866/2= 443.230433	
	18:2/16:0 PIP	C43H80O16P2	914.492166	-1	[M-H]-	913.484341	HMDB
				-2	[M-2H]-2	912.476516/2= 456.238258	
	16:0/18:1 PIP	C43H82 O16 P2	916.507816	-1	[M-H]-	915.499991	Avanti polar lipids
				-2	[M-2H]-2	914.492166/2= 457.246083	
	18:1/18:1 PIP	C45H84O16P2	942.523466	-1	[M-H]-	941.515641	Avanti polar lipids
				-2	[M-2H]-2	940.507816/2= 470.253908	
	18:2/18:0 PIP	C45H84O16P2	942.523466	-1	[M-H]-	941.5156	HMDB
				-2	[M-2H]-2	940.507816/2= 470.253908	
	18:0/20:4 PIP	C47H84O16P2	966.5235	-1	[M-H]-	965.5156	Avanti polar lipids
				-2	[M-2H]-2	964.5078/2= 482.2539	
PIP2	06:0/06:0 PIP2	C21H41O19P3	690.1455	-1	[M-H]-	689.1377	Avanti polar lipids
				-2	[M-2H]-2	688.1298/2= 344.0650	
				-3	[M-3H]-3	687.1220/3= 229.0407	
	08:0/08:0 PIP2	C25H49O19P3	746.2081	-1	[M-H]-	745.2003	Avanti polar lipids
				-2	[M-2H]-2	744.1924/2= 372.0962	
				-3	[M-3H]-3	743.1846/3= 247.7282	
	18:1/18:1 PIP2	C45H85O19P3	1022.4898	-1	[M-H]-	1021.482	Avanti polar lipids
				-2	[M-2H]-2	1020.4741/2= 510.2371	
				-3	[M-3H]-3	1019.4663/3= 339.8221	
	18:0/18:1 PIP2	C45H87O19P3	1024.505449	-1	[M-H]-	1023.497624	HMDB
				-2	[M-2H]-2	1022.489799/2= 511.2448995	
				-3	[M-3H]-3	1021.481974/3= 340.4939913	
	18:0/20:4 PIP2	C47H85O19P3	1046.4898	-1	[M-H]-	1045.482	Avanti polar lipids
				-2	[M-2H]-2	1044.4741/2= 522.2371	
				-3	[M-3H]-3	1043.4663/3= 347.8221	

PIP3	**06:0/06:0 PIP3**	C21H42O22P4	770.1118	-1	[M-H]-	769.104	Avanti polar lipids
				-2	[M-2H]-2	768.0962/2= 384.0481	
				-3	[M-3H]-3	767.0884/3= 255.6961	
				-4	[M-4H]-4	766.0805/4= 191.5201	
	08:0/08:0 PIP3	C25H50O22P4	826.1744	-1	[M-H]-	825.1666	Avanti polar lipids
				-2	[M-2H]-2	824.1588/2= 412.0794	
				-3	[M-3H]-3	823.1510/3= 274.3837	
				-4	[M-4H]-4	822.1431/4= 205.5358	
	16:0/16:1 PIP3	C41H80O22P4	1048.409181	-1	[M-H]-	1047.401357	HMDB
				-2	[M-2H]-2	1046.393532/2= 523.196766	
				-3	[M-3H]-3	1045.385707/3= 348.4619023	
				-4	[M-4H]-4	1044.377882/4= 261.0944705	
	16:0/16:0 PIP3	C41H82O22P4	1050.424832	-1	[M-H]-	1049.417007	HMDB
				-2	[M-2H]-2	1048.409181/2= 524.2045905	
				-3	[M-3H]-3	1047.401357/3= 349.1337857	
				-4	[M-4H]-4	1046.393532/4= 261.598383	
	16:0/18:1 PIP3	C43H84O22P4	1076.440482	-1	[M-H]-	1075.432657	HMDB
&	**18:0/16:1 PIP3**			-2	[M-2H]-2	1074.424832/2= 537.212416	
				-3	[M-3H]-3	1073.417007/3= 357.805669	
				-4	[M-4H]-4	1072.409181/4= 268.1022953	
	18:1/18:1 PIP3	C45H86O22P4	1102.4561	-1	[M-H]-	1101.4483	Avanti polar lipids
				-2	[M-2H]-2	1100.4405/2= 550.2203	
				-3	[M-3H]-3	1099.4327/3= 366.4776	
				-4	[M-4H]-4	1098.4248/4= 274.6062	
	18:0/18:1 PIP3	C45H88O22P4	1104.471782	-1	[M-H]-	1103.463957	HMDB
				-2	[M-2H]-2	1102.456132/2= 551.228066	
				-3	[M-3H]-3	1101.448307/3= 367.1494357	
				-4	[M-4H]-4	1100.440482/4= 275.1101205	
	18:0/20:4 PIP3	C47H86O22P4	1126.456132	-1	[M-H]-	1125.448307	Avanti polar lipids
				-2	[M-2H]-2	1124.440482/2= 562.220241	
				-3	[M-3H]-3	1123.432657/3= 374.4775523	
				-4	[M-4H]-4	1122.424832/4= 280.606208	
	18:1/20:3 PIP3	C47H86O22P4	1126.456132	-1	[M-H]-	1125.448307	HMDB
				-2	[M-2H]-2	1124.440482/2= 562.220241	
				-3	[M-3H]-3	1123.432657/3= 374.4775523	
				-4	[M-4H]-4	1122.424832/4= 280.606208	
	18:2/20:1 PIP3	C47H88O22P4	1128.471782	-1	[M-H]-	1127.463957	HMDB
				-2	[M-2H]-2	1126.456132/2= 563.228066	
				-3	[M-3H]-3	1125.448307/3= 375.1494357	
				-4	[M-4H]-4	1124.440482/4= 281.1101205	

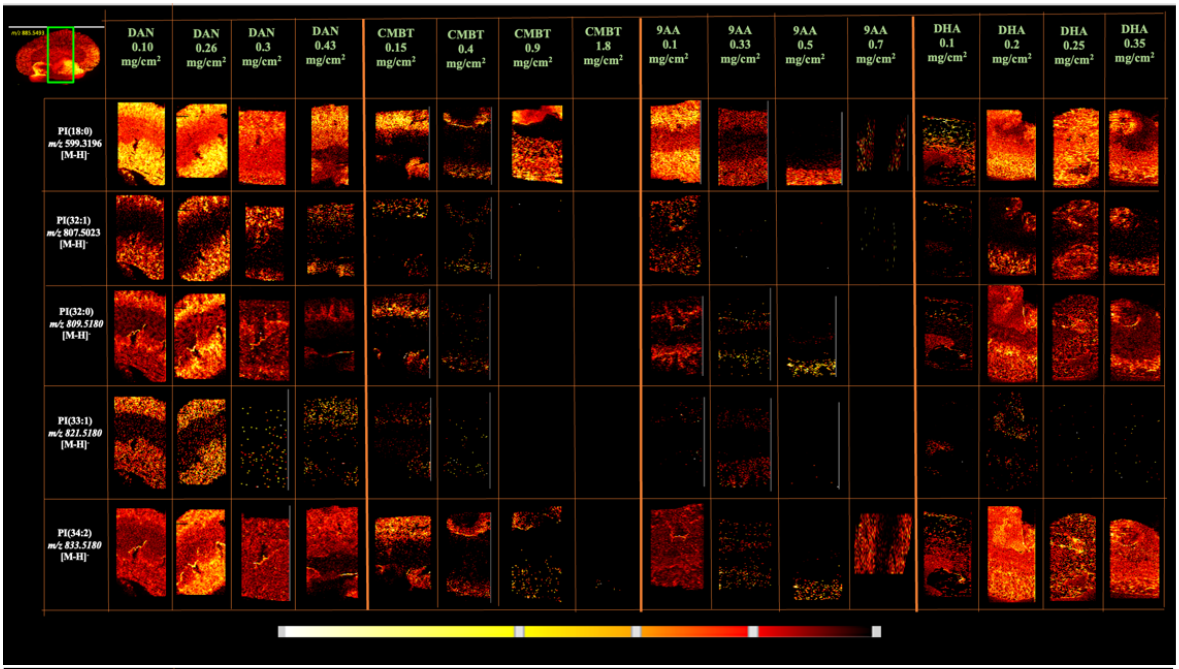
DAN 0.10 mg/cm²
DAN 0.26 mg/cm²
DAN 0.3 mg/cm²
DAN 0.43 mg/cm²
CMBT 0.15 mg/cm²
CMBT 0.4 mg/cm²
CMBT 0.9 mg/cm²
CMBT 1.8 mg/cm²
9AA 0.1 mg/cm²
9AA 0.33 mg/cm²
9AA 0.5 mg/cm²
9AA 0.7 mg/cm²
DHA 0.1 mg/cm²
DHA 0.2 mg/cm²
DHA 0.25 mg/cm²
DHA 0.35 mg/cm²
PI(18:0) m/z 599.3196 [M-H]⁻
PI(32:1) m/z 807.5023 [M-H]⁻
PI(32:0) m/z 809.5180 [M-H]⁻
PI(33:1) m/z 821.5180 [M-H]⁻
PI(34:2) m/z 833.5180 [M-H]⁻

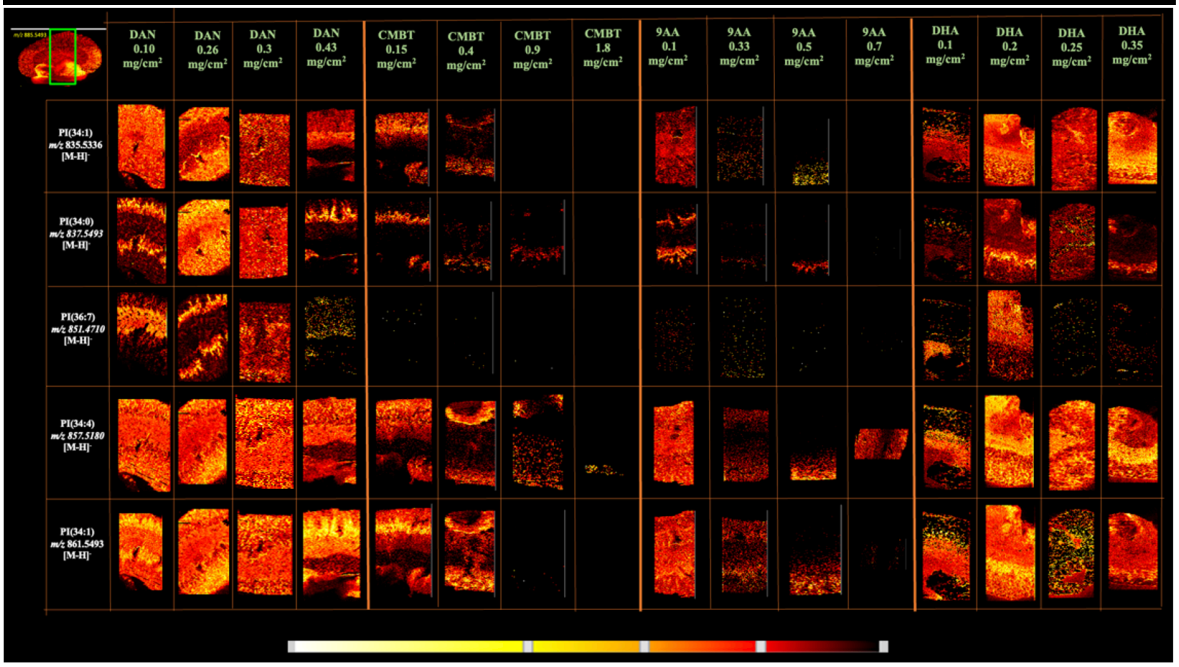
DAN 0.10 mg/cm²
DAN 0.26 mg/cm²
DAN 0.3 mg/cm²
DAN 0.43 mg/cm²
CMBT 0.15 mg/cm²
CMBT 0.4 mg/cm²
CMBT 0.9 mg/cm²
CMBT 1.8 mg/cm²
9AA 0.1 mg/cm²
9AA 0.33 mg/cm²
9AA 0.5 mg/cm²
9AA 0.7 mg/cm²
DHA 0.1 mg/cm²
DHA 0.2 mg/cm²
DHA 0.25 mg/cm²
DHA 0.35 mg/cm²
PI(34:1) m/z 835.5336 [M-H]⁻
PI(34:0) m/z 837.5493 [M-H]⁻
PI(36:7) m/z 851.4710 [M-H]⁻
PI(34:4) m/z 857.5180 [M-H]⁻
PI(34:1) m/z 861.5493 [M-H]⁻

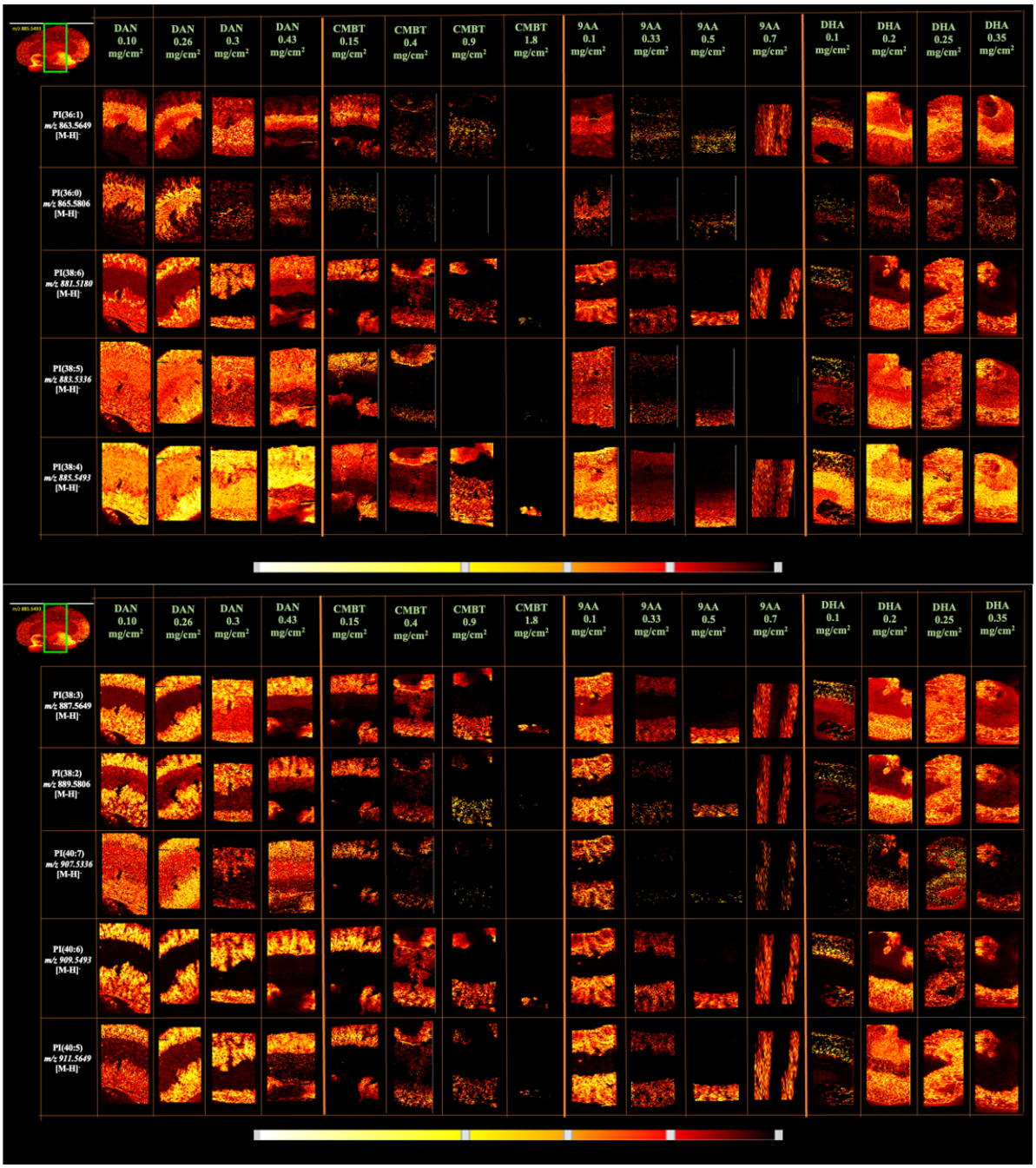
DAN 0.10 mg/cm²
DAN 0.26 mg/cm²
DAN 0.3 mg/cm²
DAN 0.43 mg/cm²
CMBT 0.15 mg/cm²
CMBT 0.4 mg/cm²
CMBT 0.9 mg/cm²
CMBT 1.8 mg/cm²
9AA 0.1 mg/cm²
9AA 0.33 mg/cm²
9AA 0.5 mg/cm²
9AA 0.7 mg/cm²
DHA 0.1 mg/cm²
DHA 0.2 mg/cm²
DHA 0.25 mg/cm²
DHA 0.35 mg/cm²
PI(36:1) m/z 863.5649 [M-H]-
PI(36:0) m/z 865.5806 [M-H]-
PI(38:6) m/z 881.5180 [M-H]-
PI(38:5) m/z 883.5336 [M-H]-
PI(38:4) m/z 885.5493 [M-H]-
PI(38:3) m/z 887.5649 [M-H]-
PI(38:2) m/z 889.5806 [M-H]-
PI(40:7) m/z 907.5336 [M-H]-
PI(40:6) m/z 909.5493 [M-H]-
PI(40:5) m/z 911.5649 [M-H]-

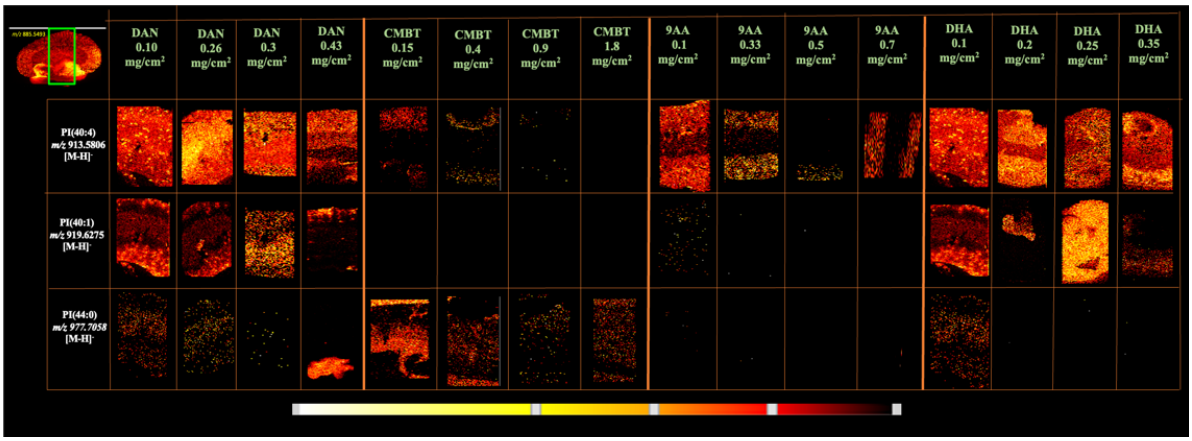

Figure C.1: Assessing the detectability or absence of specific PI molecular species across varied matrices and thicknesses. Negative ion mode MALDI-MSI analysis of mouse kidney was performed using various thicknesses (mg/cm^2) of DAN, CMBT, 9AA, and DHA matrices. The green rectangle shows the area used for the comparison of various thicknesses. Here, ion images of the most important PIs are shown. It is important to note that the thickness of the matrix layer can significantly affect the quality and quantity of ions detected in MALDI-MSI. If the matrix layer is too thin, very few ions are detected, while if it is too thick, only matrix ions are detected.